NONLINEAR SYSTEM IDENTIFICATION WITH APPLICATIONS TO DURABILITY TESTING OF GROUND VEHICLE COMPONENTS

by

Sushil Doranga

A thesis submitted to

The Faculty of Graduate Studies of

The University of Manitoba

in partial fulfillment of the requirements

of the degree of

Doctor of Philosophy

Department of Mechanical Engineering

The University of Manitoba

Winnipeg, Manitoba, Canada

December 2014

Abstract

Presently in ground vehicle industry, conducting durability tests are an essential step in evaluating the life of full vehicle, subsystem and component design. By moving the durability tests from the proving ground to the test laboratory, one can improve quality, reduce the cost associated with the testing and accelerate the product development process. The procedure of durability testing includes measuring the accelerations/strain data in a test track, generating the accelerated loading profiles (desired reference signal) and implementing them by using hydraulic actuators. In a laboratory such actuators are mounted in a fixed configuration, referred to here as a multiaxial simulation table (MAST). The time waveform replication algorithm is used, which iteratively produces an input signal used to excite a structure such that its response replicates a desired reference. The time waveform replication algorithm essentially estimates the unknown input by the inversion of the frequency response function. However, due to the presence of nonlinearities (stiffness and damping) of the test structure, the error between the test output signal and the desired reference signal is large. This results in poor reference replication whereby the validity of the test may be put into question. For such cases, the nonlinear system identification of the test structure is of essence. Such an approach is presented in this thesis, where the concept of nonlinear system identification in a test structure that is excited by using a hydraulic actuated shaker table is presented.

The methods for nonlinear system identification strictly depend on the types of excitation. The traditional nonlinear parameter identification techniques described in the existing literature are based on the excitation of forces as an input. For cases, where the excitation comes from the base motion, the above mentioned methods cannot be applied as it is impossible to measure the

motion at all degrees of freedom (DOFs) from an experiment and the mass distribution of the structure is not known a-priori.

In this thesis, two new methods, specific to the nonlinear system identification of the base excited structure, are presented. The proposed new methodologies are based on the theory of force reconstruction, base excitation and nonlinear system identification. A reverse explicit formulation is presented to reconstruct the force vector using the base excitation as an input. The formulated theory is verified by a simulated example of five degree of freedom lumped parameter model and demonstrated through experimentations. A hybrid model space is developed to determine the nonlinear restoring force at the nonlinear degrees of freedom. The first methodology shows the extraction of nonlinear parameters in the physical coordinate system while the second method shows the extraction of nonlinear parameters in the modal space.

Using a cantilever beam as an example, the proposed modal space based methodology is demonstrated. The experimental set-up, testing procedure, data acquisition and data processing are also presented. The example shows that the methods proposed here are systematic and constructive for nonlinear parameter identification for based excited structure.

As most of the vehicle components are mechanically connected, it is crucial to study the effect of joints on the dynamical behavior of assembled structures. A numerical and experimental study is carried out in a structure with bolted joint connection. Several input loading profiles are used to detect and characterize the nonlinearity. Once the nonlinearity is detected and characterized, the modal space based method is used to identify the nonlinear stiffness and damping parameters. A particular result from the experimentations is the identification of viscous damping coefficients dependent upon displacement amplitudes. The significance of this result is that the complex

phenomenon of energy dissipation in lap joints can be represented by a simple analytical model in modal space, capable of producing results that are close to the experimentally observed results.

Nomenclature

Latin symbols

$[C]$	Viscous damping matrix
$\{F\}$	Excitation force vector
$\{F\}^d$	Equivalent excitation force vector
g^{cub}	Nonlinear restoring force related to cubic stiffness nonlinearity
g^{cle}	Nonlinear restoring force related to clearance nonlinearity
g^{fri}	Nonlinear restoring force corresponding to friction nonlinearity
$\{G\}$	Nonlinear restoring force vector
$[K]$	Stiffness matrix
K_d	Tangential stiffness for stick friction
K_Z	Clearance stiffness
m	Number of measured degrees of freedom
$[M]$	Mass matrix
M_r	Number of identified modes
N	Sample measured data from the time series
$\{P^d\}$	Pseudo excited force vector

N_s	Total number of samples
$\{R_e\}$	Residual Vector
t	Time
u	Number of unmeasured degrees of freedom
$\{\tilde{U}\}$	Vector of nonlinear relative displacement amplitude
U_r	Number of unidentified modes
$\{x\}$	Displacement vector
$\{\tilde{q}\}$	Nonlinear modal response
y_c	Clearance gap distance
q	Linear modal response

Symbols

ε	Error in estimation
ζ	Modal damping ratio
$[\lambda]$	Complex eigenvalues matrix
μ	Coefficient of friction
Φ_i	Vector containing i^{th} column from mode shape matrix
$[\Phi]$	Mode shape matrix

$\sigma_x{}^2$ — Variance of the measured restoring force

ω — Excitation Frequency

ω_r — Resonance frequency of the rth mode

Subscripts

m — Index representing measured degrees of freedom

M_r — Index representing the identified modes

u — Index representing un-measured degrees of freedom

U_r — Index representing the un-identified modes

Superscripts

T — Transpose of a matrix

-1 — Inverse of a square matrix

$+$ — Pseudo-inverse of a rectangular matrix

Abbreviations

AS: Auto Spectrum

CTH: Corrected Time History

DTH: Desired Time History

ETH: Error Time History

DOFs: Degrees of Freedom

EMA: Experimental Modal Analysis

ERS: Extreme Response Spectrum

ETH: Error Time History

FDS: Fatigue Damage Spectrum

FEA: Finite Element Analysis

FEM: Finite Element Method

FFT: Fast Fourier Transform

FRF: Frequency Response Function

ID: Initial Drive

IFFT: Inverse Fast Fourier Transform

IFM: Inverse Frequency Response Function Model

MAST: Multiaxial Simulation Table

MDOF: Multi Degree-of-freedom

MSE: Mean square Error

RPC: Remote Parameter Control

MTS: Multipurpose Test Ware

RTH: Response Time History

SAST: Single Axis Simulation Table

SRS: Shock Response Spectrum

PSD: Power Spectrum Density

Table of Contents

List of Figures

List of Tables

Chapter 1

Introduction

This chapter presents a brief introduction to the subject of ground vehicle durability testing, the importance of the research in this area and its relevance to industrial applications. The terminology specific to durability testing, which is frequently used in the thesis, is explained in order to facilitate the discussion presented in the thesis. The statement of the problem along with the objectives of the research program are presented in this chapter.

1.1   Background

Newly designed commercial vehicles have to pass a number of durability tests as a pre-launch requirement in compliance with the necessary standards for safety, reliability, durability and comfort. These durability tests (field tests) are usually conducted in the proving grounds, which are designed to simulate real road environments (events). An example of a vehicle testing facility located at the Pennsylvania Transportation Institute is presented in Figure 1.1, where the vehicle durability course is shown. The vehicle durability course consists of seven different events that are expected to be encountered during the transit service. The seven events are staggered bumps; railroad crossing; one inch random chuck holes; chatter bumps; four inch chuck hole; high crown intersection; and frame twist. The geometry of the seven events is shown in Figure 1.2. During the durability test the ground vehicles need to be driven a certain distance in a durability course without exhibiting any failure, including any crack initiation, in the critical suspension, the frame and the cab systems to certify the marketability of the vehicles.

Figure 1.1: The Altoona Bus Research and Testing Center (© Pennsylvania Transportation Institute) (http://www.larson.psu.edu/testTrack)

Testing full scale vehicles in a real test track, however, is time consuming, non-repeatable and costly. A typical field test requires drivers to drive thousands of miles in a variety of operating conditions, which takes months to complete. As a result, an alternate methodology for durability testing needs to be developed.

Such an alternate to method involves testing in a laboratory set-up to simulate the driving conditions of the field tests but over a shorter period of time. To achieve successful durability results in a laboratory, certain requirements must be met [1], including : (a) the test must be suitable for the item in question, examples include a single component, sub-component, sub-assembly or the complete vehicle; (b) the test must be able to replicate the same failure mechanisms observed in the real loading environment; (c) the test should be representative of the real loading environment within known statistical margins; and, (d) the test should be accelerated, where possible, to shorten the testing process and reduce cost. However, the test should not incur unrealistically high loads that might alter the failure mechanism. Conducting

durability tests in a laboratory that satisfies the above criteria, involves two stages: in the first stage, an accelerated loading profile (test signal) is generated in the form of the power spectrum density (PSD), which has the same damage potential as that of the real environment, but in a fraction of the time. The second stage of the durability tests consists of implementing the driving test signal to the components under testing.
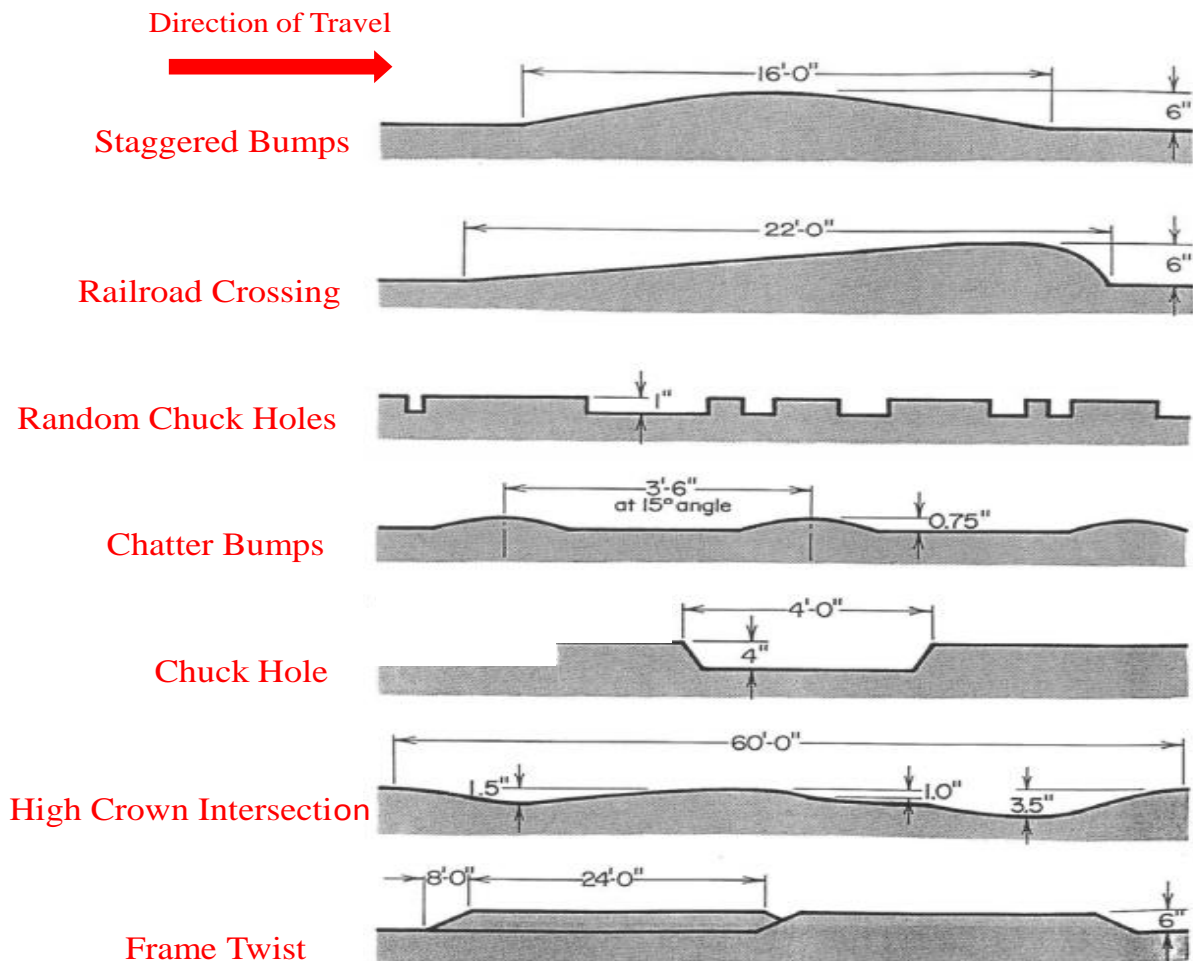
Figure 1.2: Geometry of the Seven Events (© Pennsylvania Transportation Institute)

The "Test Tailoring Approach" originally developed by Halfpenny in 2006 [2] is commonly used to generate the accelerated loading profile. The "Test Tailoring Approach" essentially consists of a two-step procedure in generating the loading profile for an accelerated test. The first

step is the Mission Profiling and the second step is the Test Synthesis. A Mission Profile comprises of recorded loading data from the field test, such as accelerations. Such loading data are correlated to the corresponding event and the PSD for each event is calculated with an estimate of the duration the vehicle might be expected to experience this event in-service. The second step is the Test Synthesis, where an accelerated loading profile is generated which has the same fatigue damage content as the Mission Profile but over a shortened test period. More detailed discussions on the "Test Tailoring Approach" are provided in references [1-3].

In the second stage of the durability tests, the accelerated test signal is replicated at the specific location of the test component. This is usually performed by using a controlled hydraulic actuator in a Multi-Axial Simulation Table (MAST). This is illustrated in Figure 1.3 for the physical testing, where the actuator is driven to replicate accelerations on the vehicle body that were previously measured for a specific road surface.

The problem of the test signal replication represents an extremely challenging problem that cannot, in most cases, be solved with current actuator controllers. As a result, an alternative methodology is widely utilized whereby the controller command signal is modified in an iterative series of experiments until the measured signal on the test component closely matches that required. All of the major suppliers of servo-hydraulic test equipment offer controller design software that can perform this iterative approach to drive file generation. Examples include MTS Systems Corporation with remote parameter control (RPC) and Instron's time waveform replication (TWR) from Illinois Tool Works Inc. Despite the variety of software packages available, all are based on the same fundamental approach that utilizes the "inverse algorithm" that was developed by engineers at General Motors in the 1970s [4]. The durability testing

4

companies, such as MIRA and DYNATEX use the RPC software to replicate the test signal at a specific location of the component under testing.
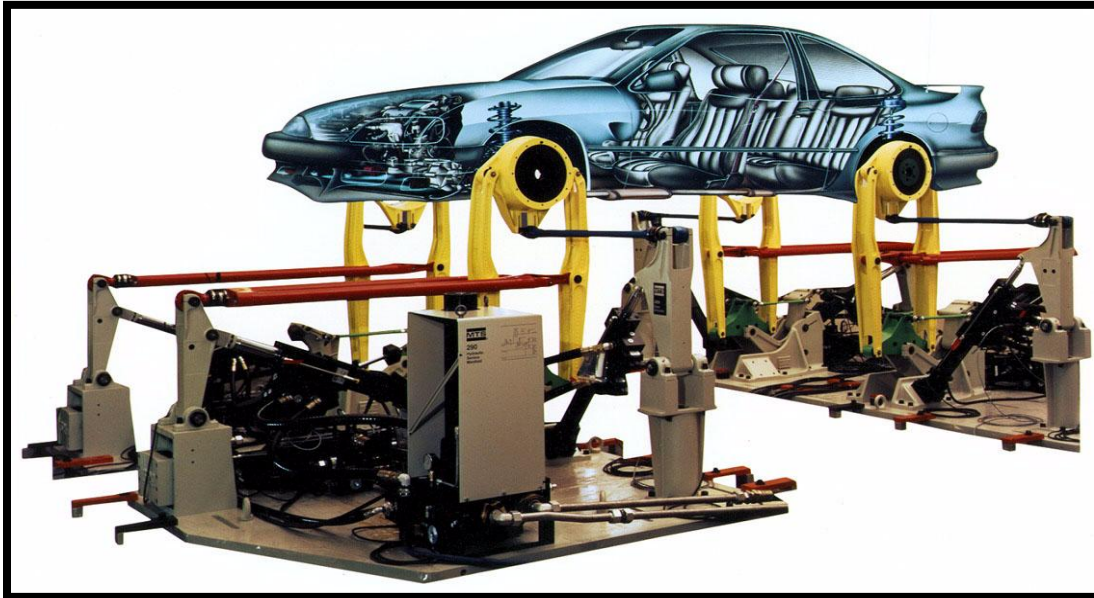
Figure 1.3: Durability Testing of Variety of Components or Assemblies (© Westest, Canada)

(http://www.westest.ca/)

The algorithm for the test signal replication works on the frequency domain data and consists of two parts. In the first part, the frequency response function (FRF), also known as the forward system model (MAST and the test component), is calculated. The calculated FRF is based on the assumption that the behavior of the whole system is linear. The second part of the test signal replication involves the calculation of the excitation (driving signal) to the MAST from the accelerated loading profile using the inverse of the above FRF. Another test methodology, which is used by Western Canada Testing Inc. (Westest), is that the test signal is replicated in the MAST instead of the component under testing. However, the principle behind the test signal replication remains the same.

In spite of advancements in durability testing technologies, the accuracy in implementing the desired accelerated loading profile is often unsatisfactory. The engineering problem associated with the replication of accelerated loading profile is due to (a) the unknown dynamics of the test component; (b) the presence of significant structural resonance in the test component; and, (c) the poor performance of the controller. There are two ways of addressing this problem. The first is to develop robust control algorithms that can minimize the error between the desired loading profile and the achieved one. The second is to improve the performance of the controller by identifying the unknown dynamics of the test component such as, stiffness and damping through nonlinear system identification. There are several companies and academic institutions working to address the first of these approaches. Examples include Turbo RPC developed by MTS and New Iterative Control Methods which is under development at the Automatic Control and Systems Engineering department at the University of Sheffield, UK [4]. The Turbo RPC is found to be working properly if there is significant structural resonance presence in the test component and if the nonlinearity (dynamics) of the structure is known a-priori [5]. The research presented in this thesis focuses on the second approach; namely, to identify the dynamics of the test component, such that the accelerated test signals can be implemented with satisfactory accuracy.

1.2   Nonlinear System Identification

The term 'Nonlinear' is quite a broad term and has different meanings in the context of different engineering disciplines. From a structural dynamics point of view, nonlinearity refers to the dynamics which causes the system to violate the principle of superposition, homogeneity and reciprocity. Mathematically, nonlinear systems are represented by a set of differential equations with nonlinear terms. The natural frequencies and the mode shapes of such systems are dependent on the excitation amplitude. Various domains of engineering, like aerospace,

6

automobile, civil and structural engineering encounter nonlinear systems in one form or other [6]. Some common occurrence of nonlinearities in engineering are the friction induced nonlinearities in bolted joints and the polynomial stiffness nonlinearities observed in beams, plates and engine-wing of an aero structure etc.

Linear system identification, which attempts to determine mathematical models of linear dynamic systems from vibration measurements, is an established area of study. The tool like modal testing and analysis [6-8] is the powerful and universally accepted tool for linear system identification. For linear systems, the transfer function, relating the input of the system to its output, remains constant at all excitation levels. Thus, the mathematical model obtained through the identification at one operating point can later be used for prediction at any other operating point. For a nonlinear system, it is impossible to obtain a universal mathematical model of the system by performing the system identification only at a single excitation level. A model obtained at a given operating condition can, at best, provide the equivalent linear system at that point with some contribution of nonlinearities. Figure 1.4 shows the difference between linear and nonlinear systems. From the system identification perspective, the transfer function is dependent upon the input for a nonlinear system, as indicated by Figure 1.4.

$X(\omega)$ → $H(\omega)$ → $Y(\omega)$

Linear System

$X(\omega)$ → $H(\omega, X)$ → $Y(\omega)$
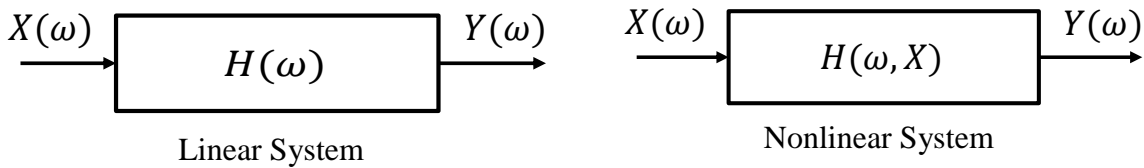
Nonlinear System

Figure 1.4: Difference between Linear and Nonlinear Systems

1.2   Objectives of the Thesis

The overall goal of this thesis is to address the problem associated with the test signal replication at a specific location of the component in a typical durability test. In this thesis, at first, the available methodologies and their limitations for the nonlinear system identification are investigated. The current literature shows that, the available methodologies are only useful for the cases where the excitation is in the form of forces. While, the most testing components under durability testing are structures excited with base motion, the methodology developed for force excited system, as described in the existing literature, cannot be applied to base excited structure.

The specific objectives of this research project are:

(a)   To develop a nonlinear system identification methodology, such that it bridges the gap between force excited systems and base excited systems

(b)   To develop the methodology for force reconstruction in a vibrating structure, where the excitation comes from the moving base

(c)   To develop the methodology for the nonlinear parameter identification in a base excited system such that the well known force state mapping principle can be used in the modal space

(d)   To develop an experimental approach to demonstrate the proposed methodology

(e)   To develop the nonlinearity detection, characterization, and identification algorithm for a joint structure and validate this algorithm through numerical simulations and experimentations

1.2   Organization of the Thesis

The material in the thesis is arranged sequentially, starting with the survey of the literature in the area of nonlinear structural identification, which is presented in Chapter 2. Chapter 3 presents the force reconstruction procedure in base excited structure. The new methodology for the nonlinear system identification in base excited structure is presented in Chapter 4. Chapter 5 presents the design of experimental setup and the demonstration of the nonlinear system identification through experimental observations. The application of this method to the joint structure is presented in Chapter 6. In the last chapter of the thesis, Chapter 7, some concluding remarks on the research, contributions of the thesis and suggestion for the future works are listed.

Chapter 2

Literature Review

This chapter presents a survey of the literature in the area of nonlinear structural dynamics. The survey presented is not at all comprehensive but more specific to the topics related to the thesis. The literature, which helped me to develop the new methodology for nonlinear system identification, and is closely related to the research presented in the thesis is dealt with in detail. The excellent review articles [9-12] on this topic and the books by Nayfeh and Mook [13] and Worden and Tomlinson [14] serve as a good starting point for the researchers who are new to this area. The review in this chapter is organized methodologically. In the last section of this chapter, the summary of the literature review describing the gaps in current knowledge is presented.

Nonlinear structural dynamics has been of interest to the researchers for more than four decades. Tremendous efforts have been devoted to predict the accurate methods for nonlinear system identification in order to reduce the time and cost involved with the durability testing of ground vehicles. Such a need coupled with the availability of computational resources acted as a stimulus to the research in this area.

The nonlinear system identification is an inverse problem. It attempts to identify the system in its mathematical form by knowing the input and output. The nonlinear system identification has three steps: (i) nonlinearity detection, (ii) nonlinearity characterization and (iii) nonlinear parameter extraction. The methods for nonlinearity detection are well established and are widely used in the aerospace and automobile industries. The methods for the characterization of nonlinearity types are still not reliable for industrial applications. An experience based subjective

judgments is widely used in the industry for nonlinearity characterization. Extraction of the nonlinear parameters poses even the large scale of challenges. Since my research focuses on nonlinear parameter identification, the review of relevant literature is presented here.

Many approaches for linear system identification are in practice, such as output only analysis for linear system identification [15], complex mode shapes analysis for non-proportional damped structures [16] and mode shapes identification for geometrical discontinuous structures [17]. All those analyses yield a final model based on modal parameters, such as natural frequencies, mode shapes, modal damping ratios and modal masses. Therefore, it would not be injustice to say that the methods for linear system identification are mature. In practice, most structures show some nonlinear behaviors and there is a considerable interest in the identification of the nonlinear dynamic systems. However, methods developed for linear system identification cannot be directly applied to nonlinear system identification.

The research in the field of nonlinear system identification started more then four decades ago [18-20]. During the early stage, due to limited mathematical tools and experimental techniques, it was perceived that the linear system identification is enough for the practical applications of structures. The research later gained the popularity and general acceptance when it was understood that the behaviors of all engineering structures are nonlinear to some extents. Rosenberg [21] in the 1960s proposed a new concept of nonlinear normal modes (NNMs) as a motion in which all points of the system vibrate with the same phase. This theory is the extension of the definition of normal modes used for linear systems. Later Shaw [22] and Pierre [23] generalized Rosenberg's definition by proposing the concept of an invariant manifold. They represented nonlinear normal modes as surfaces in a phase plane. This invariant manifold concept is used to find out the amplitude dependent mode shapes. The Nonlinear normal modes

11

theory is based on rigorous mathematics, and it explains various nonlinear phenomena, such as internal resonance and mode bifurcations. Since the introduction of this concept, a number of articles have been published that deals with NNMs. Nayfeh and Nayfeh [24-26] used two dimensional manifold concepts to formulate the nonlinear natural frequencies and mode shapes of a cantilever beam. This study was extended by Khadem and Mahmoodi [27] by including the nonlinear damping terms. The nonlinear normal modes theory enables one to describe complex physics, but it is difficult to apply in practical engineering applications. It is due to the fact that nonlinear phenomenon such as internal resonance and mode bifurcations are difficult to capture during the experimental observation.

Addressing the challenge of implementation, many researchers have attempted to express the nonlinearities either in a modal space or in a physical coordinate system. Marsi and Caughey developed a pioneer theory which is essentially nonparametric and expressed the nonlinearities in a physical coordinate system [28]. They proposed a method called restoring force surface (RFS) in which the restoring force is plotted against instantaneous values of displacement and velocity in a phase plane. The surface is then approximated by the double chebyshev polynomials to identify the nonlinear parameters. The most important restriction made on their method is that, it is not suitable for a nonlinear system with discontinuous nonlinearities.

Richard and Singh [29] proposed a method for nonlinear system identification named as conditioned reverse path (CRP). The idea of this method is to separate the nonlinear distortions from the measured FRFs using spectral conditioning. The method is applicable to such structures where the location and the type of nonlinearities are known. Another method similar to CRP method is presented in reference [30], which is commonly known as nonlinear identification through feedback of the output (NIFO). In this method, nonlinear restoring forces are modeled as

12

an internal feedback into a closed loop linear system. The compact formulation of this method makes it easier to implement in the real life structure.

He and Ewins [31] proposed a new method based on the inverse receptance analysis. Their method attempted to find the natural frequency and the damping ratio for each mode based on a single DOF assumption that one and only one mode is excited. The effects due to other modes were neglected. While dealing with large MDOF systems it is almost impossible to separate the cross coupling terms, which is the limitation of this method in a practical situation. The method proposed by He and Ewins [31] also assumed that the mode shapes of the nonlinear system are the same as the mode shapes of the corresponding linear system.

Feldman in his research [32] developed methods for free vibration and forced vibration analysis, named as FREEVIB and FORCEVIB. The variation of natural frequencies and damping ratios with the amplitude of vibration was shown in his method [32]. Platten et al. [33-34] proposed a new concept of the nonlinear resonant decay method for nonlinear system identification in a modal space and showed the possibility to excite experimentally individual linear undamped modes. Their method [33-34] consists of two stages, (i) linear parameters are identified with low level frequency response functions (FRF) data and (ii) apply the high level force in the mode to excite it nonlinearly. To achieve this, an optimum force pattern is required. Platten et al. [33-34] found the optimum force pattern through a multivariate mode indicator function (MMIF). This high level force will induce nonlinearities between the individual and cross coupled modes. The method proposed by Platten et al. [33-34], compared to existing methods, is more accurate and robust in analyzing large MDOF systems. However, there are some limitations, like the force drop-out at resonance and shaker structure interaction, etc. Platten et.al. [33-34] further proposed

the acoustic excitation as an alternative to the shaker excitation to reduce those problems in modal testing.

Elizalde [35] used the nonlinear modal vector approach to distinguish the level of nonlinearity in a nonlinear system as lightly nonlinear, moderately nonlinear and highly nonlinear. It was shown that for a highly nonlinear system, the ratio of nonlinear modal vectors to input forces exceeds 10. To extract the nonlinear modal vectors, all the measured DOFs are excited by the input forces. These classifications are based on the extreme theoretical simulations. Elizalde [35] used a hybrid model to define the modes that are particularly affected by the nonlinearity and the modes which are linear and can be neglected from further analysis. Elizalde's research presents the procedure and practical advices for readers who are interested in analyzing the nonlinear system in a modal space.

Jalali [36] used the approach of "Sensitivity of Frequency Response Functions" for nonlinear system identification. He proposed an identification approach for nonlinear MDOF systems when there is a single nonlinear element in the system and its location is known. This proposed method is an extension of the FRF sensitivity method used in the linear system. This method uses measured nonlinear FRFs and employs a reduced order model for sensitivity calculations. Jalai in his another work [37] proposed the method called the describing functions inversion method. In his method the describing functions were obtained using the linearized FRFs. The linearized FRFs were obtained by taking the response of the system to harmonic excitation forces at the frequency range close to the natural frequencies. The nonlinear parameters were identified based on the calculation of the experimental describing functions and the system response corresponding to the nonlinear DOF. The method was verified using the 2 DOF lumped parameter model with cubic stiffness nonlinearity. The aim of the describing functions method is

14

to obtain equivalent amplitude dependent stiffness and damping coefficients at the nonlinear DOF. Many researchers in the past had applied the describing functions method for the identification of different types of nonlinearities of a nonlinear system. Kul and Chen [38] applied the describing functions method for the identification of the hysteretic type nonlinearities. Watanabe and Sato [39] used the first order describing functions and obtain the nonlinear stiffness of a beam structure. Kuran and Ozguven [40] used the describing functions method to obtain the cubic stiffness nonlinearity of a MDOF system. Besancon-Voda and Blaha [41] developed a multi-input describing function for the friction damping nonlinearity. Ozer et.al. [42] proposed a method for calculating describing functions by using the harmonic response of a MDOF nonlinear system. In their method the restoring forces of the nonlinear system was obtained using the curve fitting approach. Despite the facts of the use of describing functions methods by various researchers, the major drawback of this describing functions method is that it required the location and the functional form of the nonlinearity which may limits the application of this method in a practical structure.

Rogers et.al. [43] presented the approach to detect the presence of real normal modes. A brief theory for generating the multivariate mode indicator function and the procedure to extract the modal parameters are presented in their research. They demonstrated the theory by applying in a typical aerospace structure which consists of closely spaced modes in a narrow frequency range.

Wright et.al. [44] presented a method of physically exciting and measuring the undamped natural frequencies and normal mode shapes of a structure. They verified the method using the simulated response data and is demonstrated experimentally using an aluminum plate. A viscous damper was placed at one corner of the aluminum plate so as to yield the non-proportional damping. Their experimental results conclude that the proposed technique offer a way forward for

nonlinear system identification in a modal model form. However, the method has some disadvantages like: requirement of the long testing time and the need for adequate placement of the exciters.

Sinapius [45-47] performed the normal mode tuning using the multiaxial base excited shaker table. His research presented the theoretical background on the test method with the particular emphasis on the estimation of damping, modal mass and on finding the suitable base axis combination of the 6 DOF base excited shaker table.

One of the major difficulties of nonlinear system identification is that the functional form of the nonlinearity which maps the input signal to the output signal is usually unknown beforehand. Physical insight is necessary to select a reasonable accurate model of the nonlinearity. If the physical insight is completely lacking, it is then time to move to nonlinear black box modeling. A nonlinear black box model of a structure is a model that is prepared to describe virtually any nonlinear dynamics on the basis of the measured input output data. Sjöberg et al. [48] presented the approach based on nonlinear black-box modeling. In their research the nonlinear dynamics of the structure was approximated with three black box model: wavelet based model, neural network based model and the fuzzy based model. Their research highlighted the common features of the above mentioned three black box model and the choice of the model that have to be made for successful system identification.

Allison [49] used the proper orthogonal decomposition method for the identification of the nonlinear dynamic systems. In his method the proper orthogonal decomposition of the measured response data was combined with linear system theory to construct a model of an arbitrary linear or nonlinear system without any knowledge of the equations of motion. The method was verified

by using the simulated numerical data. The major disadvantage of the method proposed by Allison [49] is that his method is developed for the situations where the displacements are measured as an output and the forces are applied as an input. However, in many cases, vibration tests are performed by applying base excitations instead of loads. Acceleration, strain or stress output may be of more interest than displacements.

Sadat et.al. [50] used an intelligent parameter varying approach for nonlinear system identification in a base excited structure. They used a radial basis function neural network to fit the measured nonlinear restoring force. In their method, the structure has been treated as a lumped mass system, which is beyond the scope of this research. This is the only literature documented so far for nonlinear system identification in a base excited structure.

2.1   Gap in Knowledge

In spite of the research efforts to develop methods for nonlinear parameter identification, most of the methods available in the literature are presented for few DOF lumped mass systems or simple continuous systems of academic interest. Recently, some attempts have been made to use the identification methods on complex engineering structures [33]. The methods discussed in the literature have their application region within which they succeed. Although the research in the field of nonlinear system identification progressed for the last four decades, the research has not yet proposed the universal methodology for the nonlinear system identification. The proposed methodologies in the literatures for nonlinear system identification depend on three parameters. The three parameters are: (i) type of excitations used (force, displacement, and acceleration), (ii) number of excitations used, for example, multi force input, and (iii) test set-up (hammer, modal shaker, base excited mechanical shaker). A lot of research has been progressed in developing the methodologies that uses the modal shaker as a test setup. However, significant research has not

17

been carried out in developing the methodologies that use the base excited shaker as the test set-up. There are some limitations when applying the above mentioned methods (Force excited system) to real-life engineering structures, such as the cases where the excitation comes from the base motion (base excited system). Such issue include (i) it is impossible to measure the response at all DOFs from the experiments, (ii) the mass distribution of the structures are not always known a-priori and (iii) the input force to the system is difficult or even impossible to measure. Even today, the testing industry is waiting for a method for nonlinear system identification which can be used alongside with the main-stream tools like linear modal analysis and Finite element analysis (FEA) and is applicable for complex real-life structures.

Chapter 3

Force Reconstruction Using the Base Excitation as an Input

It is mandatory to evaluate the dynamic performance and durability of the important mechanical components of aircraft structures and ground vehicles under service loading. The testing is often carried out by mounting the components to a shaker table, making the tested components a base excited mechanical system. Similarly, civil structures, like bridges, buildings, and dams, are often designed to resist the transmissibility of ground vibrations. For laboratory testing of civil structures, a scaled model of the structure is mounted on a shaker table, and it is given a displacements/accelerations input at the base to simulate operating conditions. In this kind of testing the excitation comes from the moving base which is in the form of displacements/accelerations. In such cases the excitation forces do not act locally, but they are distributed throughout the structure depending on the mass distribution of the structures. Thus, it is not possible and feasible to measure the excitation forces directly.

This chapter presents a new method for the force reconstruction of a base excited structure with controlled displacements/accelerations input. The main contribution presented in this chapter is the derivation of an analytical expression for the input force vector using the base motion as an input. It makes more sense; at least when dealing with experimentally derived data, to be able to formulate the input excitation force vector at the measured DOFs only. This approach can mimic the conditions of incomplete measurements of motion for a continuous system and pleased for discrete lumped parameter system. The proposed methodology is based on previous work by Aditya *et al*. [18] and Elizalde and Imregun [35], who used the hybrid model concept for system identification in a force excited structure. For the sake of clarity, the methodology presented is validated by using the lumped parameter model and is applied to a cantilever beam for

demonstration. The detailed mathematical concepts, the procedure to extract the input force vector, and the validation of this theory are presented in this chapter.

3.1 Theoretical Formulation for the Extraction of a Pseudo Excitation Force Vector

In this section, the theoretical formulation for the extraction of a pseudo excitation force[1] vector at the measured DOFs is presented. A linear mathematical equation developed in references [39, 40] for a moving base system can be used if the motion, e.g., acceleration, can be measured at all degrees of freedom (DOFs). Since such measurements can be made only in finite DOFs, there are some questions that need to be addressed in order to use the methodology [45, 46]. For example, what is the contribution of the motion at the unmeasured DOFs to the system equation? How are the specific DOFs selected for measurements? What is the effect of unidentified modes on the estimated pseudo excitation force vector? To address these questions, the same equations as those in references [45, 46] are first represented in a mixed (physical/modal) form, also known as the hybrid model of the system. A system with a moving base configuration can be represented as an equivalent system to the fixed base configuration if the displacement vector is represented as a vector relative to the base displacement [45, 46]. Thus, the equation of motion for a linear multi-degree-of-freedom (MDOF) system excited by the acceleration input at the base can be written as the equivalent fixed base configuration as:

$$[M]\{\ddot{u}\} + [K]\{u\} + [C]\{\dot{u}\} = -[M]\{l\}\ddot{y} \qquad (3.1)$$

Where, $[M]$, $[K]$, and $[C]$ are the mass, stiffness, and proportional damping matrices of the system in a fixed base configuration, $\ddot{y}$ is the input acceleration, $\{u\}$ is the displacement vector

---

[1] The reconstructed input force vector using the base motion as an input is referred to as pseudo excited force vector.

relative to the base, and $\{l\}$ is the transformation vector $(\{l\}_i = Cos(\theta)_i)$, where, $(\theta)_i$ is the angle between the ith DOF and the direction of base motion.

Transforming Equation (3.1) to the frequency domain we have,

$$[-w^2[M] + [K] + iw[C]]\{u\} = w^2[M]\{l\}y \qquad (3.2)$$

Where $i = \sqrt{-1}$. The right hand side of Equation (3.2) represents the equivalent excitation force vector, which is dependent on the distribution of mass in the system. The equivalent force vector remains constant throughout the analysis frequencies if a constant acceleration as a function of frequencies is applied to the base. The equivalent force vector will vary as a quadratic function of the excitation frequency if the constant displacement as a function of frequencies is applied to the base. The linear modal analysis of Equation (3.2) yields mode shapes, natural frequencies and modal mass of the structure. To find out the pseudo excitation force vector at the measured DOFs, Equation (3.2) is analyzed in the hybrid model form, where the relative response vectors are in the physical coordinates and the remaining parameters in the modal space. Denoting $w^2[M]\{l\}y$ by $\{F^d\}$, Equation (3.2) can be written as,

$$[-w^2[M] + [K] + iw[C]]\{u\} = \{F^d\} \qquad (3.3)$$

Multiplying both sides of Equation (3.3) by modal matrix $[\Phi]^T$ and introducing the term $[\Phi][\Phi]^{-1} = I$, Equation (3.3) becomes

$$[-w^2[\Phi]^T[M][\Phi][\Phi]^{-1} + [\Phi]^T[K][\Phi][\Phi]^{-1} + iw[\Phi]^T[C] [\Phi][\Phi]^{-1}]\{u\} = [\Phi]^T\{F^d\} \qquad (3.4)$$

For mass normalized mode shapes and proportional damping assumptions, the orthogonal properties of the linear modal matrix $[\Phi]$, can be written as,

$$[\Phi]^T[M][\Phi] = I \tag{3.5}$$

$$[\Phi]^T[K][\Phi] = [w_r{}^2]_{diag} \tag{3.6}$$

$$[\Phi]^T[C][\Phi] = [2\zeta_r w_r]_{diag} \tag{3.7}$$

Let, $[[w_r{}^2]_{diag} + iw[2\zeta_r w_r]_{diag} - w^2 I] = \lceil \lambda - w_r{}^2 \rfloor$ where, the brackets $"\lceil\ \rfloor"$ denotes a diagonal matrix. Using this property, Equation (3.4) can be written in a more concise form as,

$$\lceil \lambda - w_r{}^2 \rfloor [\Phi]^{-1}\{u\} = [\Phi]^T\{F^d\} \tag{3.8}$$

$$\{u\} = [\Phi]\lceil \lambda - w_r{}^2 \rfloor^{-1}[\Phi]^T\{F^d\} \tag{3.9}$$

Equation (3.9) is the extended form of Equation (3.1) and it represents the modal model of the linear system with the relative displacement vector in the physical coordinates system. Equation (3.9) is named as the hybrid model of the system due to the fact that the response vectors are in the physical coordinates while the remaining parameters are kept in the modal space. Equation (3.9) represents the dynamics of the system when the full model of the system is known. A full model refers to the response at all DOFs and all the modes are available. For making use of Equation (3.9) in practical cases, there are two major difficulties: (i) measurements of motion, e.g., accelerations, at all DOFs are impossible and (ii) the modal model derived via the experimental route is incomplete. So for the extraction of the pseudo excited force vector, Equation (3.9) is partitioned at the measured and unmeasured DOFs. Let the subscript M represent the measured DOFs and the subscript U represent the unmeasured DOFs. Similarly, M_r represents the identified modes and U_r represents the unidentified modes then, partitioning Equation (3.9) at measured and unmeasured DOFs, we have,

$$\begin{Bmatrix} u_M \\ u_U \end{Bmatrix} = \begin{bmatrix} \Phi_{MM_r} & \Phi_{MU_r} \\ \Phi_{UM_r} & \Phi_{UU_r} \end{bmatrix} \begin{bmatrix} [\lambda - w_r{}^2]_{M_r} & 0 \\ 0 & [\lambda - w_r{}^2]_{U_r} \end{bmatrix}^{-1} \begin{Bmatrix} F^d{}_M \\ F^d{}_U \end{Bmatrix} \tag{3.10}$$

$$\{u_M\} = [\Phi_{MM_r}][\lambda - w_r{}^2]_{M_r}{}^{-1}[\Phi_{M_rM}]\{F^d{}_M\} + [\Phi_{MU_r}][\lambda - w_r{}^2]_{U_r}{}^{-1}[\Phi_{U_rM}]\{F^d{}_M\} +$$

$$[\Phi_{MM_r}][\lambda - w_r{}^2]_{M_r}{}^{-1}[\Phi_{M_rU}] + \{F^d{}_U\} + [\Phi_{MU_r} + [\lambda - w_r{}^2]_{U_r}{}^{-1}[\Phi_{U_rU}]\{F^d{}_U\} \tag{3.11}$$

Let,

$$\alpha_{MM} = [\Phi_{MM_r}][\lambda - w_r{}^2]_{M_r}{}^{-1}[\Phi_{M_rM}] \tag{3.12}$$

$$\alpha_{MU} = [\Phi_{MU_r}][\lambda - w_r{}^2]_{U_r}{}^{-1}[\Phi_{U_rM}] \tag{3.13}$$

$$\alpha_{UM} = [\Phi_{MM_r}][\lambda - w_r{}^2]_{M_r}{}^{-1}[\Phi_{M_rU}] \tag{3.14}$$

$$\alpha_{UU} = [\Phi_{MU_r}][\lambda - w_r{}^2]_{U_r}{}^{-1}[\Phi_{U_rU}] \tag{3.15}$$

The relative displacement vector at the measured DOFs can be written as,

$$\{u_M\} = [\alpha_{MM}]\{F^d{}_M\} + [\alpha_{MU}]\{F^d{}_M\} + [\alpha_{UM}]\{F^d{}_U\} + [\alpha_{UU}]\{F^d{}_U\} \tag{3.16}$$

Equation (3.15) represents the response of the relative displacement vector at the measured DOFs. Multiplying both sides by $[\alpha_{MM}{}^{-1}]$ to Equation (3.15), we have,

$$[\alpha_{MM}{}^{-1}]\{u_M\} = \{F^d{}_M\} + [\alpha_{MM}{}^{-1}][\alpha_{MU}]\{F^d{}_M\} + [\alpha_{MM}{}^{-1}][\alpha_{UM}]\{F^d{}_U\} +$$

$$[\alpha_{MM}{}^{-1}][\alpha_{UU}]\{F^d{}_U\} \tag{3.16}$$

$[\alpha_{MM}{}^{-1}]\{u_M\}$ is the pseudo excited projected force at the measured DOFs. This can be extracted solely from the measured data. Denoting it by $\{P^d\}$, the final equation can be written as,

$$\{P^d\} = \{F^d{}_M\} + [\alpha_{MM}{}^{-1}][\alpha_{MU}]\{F^d{}_M\} + [\alpha_{MM}{}^{-1}][\alpha_{UM}]\{F^d{}_U\} + [\alpha_{MM}{}^{-1}][\alpha_{UU}]\{F^d{}_U\} \quad (3.17)$$

Equation (3.17) represents the closed-form expression for the pseudo excited force vector projected at the measured DOFs. The last three terms shown in Equation (3.17) are the linear residuals. These three terms of the Equation (3.17) project the force from unmeasured DOFs to the measured DOFs. The pseudo excited force vector $\{P^d\}$ is obtained solely from the dynamics of the system as shown by Equation (3.16). Analyzing each term of the Equation (3.17), one can make a conclusion that the reconstructed input force vector is equal to the equivalent excitation force vector for a lumped parameter model. An example of this type of system includes: Multi-storey building where each storey represent the floor lumped mass and that the springs and dampers represent the collective structural stiffness and damping between adjacent floors. The reconstructed force vector is not equal to the equivalent excitation force vector for a continuous system as the last three terms of the Equation (3.17) project the force from the unmeasured DOFs to the measured DOFs. Examples of a continuous system include beams, plates, and, shells.

3.2 Illustration of Force Reconstruction Technique

Clearly what is of interest is to show that the reverse explicit formulation theory for input force reconstruction presented in Section 3.1 is true. Here, a five degree of freedom (DOF) lumped parameter system subjected to a base excitation is used for the validation of the above mentioned theory.

The system chosen is shown in Figure 3.1. The system comprises of five masses each connected with a spring and a damper. The two end supports are subjected to base displacement of x_g. The parameters used for this simulation are $m = 1$ kg, $c = 4.8$ Ns/m, $k = 4 \times 10^3$ N/m and $x_g = 2\sin(w.t)$. Where w is the excitation frequency. If the displacement of the mass 1, mass 2,

24

mass 3, mass 4 and mass 5 are represented by x_1, x_2, x_3, x_4 and x_5, the equation of motion in the direction of base motion can be derived by using the Newton's second law of motion.
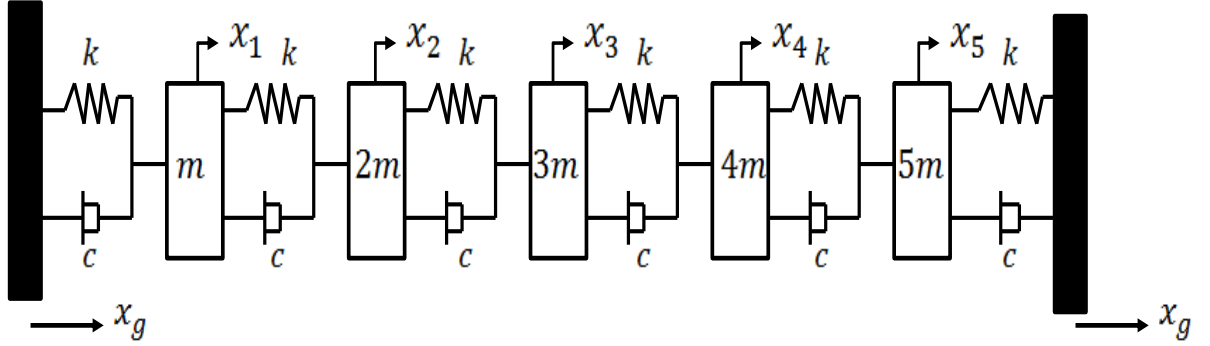
Figure 3.1: Five DOF Lumped Parameter System

In accordance with Newton's second law, the equations of motion can be expressed as:

$$-5m\ddot{x}_5 - c(\dot{x}_5 - \dot{x}_g) - c(\dot{x}_5 - \dot{x}_4) - k(x_5 - x_g) - k(x_5 - x_4) = 0 \tag{3.18}$$

$$-4m\ddot{x}_4 - c(\dot{x}_4 - \dot{x}_5) - c(\dot{x}_4 - \dot{x}_3) - k(x_4 - x_5) - k(x_4 - x_3) = 0 \tag{3.19}$$

$$-3m\ddot{x}_3 - c(\dot{x}_3 - \dot{x}_4) - c(\dot{x}_3 - \dot{x}_2) - k(x_3 - x_4) - k(x_3 - x_2) = 0 \tag{3.20}$$

$$-2m\ddot{x}_2 - c(\dot{x}_2 - \dot{x}_3) - c(\dot{x}_2 - \dot{x}_1) - k(x_2 - x_3) - k(x_2 - x_1) = 0 \tag{3.21}$$

$$-m\ddot{x}_1 - c(\dot{x}_1 - \dot{x}_2) - c(\dot{x}_1 - \dot{x}_g) - k(x_1 - x_2) - k(x_1 - x_g) = 0 \tag{3.22}$$

Alternately, these state Equations (3.18-3.22) can be written in terms of mass drifts[2] u_1, u_2, u_3, u_4 and u_5 :

$$-5m\ddot{u}_5 - c\dot{u}_5 - c(\dot{u}_5 - \dot{u}_4) - ku_5 - k(u_5 - u_4) = m_5\ddot{x}_g \tag{3.23}$$

$$-4m\ddot{u}_4 - c(\dot{u}_4 - \dot{u}_5) - c(\dot{u}_4 - \dot{u}_3) - k(u_4 - u_5) - k(u_4 - u_3) = m_4\ddot{x}_g \tag{3.24}$$

---

[2] Relative displacement of the masses with respect to the moving base.

$$-3m\ddot{u}_3 - c(\dot{u}_3 - \dot{u}_4) - c(\dot{u}_3 - \dot{u}_2) - k(u_3 - u_4) - k(u_3 - u_2) = m_3\ddot{x}_g \tag{3.25}$$

$$-2m\ddot{u}_2 - c(\dot{u}_2 - \dot{u}_3) - c(\dot{u}_2 - \dot{u}_1) - k(u_2 - u_3) - k(u_2 - u_1) = m_2\ddot{x}_g \tag{3.26}$$

$$-m\ddot{u}_1 - c(\dot{u}_1 - \dot{u}_2) - c\dot{u}_1 - k(u_1 - u_2) - ku_1 = m_1\ddot{x}_g \tag{3.27}$$

Where:

$$u_1 = x_1 - x_g,\ u_2 = x_2 - x_g,\ u_3 = x_3 - x_g,\ u_4 = x_4 - x_g \text{ and } u_5 = x_5 - x_g \tag{3.28}$$

Rewriting the Equations (3.23-3.27) in a matrix form,

$$
\begin{bmatrix}
m & 0 & 0 & 0 & 0 \\
0 & 2m & 0 & 0 & 0 \\
0 & 0 & 3m & 0 & 0 \\
0 & 0 & 0 & 4m & 0 \\
0 & 0 & 0 & 0 & 5m
\end{bmatrix}
\begin{Bmatrix}
\ddot{u}_1 \\ \ddot{u}_2 \\ \ddot{u}_3 \\ \ddot{u}_4 \\ \ddot{u}_5
\end{Bmatrix}
+
\begin{bmatrix}
2c & -c & 0 & 0 & 0 \\
-c & 2c & -c & 0 & 0 \\
0 & -c & 2c & -c & 0 \\
0 & 0 & -c & 2c & -c \\
0 & 0 & 0 & -c & 2c
\end{bmatrix}
\begin{Bmatrix}
\dot{u}_1 \\ \dot{u}_2 \\ \dot{u}_3 \\ \dot{u}_4 \\ \dot{u}_5
\end{Bmatrix}
$$

$$
+
\begin{bmatrix}
2k & -k & 0 & 0 & 0 \\
-k & 2k & -k & 0 & 0 \\
0 & -k & 2k & -k & 0 \\
0 & 0 & -k & 2k & -k \\
0 & 0 & 0 & -k & 2k
\end{bmatrix}
\begin{Bmatrix}
u_1 \\ u_2 \\ u_3 \\ u_4 \\ u_5
\end{Bmatrix}
= -
\begin{bmatrix}
m & 0 & 0 & 0 & 0 \\
0 & 2m & 0 & 0 & 0 \\
0 & 0 & 3m & 0 & 0 \\
0 & 0 & 0 & 4m & 0 \\
0 & 0 & 0 & 0 & 5m
\end{bmatrix}
\begin{Bmatrix}
1 \\ 1 \\ 1 \\ 1 \\ 1
\end{Bmatrix}
\ddot{x}_g \tag{3.29}
$$

Equation (3.29) can be written as,

$$[M]\{\ddot{u}\} + [K]\{u\} + [C]\{\dot{u}\} = -[M]\{l\}\ddot{x}_g \tag{3.30}$$

Where:

$$
[M] =
\begin{bmatrix}
m & 0 & 0 & 0 & 0 \\
0 & 2m & 0 & 0 & 0 \\
0 & 0 & 3m & 0 & 0 \\
0 & 0 & 0 & 4m & 0 \\
0 & 0 & 0 & 0 & 5m
\end{bmatrix},
[C] =
\begin{bmatrix}
2c & -c & 0 & 0 & 0 \\
-c & 2c & -c & 0 & 0 \\
0 & -c & 2c & -c & 0 \\
0 & 0 & -c & 2c & -c \\
0 & 0 & 0 & -c & 2c
\end{bmatrix}
$$

$$[K] = \begin{bmatrix} 2k & -k & 0 & 0 & 0 \\ -k & 2k & -k & 0 & 0 \\ 0 & -k & 2k & -k & 0 \\ 0 & 0 & -k & 2k & -k \\ 0 & 0 & 0 & -k & 2k \end{bmatrix}, \quad \{u\} = \begin{Bmatrix} u_1 \\ u_2 \\ u_3 \\ u_4 \\ u_5 \end{Bmatrix} \text{ and } \{l\} = \begin{Bmatrix} 1 \\ 1 \\ 1 \\ 1 \\ 1 \end{Bmatrix} \tag{3.31}$$

The resulting natural frequencies and mode shapes of the undamped system are obtained by solving the undamped free vibration Equation (3.30), given by Equation (3.32). The natural frequencies and mode shapes are tabulated in Table 3.1.

$$[M]\{\ddot{u}\} + [K]\{u\} = 0 \tag{3.32}$$

Using Equation (3.16) requires the linear response, modal damping ratio and modal stiffness. The experimental measurements of the signal involve measuring the acceleration response and integration of the acceleration response to velocity and displacement. In order to eliminate any phase distortion in numerically integrated displacement and velocity signal a single- frequency harmonic excitation is used. The response of the structure will be harmonic too and generally contains higher harmonics in the response. Considering that the excitation frequency is w radian/sec, the steady state measured acceleration signal may be represented using,

Table 3. 1: Frequencies and Mode Shapes of 5 DOF Simulated System

Modal frequencies (Hz)	Mode shapes				
	1	2	3	4	5
2.9429	-0.1258	-0.2076	-0.2447	-0.3511	-0.8706
5.8464	-0.2409	-0.3452	-0.3262	-0.3198	0.3378
8.2187	-0.3147	-0.2499	0.0272	0.4081	-0.0672
10.5050	-0.3079	0.0983	0.3262	-0.1975	0.0090
15.5550	-0.1958	0.3139	-0.2447	0.0573	-0.0009

$$\ddot{u}(t) = \sum_{i=1}^{n}(A_n \sin(nwt) + B_n \cos(nwt)) \tag{3.33}$$

Writing Equation (3.33) in each time instant and using a least-square procedure the coefficients A_n and B_n can be identified. Once the coefficients of Equation (3.33) are known, the velocity and displacements are obtained by analytical integration,

$$\dot{u}(t) = \sum_{i=1}^{n}\frac{1}{nw}(-A_n \cos(nwt) + B_n \sin(nwt)) + C_1 \tag{3.34}$$

$$u(t) = \sum_{i=1}^{n}\frac{1}{(nw)^2}(-A_n \sin(nwt) - B_n \cos(nwt)) + C_1 t + C_2 \tag{3.35}$$

The mean values of the velocity and the displacement signals have to be zero, which means that $C_1 = 0$ and $C_2 = 0$.

3.3 Solution Methodology

The excitation frequency is varied in a frequency band around the first natural frequency of a 5 DOF system and the time domain acceleration, velocity and displacement response are determined using a Runge-Kutta procedure. By employing Equation (3.33) the governing equation of the steady state acceleration is estimated and the coefficients A_n and B_n are calculated. By knowing these coefficients and using Equations (3.34 and 3.35), the velocity and displacement of the steady state response are calculated. The result of the true and least square fitted acceleration signal is shown in Figure 3.2. In Figure 3.2, the true acceleration signal is the signal obtained from Runge-Kutta integration while the least square fitted signal is the estimated signal obtained by using Equation (3.33) in the true signal. Similarly in Figure 3.3, the true velocity is the velocity obtained from Runge-Kutta integration while the analytically integrated velocity signal is the signal obtained by using Equation (3.34). The same procedure follows for Figure 3.4. Having displacement, velocity, acceleration response and mode shapes matrix, it is

possible to reconstruct the input excitation force vector using Equation (3.16). The reconstructed force vector is than compared with the equivalent excitation force vector so as to validate the theory. Figures (3.2-3.6) show the plot of the reconstructed and equivalent excitation force vector at each excitation frequency projected at each DOF. The reconstructed force vector and the equivalent excitation force vector are very close to each other and are varying as a quadratic function of the excitation frequencies. The results (Figures 3.5-3.9) show that the theory presented is true and pleased for lumped parameter system. The demonstration of this theory for a continuous system is presented in Chapter 5 by taking the cantilever beam as an example.
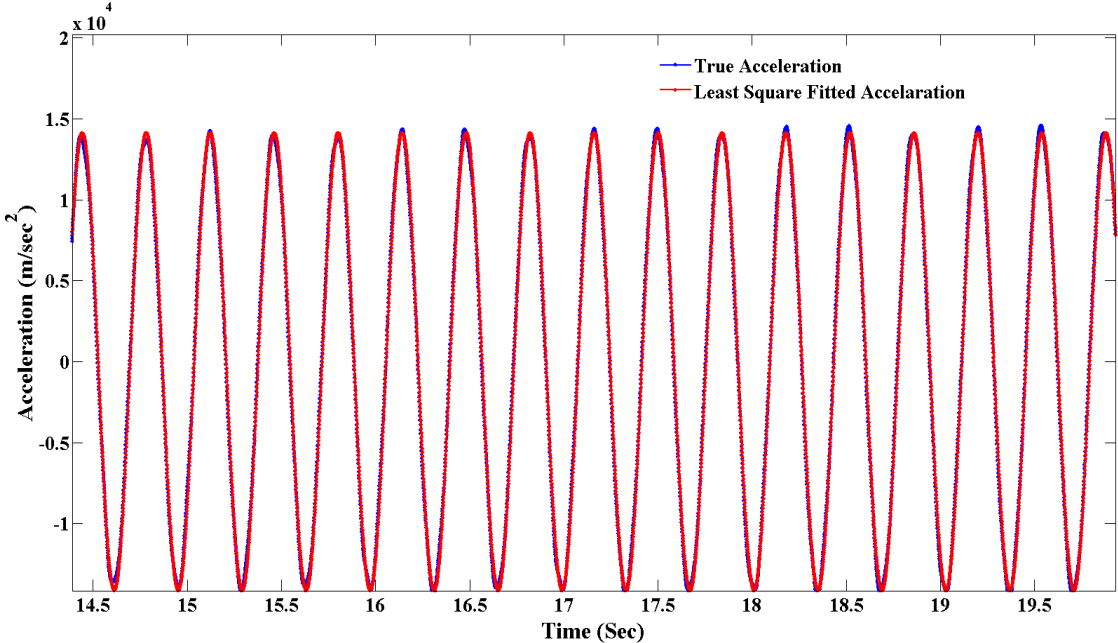
Figure 3.2: True and Least Square Fitted Acceleration Signal (Excitation Frequency 2.9429Hz)
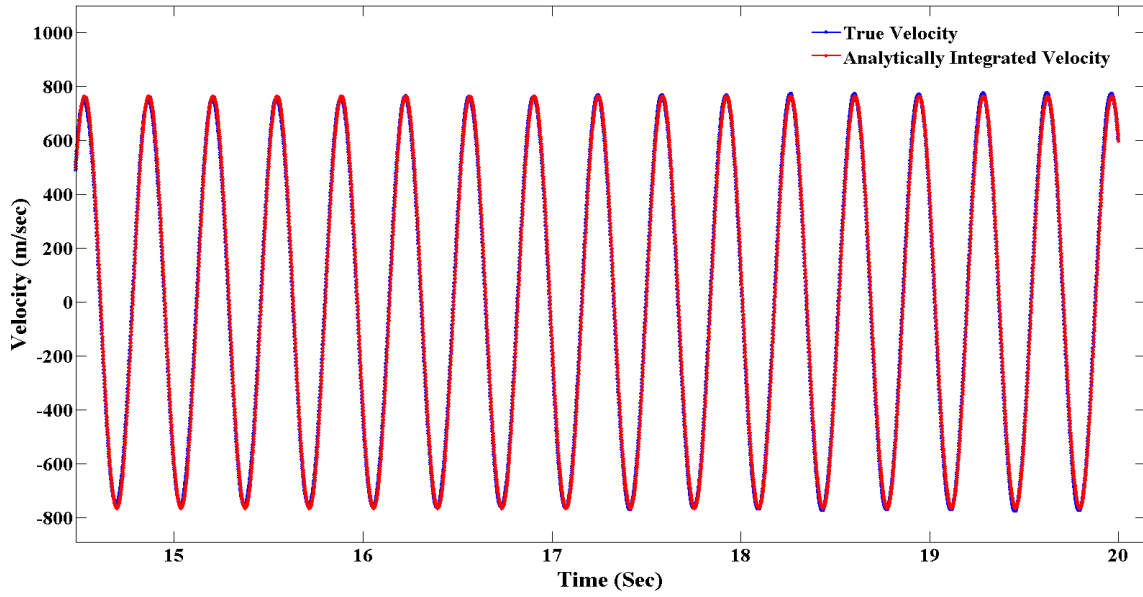
Figure 3.3: True and Analytically Integrated Velocity Signal (Excitation Frequency 2.9429Hz)
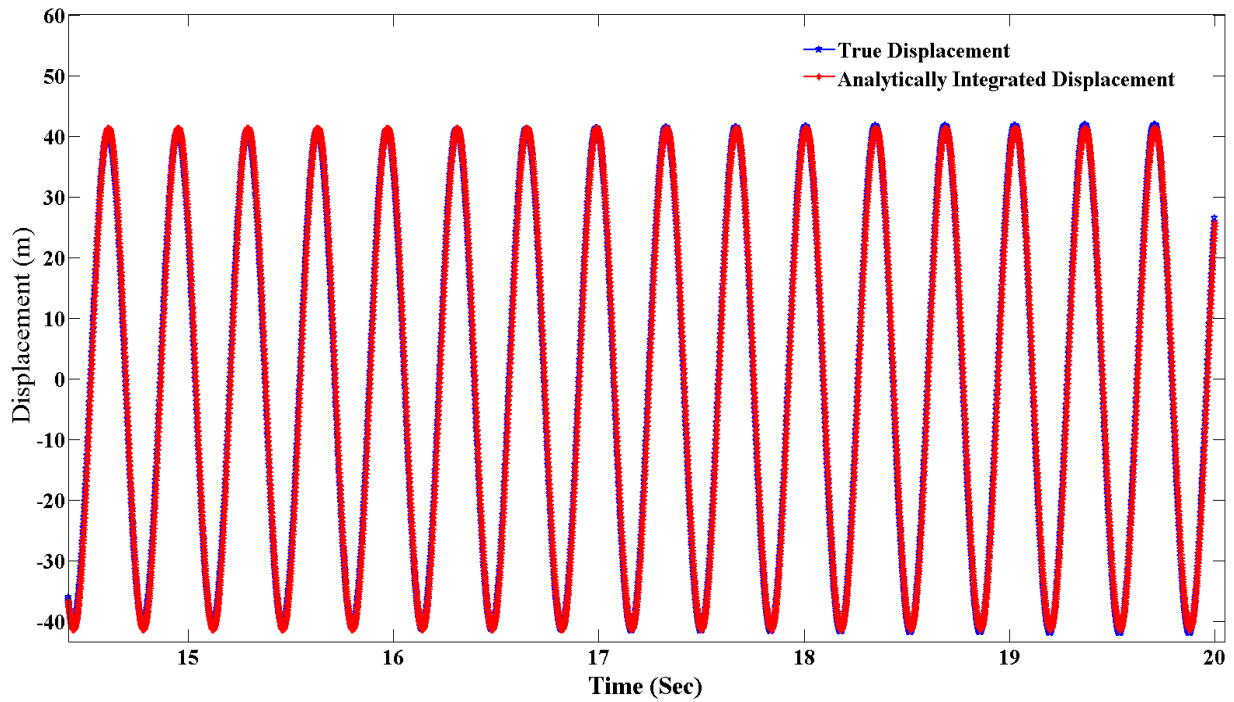
Figure 3.4: True and Analytically Integrated Displacement Signal (Excitation Frequency 2.9429Hz)
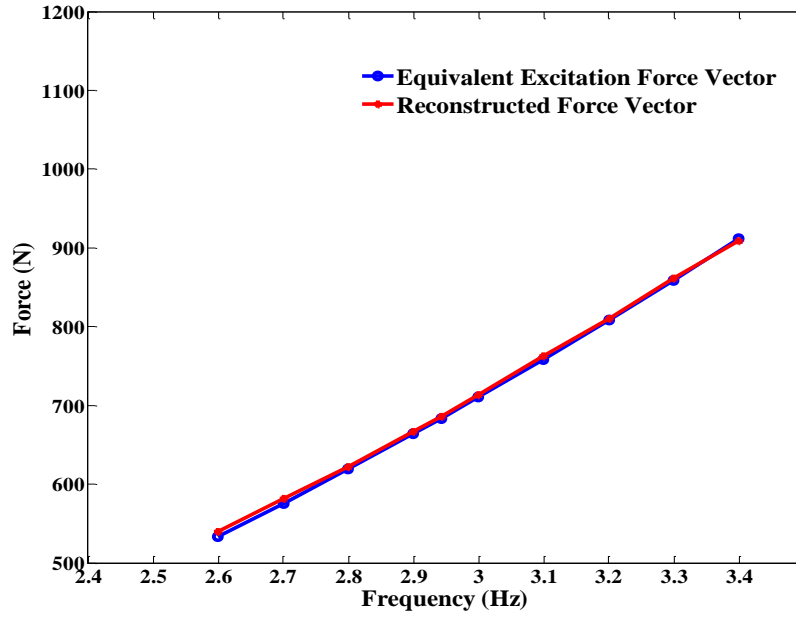
Figure 3.5: Comparison of Reconstructed Force Vector and Equivalent Excitation Force Vector Acting at Mass 1
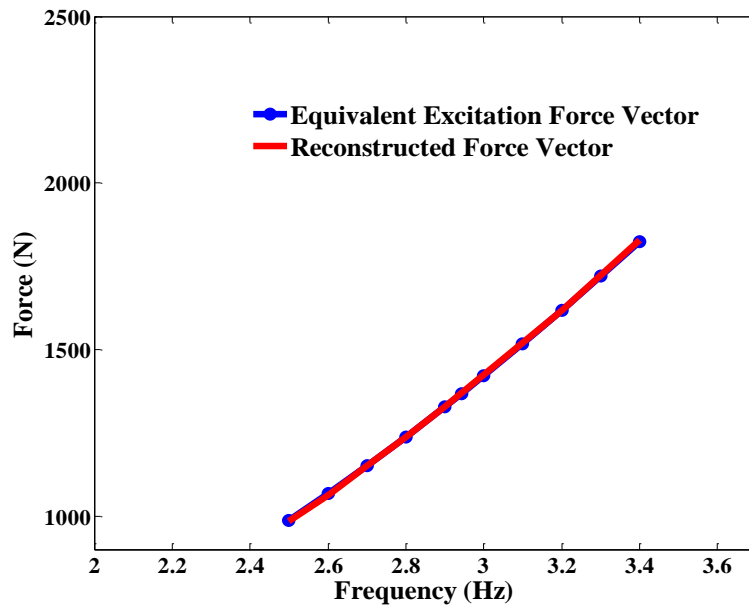
Figure 3.6: Comparison of Reconstructed Force Vector and Equivalent Excitation Force Vector Acting at Mass 2
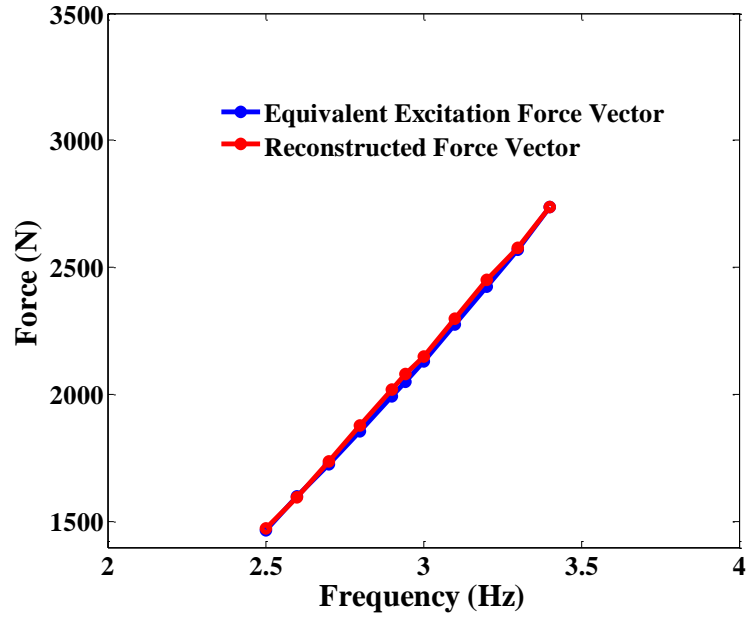
Figure 3.7: Comparison of Reconstructed Force Vector and Equivalent Excitation Force Vector Acting at Mass 3
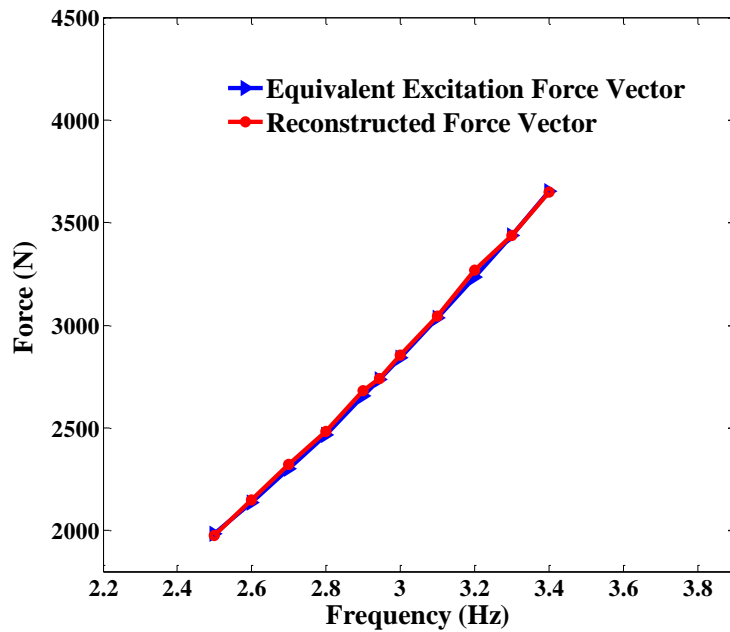
Figure 3.8: Comparison of Reconstructed Force Vector and Equivalent Excitation Force Vector Acting at Mass 4
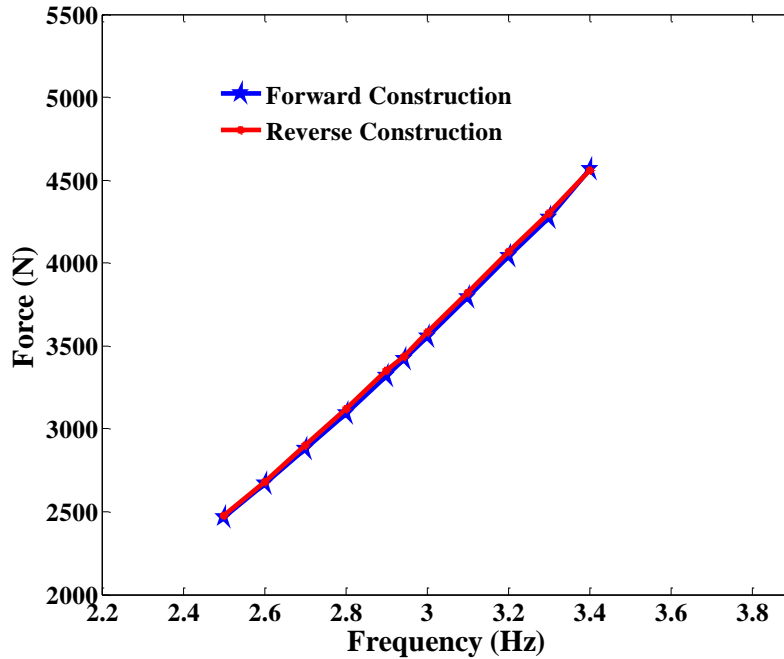
Figure 3.9: Comparison of Reconstructed Force Vector and Equivalent Excitation Force Vector Acting at Mass 5

3.4   Summary

A methodology for the force reconstruction technique for a base excited structure is presented in this section. A closed form solution is derived by partitioning the system equation at the measured and the unmeasured DOFs. The proposed methodology is illustrated by using a 5 DOF lumped parameter model with a constant displacement input at the base. Simulation results show that the proposed methodology is accurate for a lumped parameter model. The experimental demonstration of this methodology for a continuous system is presented in Chapter 5 of this thesis.

Chapter 4

Nonlinear System Identification in Base Excited Structure

The conventional nonlinear system identification techniques described in the existing literatures require force and response information at all excitation DOFs for their successful implementation. For cases where the excitation comes from the base motion/support motion, these requirements can be met only if the motions at all DOFs are measured and the mass distribution of the structure is known a-priori. Thus, in practical cases it is not possible to use the available nonlinear system identification methods directly.

This chapter presents two new methods for nonlinear system identification of a base excited structure with the controlled displacement/acceleration input. Both methods are based on the theory of force reconstruction, base excitation and the nonlinear system identification. Combining these three theories, the new theory/new approach is developed which is the original contribution of this chapter. The first method bridges the gap of nonlinear system identification between the force excited systems and the base excited systems which addresses objective (a) and identifies the nonlinear parameters in the physical coordinates system. The second method addresses the objective (b) and identifies the nonlinear parameters in the modal space. The modal space is used to find out the maximum normal and cross-couplings nonlinear terms. Both methods are entirely based on measured data from the experiment with no need for a finite element model. The detailed mathematical concept, the procedure to extract the nonlinear parameters and the advantages and limitations of both methods are presented in this chapter.

4.1 Theoretical Formulation of Nonlinear System Identification in the Physical Coordinates System

The proposed method works in three stages to estimate the nonlinear parameters of a system. The three stages are: (1) Reconstruction of the input force vector at the measured DOFs, (2) Recovery of the nonlinear restoring force vector using the reconstructed force vector in a nonlinear system and (3) extraction of nonlinear parameters. In chapter 3 of this thesis the closed form solution for the reconstructed force vector is presented so in this chapter the theory for nonlinear restoring force vector extraction, nonlinear parameter extraction and the new theory /approach which combines these three theories is presented.

4.1.1 Theoretical Formulation for the Nonlinear Restoring Force Vector at the Measured DOFs

This section illustrates the theoretical formulation for the nonlinear restoring force extraction from the measured data at the measured DOFs. The hybrid model for the nonlinear system is shown such that the linear response of the system is in the modal domain while the nonlinearities are expressed in the physical coordinates system. In this model the nonlinear residual are approximated as the linear residual. This can be achieved in practical scenario by setting the analysis frequency to be high [35]. The model assumes that when the magnitude of excitation to the base is sufficiently high, the response from the structure attached to the base is no longer linear [19, 35, 37, 39 and 41].

The general Equation of motion for a MDOFs nonlinear system, subjected to base excitation can be written as,

$$[M]\{\ddot{\tilde{u}}\} + [C]\{\dot{\tilde{u}}\} + [K]\{\tilde{u}\} + \{G(\tilde{u}, \dot{\tilde{u}}\} = -[M]\{l\}\ddot{y} \tag{4.1}$$

Where, $\{\tilde{u}\}$ is the nonlinear displacement vector relative to the base,$\{G\}$ is the nonlinear restoring force vector.

Transforming Equation (4.1) to the frequency domain we have,

$$[-w^2[M] + [K] + iw[C]]\{\tilde{u}\} + \{G(\tilde{u},w)\} = w^2[M]\{l\}y \qquad (4.2)$$

Where, $w^2[M]\{l\}y$ is the Equivalent excitation force vector which is denoted by $\{F^d\}$ in Chapter 3. Using the same notation Equation (4.2) becomes,

$$[-w^2[M] + [K] + iw[C]]\{\tilde{u}\} + \{G\} = \{F^d\} \qquad (4.3)$$

Multiplying both sides of Equation (4.3) by modal matrix $[\Phi]^T$ and introducing the term $[\Phi][\Phi]^{-1} = I$, Equation (4.3) becomes,

$$[-w^2[\Phi]^T[M][\Phi][\Phi]^{-1} + [\Phi]^T[K][\Phi][\Phi]^{-1} + iw[\Phi]^T[C][\Phi][\Phi]^{-1}]\{\tilde{u}\} + [\Phi]^T\{G\} =$$
$$[\Phi]^T\{F^d\} \qquad (4.4)$$

For mass normalized mode shapes and proportional damping assumptions, the orthogonal properties of the linear modal matrix $[\Phi]$, can be written as,

$$[\Phi]^T[M][\Phi] = I \qquad (4.5)$$

$$[\Phi]^T[K][\Phi] = [w_r{}^2]_{diag} \qquad (4.6)$$

$$[\Phi]^T[C][\Phi] = [2\zeta_r w_r]_{diag} \qquad (4.7)$$

Let, $[[w_r{}^2]_{diag} + iw[2\zeta_r w_r]_{diag} - w^2 I] = \lceil \lambda - w_r{}^2 \rfloor$ where, the brackets "$\lceil \ \rfloor$" denotes a diagonal matrix. Using this property, Equation (4.4) can be written in a more concise form as,

$$\lceil \lambda - w_r{}^2 \rfloor [\Phi]^{-1}\{\tilde{u}\} + [\Phi]^T\{G\} = [\Phi]^T\{F^d\} \qquad (4.8)$$

$$\{\tilde{u}\} = [\Phi][\lambda - w_r{}^2]^{-1}[\Phi]^T(\{F^d\} - \{G\}) \tag{4.9}$$

Equation (4.9) represents the hybrid model for nonlinear MDOFs systems undergoing base excitation, where the nonlinear response vector is kept in the physical domain while the remaining parameters in the modal space. Using Equation (4.9) directly in practical cases has two major difficulties: (i) the measurement of nonlinear response vector at all DOFs is impossible and (ii) the modal model derived via an experimental route is incomplete. In order to mimic the condition of incomplete measurements, Equation (4.9) is partitioned at the measured and the unmeasured DOFs. Partitioning Equation (4.9) at the measured and the unmeasured DOFs Equation (4.9) can be written as,

$$\begin{Bmatrix} \tilde{u}_M \\ \tilde{u}_U \end{Bmatrix} = \begin{bmatrix} \Phi_{MM_r} & \Phi_{MU_r} \\ \Phi_{UM_r} & \Phi_{UU_r} \end{bmatrix} \begin{bmatrix} [\lambda - w_r{}^2]_{M_r} & 0 \\ 0 & [\lambda - w_r{}^2]_{U_r} \end{bmatrix}^{-1} \begin{bmatrix} \Phi_{M_rM} & \Phi_{M_rU} \\ \Phi_{U_rM} & \Phi_{U_rU} \end{bmatrix} \left[\begin{Bmatrix} F^d{}_M \\ F^d{}_U \end{Bmatrix} - \begin{Bmatrix} G_M \\ G_U \end{Bmatrix} \right] \tag{4.10}$$

Let,

$$\alpha_{MM} = [\Phi_{MM_r}] [\lambda - w_r{}^2]_{M_r}{}^{-1} [\Phi_{M_rM}] \tag{4.11}$$

$$\alpha_{MU} = [\Phi_{MU_r}] [\lambda - w_r{}^2]_{U_r}{}^{-1} [\Phi_{U_rM}] \tag{4.12}$$

$$\alpha_{UM} = [\Phi_{MM_r}] [\lambda - w_r{}^2]_{M_r}{}^{-1} [\Phi_{M_rU}] \tag{4.13}$$

$$\alpha_{UU} = [\Phi_{MU_r}] [\lambda - w_r{}^2]_{U_r}{}^{-1} [\Phi_{U_rU}] \tag{4.14}$$

The nonlinear response at the measured DOFs can be written as,

$$\{\tilde{u}_M\} = [\alpha_{MM}](\{F^d{}_M\} - \{G\}_M) + [\alpha_{MU}] (\{F^d{}_M\} - \{G\}_M) + [\alpha_{UM}](\{F^d{}_U\} - \{G\}_U) +$$

$$[\alpha_{UU}](\{F^d{}_U\} - \{G\}_U) \tag{4.15}$$

The term $[\alpha_{MU}](\{F^d{}_M\} - \{G\}_M)$ is the nonlinear residual. This is the contribution of the unidentified modes to the response at the measured DOFs. It should be noted that the nonlinear residual can be approximated as a linear residual, if the analysis frequency is set to be high [35]. If the nonlinearities are confined to the measured zone, by using the nonlinearity detection methodologies $\{G\}_U$ can be set to zero. Replacing nonlinear residual by the linear residual and multiplying both sides of the Equation (19) by $[\alpha_{MM}{}^{-1}]$, we get,

$$[\alpha_{MM}{}^{-1}] \{\tilde{u}_M\} = \{F^d{}_M\} - \{G\}_M + [\alpha_{MM}{}^{-1}][\alpha_{MU}]\{F^d{}_M\} + [\alpha_{MM}{}^{-1}][\alpha_{UM}]\{F^d{}_U\} +$$

$$+[\alpha_{MM}{}^{-1}][\alpha_{UU}]\{F^d{}_U\} \tag{4.16}$$

$\{F^d{}_M\} + [\alpha_{MM}{}^{-1}][\alpha_{MU}]\{F^d{}_M\} + [\alpha_{MM}{}^{-1}][\alpha_{UM}]\{F^d{}_U\} + [\alpha_{MM}{}^{-1}][\alpha_{UU}]\{F^d{}_U\}$ is the pseudo excited force vector (Reconstructed Force Vector) projected to the measured DOFs, which is equivalent to $\{P^d\}$. Therefore,

$$\{G\}_M = \{P^d\} - [\alpha_{MM}]^{-1} \{\widetilde{u_M}\} \tag{4.17}$$

Equation (4.17) gives the nonlinear restoring force vector at the measured DOFs. Once such a force vector is obtained, the nonlinear parameters can be extracted by the conventional technique, which is shown in the Appendix A. The system identification strategy in a physical coordinate system for a base excited structure that addresses the objective (i) is illustrated in Figure 4.1.
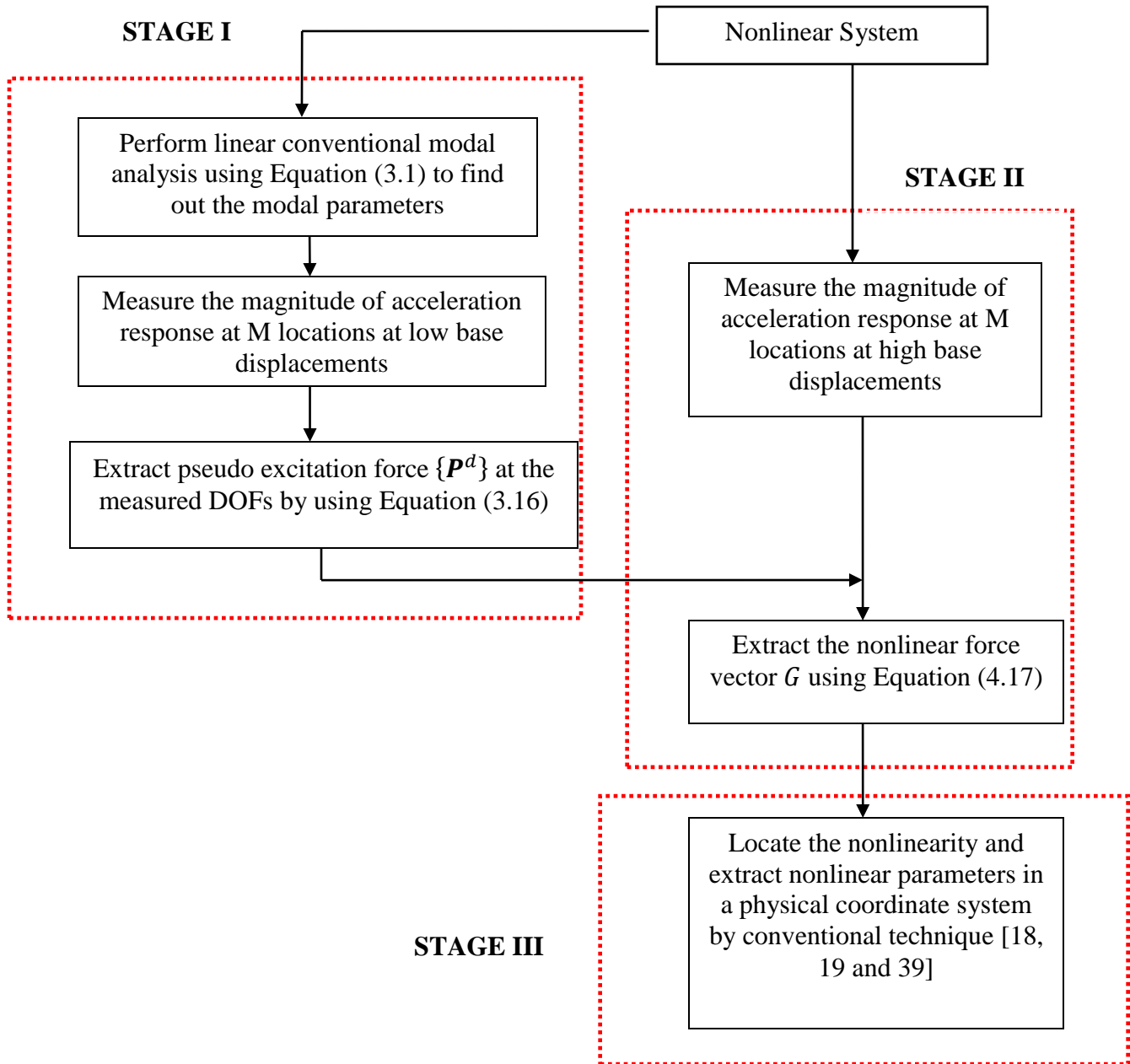
Figure 4.1: Flow Chart for Nonlinear System Identification in a Physical Coordinate System

4.1.2 Implementation of Nonlinear System Identification in the Physical Coordinates System

The proposed method, shown in Figure 4.1, involves three stages. In the first stage, the pseudo excited force vector at the measured DOFs is extracted using Equation (3.16). Prior to it, the

modal parameters of the underlying linear structure such as modal damping ratios and the modal matrix are obtained by performing conventional modal analysis using Equation (3.1). In the second stage the nonlinear restoring force vector at the measured DOFs is extracted using Equation (4.17). To use Equation (4.17), the nonlinear acceleration vector is measured by subjecting the structure to high displacement/acceleration input at the base. In the third stage of this method, the nonlinear parameters are extracted according to references [18, 19 and 39]. The nonlinear parameter extraction technique is detailed in the Appendix A.

4.2   Theoretical Formulation for Nonlinear System Identification in a Modal Space

The traditional nonlinear parameter identification technique proposed in references [18, 19 and 39] is based on the first order describing functions method. This method is well suited for frequency domain data. However, it is highly inaccurate for the time domain representation as discussed in literature [34]. It may require the location as well as the functional form of the nonlinearity to extract the nonlinear parameters. Though the above mentioned method [18, 19, 39] extracts the nonlinear parameters at the physical coordinates of the system, it does not give any information about the model and the nonlinear coupling effect.

A new method is proposed here to extract the nonlinear parameters along with the nonlinear model in a modal space. It has the advantages over other methods in that it shows the normal and cross coupling nonlinearity between the modes, extracts the maximum nonlinearity of the system and does not required the location and the functional form of the nonlinearity. The proposed method involves the extraction of the pseudo excited force vector at the undamped natural frequency of the system, the calculation of the nonlinear modal restoring force in the modal space and the extraction of the nonlinear parameters (normal and cross-coupling) nonlinearities in a modal space by using the restoring force state mapping principle.

Although the mathematical formulation for the pseudo force extraction and the nonlinear restoring force extraction remain identical as Equations (3.16) and (4.17), the transformation of the nonlinear restoring force in a modal space is different. Moreover, the measured nonlinear response data are at the physical coordinates and need to be transformed to the modal space. The formulation presented in this section shows the methodology to transform the nonlinear response data and nonlinear restoring force in a nonlinear modal space. The theoretical formulation of the nonlinear system identification in a modal space includes: (a) decoupling a nonlinear modal equation and performing the mode by mode analysis; (b) analyzing the effect of nonlinear mode shapes matrix on the response of the system; (c) investigating perfect and imperfect excitations in modal analysis; (d) evaluating nonlinear parameter extraction in the case of imperfect excitation for the closely spaced modes and the use of suitable basis function for the extraction of nonlinear parameters through curve fittings; and, (e) examining the type of established algorithms used for curve fitting in modal space.

4.2.1 Theoretical Formulation for the Extraction of Nonlinear Response Data and the Nonlinear Restoring Force in a Modal Space

The nonlinear response of a MDOF system with base excitations can be represented as,

$$[M]\{\ddot{\tilde{u}}\} + [K]\{\tilde{u}\} + [C]\{\dot{\tilde{u}}\} + \{\tilde{G}(u,\dot{u})\} = \{F^d\} \tag{4.18}$$

Where $\tilde{u}$ is the relative nonlinear response vector at the measured DOFs. With the single harmonic assumptions (the output signal is at same harmonic to input) one can write the Equation (4.18) in the frequency domain as,

$$[-w^2[M] + [K] + iw[C]]\{\tilde{u}\} + \{\tilde{G}(w,\tilde{u})\} = \{F^d\} \tag{4.19}$$

Expressing the response vector in the modal space we can write,

$$\{\tilde{u}\} = [\Phi + \widetilde{\Delta\Phi}\,]\{\tilde{q}(t)\} \tag{4.20}$$

Where, $\{\tilde{q}(t)\}$ is the nonlinear modal response. $[\Phi]$ is the matrix of linear eigenvectors, which is independent of the excitation amplitude and the frequency. $\widetilde{\Delta\Phi}$ is the matrix of nonlinear eigenvectors, which is dependent on both the amplitude and the frequency of the excitation. Using the above relation (Equation (4.20)) in Equation (4.19) and multiplying both sides of Equation (4.19) by $[\Phi]^T$, we have,

$$[\Phi]^T[-w^2[M] + [K] + iw[C]\,][\Phi + \widetilde{\Delta\Phi}\,]\{\tilde{q}(t)\} + [\Phi]^T\{\tilde{G}\} = [\Phi]^T\{F^d\} \tag{4.21}$$

Further expanding Equation (4.21) the following equation is obtained,

$$\left[-w^2[\Phi]^T[M][\Phi] + [\Phi]^T[K][\Phi] + iw[\Phi]^T[C][\Phi]\right]\tilde{q}(t) + [-w^2[\Phi]^T[M][\Phi][\Phi]^{-1}\widetilde{\Delta\Phi} +$$

$$[\Phi]^T[K][\Phi][\Phi]^{-1}\widetilde{\Delta\Phi} + iw[\Phi]^T[C][\Phi][\Phi]^{-1}\widetilde{\Delta\Phi}\,]\tilde{q}(t) + [\Phi]^T\{\tilde{G}\} = [\Phi]^T\{F^d\} \tag{4.22}$$

Applying the orthogonal properties of the mass normalized mode shapes, Equation (4.22) can be written as,

$$[\lambda - w_r^2]\left(I + [\Phi]^{-1}\widetilde{\Delta\Phi}\,\right)\tilde{q}(t) + [\Phi]^T\{\tilde{G}\} = [\Phi]^T\{F^d\} \tag{4.23}$$

Equation (4.23) is the mathematical representation of the MDOF nonlinear system in a modal space for a base excited structure. Observed that neither mathematical assumptions nor approximations are made in formulating this equation.

From the theoretical point of view, Equation (4.23) represents the model equivalent to nonlinear normal modes[3], which has been the subject of research for the last four decades. The nonlinear normal modes are usually considered orthogonal, i.e., they are independent of each other. These nonlinear normal modes are affected by the nonlinearities at resonance only, otherwise they behave linearly. Comparing Equation (4.23) with its linear counterpart in Equation (3.9) there are two nonlinear terms; the nonlinear mode shapes $\widetilde{\Delta\Phi}$ and the nonlinear restoring force vectors $[\Phi]^T\{\tilde{G}\}$. These two terms make Equation (4.23) in the coupled form and cause the nonlinear modal behaviors as compared to Equation (3.9) as its linear counterpart in an uncoupled form. To understand this scenario, it is important to analyze each term of the Equation (4.23) separately.

It is clear from Equation (4.23) that the rth modal coordinate response $\tilde{q}_r(t)$ contains components belonging to all other modes, caused by the nonlinear term $([\Phi]^{-1}\widetilde{\Delta\Phi}$). This term is directly responsible for modal coupling effects by introducing non-diagonal entries in the mode shapes matrix. This further invalidates the assumption of modal superposition stating that modes are linearly independent of each other (or orthogonal). Thus, it is important to analyze the significance of this term with respect to the total response.

It has been observed in the existing literature that the total nonlinear variation of $\left[\widetilde{\Delta\Phi}\right]$ is quite small, between 1-20 % [35]. The term $[\Phi]^{-1}\widetilde{\Delta\Phi}$, in the vicinity of resonance is negligible as compared to the modal response $\tilde{q}(t)$. Away from the resonance, $[\Phi]^{-1}\widetilde{\Delta\Phi}$ has a higher magnitude, as compared to modal response $\tilde{q}(t)$. So, if the system can be excited at the undamped natural frequencies (modal frequencies) of the system, the contribution due to

---

[3] The nonlinear normal mode is usually multi-harmonic in nature.

43

$[\Phi]^{-1}\widetilde{\Delta\Phi}$ can be neglected. Since the effect of $[\Phi]^{-1}\widetilde{\Delta\Phi}$ is negligible, the nonlinear modal equation is decoupled to each mode. The term $[\Phi]^T\{\tilde{G}\}$ has the coupling effect between the modes. These nonlinear coupling terms between the modes are extracted by using the multilinear least square regression algorithm in the modal space. This is the main concept which is used in this research to extend the nonlinear response in the modal space. The term $[\Phi]^T\{\tilde{G}\}$ is the nonlinear modal restoring force. This is obtained by multiplying Equation (4.17) with the transpose of the mode shapes matrix $[\Phi]^T$. The measured nonlinear response data is transformed to the nonlinear modal space by using Equation (4.20).

The modal model formed by exciting one mode at a time (exciting at the modal frequency) may have cross couplings of nonlinear terms with other modes. If only one mode is excited at a time during a linear response corresponding to low base displacement, then we can say that the response in other modes during high base displacement is due to the cross coupling nonlinearity between the modes.

The perfect excitation is the excitation in which a linear mode can be excited one at a time. In a single base motion even in a very small base displacement/acceleration, i.e. in a linear modal analysis, it is impossible to excite one mode only, i.e. other modes are also excited by a small amount. This leads to the imperfect excitation. This imperfect excitation causes linear as well as cross-coupling excitation during high level base displacement/acceleration. In this way, if we perform a linear regression in a nonlinear modal space between the modes, part of the linear response also appears during regression. This linear response will affect the accuracy of the indentified cross coupling terms, while the direct nonlinear terms associated with that mode will

be accurate. The true cross coupling terms can be obtained accurately when several modes are tested based on mode by mode analysis principle and using Equation (4.20).

A nonlinear restoring force extracted by performing mode by mode analysis now needs to be fitted to the measured pseudo force and response data in the least square sense to extract the nonlinear parameters. It is important to describe the nonlinear restoring force by a mathematical model. The usual way is to fit to the restoring force a model of the form,

$$G(q, \dot{q}) = \sum_{i=0}^{m} \sum_{j=0}^{n} (a_{ij} q_i \dot{q}_j) \qquad (4.24)$$

Where $\sum_{i=0}^{m} \sum_{j=0}^{n} a_{ij} q_i \dot{q}_j = a_{11} q_1{}^3 + a_{12} q_1{}^2 q_2 + a_{13} q_2{}^2 q_3 + a_{14} q_1 \dot{q}_1 \ldots \ldots \ldots \ldots \ldots \ldots$ (4.25)

The least square parameter estimation technique is used to obtain the values of the coefficients a_{ij}. The normalized Mean-Square Error (MSE) between the measured and the predicted restoring force is defined as,

$$MSE\ (G) = \frac{100}{N_s \sigma_x{}^2} \sum_i (G(q, \dot{q}) - \hat{G}(q, \dot{q})) \qquad (4.26)$$

Where N_s is the total number of samples and $\sigma_x{}^2$ is the variance of the measured restoring force. Research shows that a MSE value of less than 5% indicates good agreement while a value of less than 1% reflects an excellent fit [33]. Potentially, a large number of nonlinear terms exist as indicated by Equation (4.25). To determine which terms are significant and which terms can be safely discarded in Equation (4.25), the significant factor is used which is defined as,

$$s_\theta = 100 \frac{\sigma^2{}_\theta}{\sigma^2{}_m} \qquad (4.27)$$

Where $\sigma^2{}_m$ corresponds to the variance of the sum of all the terms of the model and $\sigma^2{}_\theta$ is the variance of the considered term. A stepwise regression technique is used so as to achieve a desired level of MSE. The nonlinear system identification flow chart is shown in Figure 4.2.

```
STAGE I                              Nonlinear system

   Perform linear conventional modal
   analysis in Equation (3.1) to find out
          the modal parameters
                                            STAGE II

   Measure the acceleration response at M       Measure the acceleration
   locations at low base displacement at the    response vectors at M locations
          modal frequency                       at high base displacement at
                                                     the modal frequency

   Extract pseudo excitation force {Pᵈ} at the
   measured degrees of freedom by using
          Equation (3.16)

                                            Transform all the response and
                                            Pseudo force to the modal
                                                     space

                                            Extract the modal nonlinear
                                            restoring force vector

   STAGE III                                Perform multilinear least square

                                            regression to find out the normal and

                                            cross-coupling nonlinear terms
```

Figure 4.2: Flow Chart for Nonlinear System Identification in the Modal Space

4.2.2 Implementation of Nonlinear System Identification in the Modal Space

The flowchart for nonlinear system identification methodology in the modal space is shown in Figure 4.2, which involves three stages. During the first stage, the pseudo excited force vector at the measured DOFs is extracted using Equation (3.16). Prior to it, the modal parameters and the response at modal frequencies are needed. Such modal parameters are extracted by using Equation (3.1) and the response at modal frequencies is obtained by exciting the system at the corresponding frequencies. The second stage of this method consists of extracting the nonlinear modal restoring force vector. For this purpose, the system is excited with high base displacement/acceleration at the same modal frequencies and all the response vector and the nonlinear restoring force vector are transformed to the modal space. The third stage of this method consists of performing the multilinear least square regression in the excited mode to obtain the normal and cross-coupling nonlinearities.

4.2.3 Illustration of Nonlinear System Identification in a Modal Space

The overall methodology of nonlinear system identification which combines these three theories of force reconstruction, base excitation and nonlinear system identification will be illustrated at this stage using a 5 DOF nonlinear system where all the modes are affected by nonlinearities. A complex system with a maximum of 35 nonlinear terms is chosen to demonstrate the method, as shown by the Equations (4.34-4.38).

The system chosen is shown in Figure 4.3. The system has hardening cubic stiffness nonlinearity between Masses 2 and 4. If the nonlinear relative displacements response of mass 1, mass 2, etc. are denoted by $\tilde{u}_1, \tilde{u}_2$ etc., the unforced equations of motion in terms of relative displacement vector can be written as,
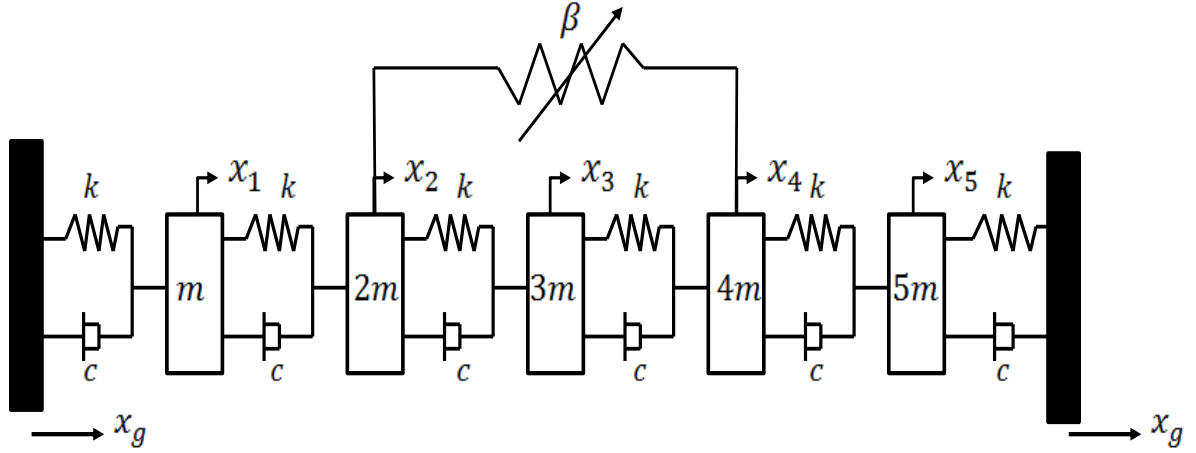
Figure 4.3: Five DOF Lumped Parameter Model

$$\begin{bmatrix} m & 0 & 0 & 0 & 0 \\ 0 & 2m & 0 & 0 & 0 \\ 0 & 0 & 3m & 0 & 0 \\ 0 & 0 & 0 & 4m & 0 \\ 0 & 0 & 0 & 0 & 5m \end{bmatrix} \begin{Bmatrix} \ddot{\tilde{u}}_1 \\ \ddot{\tilde{u}}_2 \\ \ddot{\tilde{u}}_3 \\ \ddot{\tilde{u}}_4 \\ \ddot{\tilde{u}}_5 \end{Bmatrix} + \begin{bmatrix} 2c & -c & 0 & 0 & 0 \\ -c & 2c & -c & 0 & 0 \\ 0 & -c & 2c & -c & 0 \\ 0 & 0 & -c & 2c & -c \\ 0 & 0 & 0 & -c & 2c \end{bmatrix} \begin{Bmatrix} \dot{\tilde{u}}_1 \\ \dot{\tilde{u}}_2 \\ \dot{\tilde{u}}_3 \\ \dot{\tilde{u}}_4 \\ \dot{\tilde{u}}_5 \end{Bmatrix}$$

$$+ \begin{bmatrix} 2k & -k & 0 & 0 & 0 \\ -k & 2k & -k & 0 & 0 \\ 0 & -k & 2k & -k & 0 \\ 0 & 0 & -k & 2k & -k \\ 0 & 0 & 0 & -k & 2k \end{bmatrix} \begin{Bmatrix} \tilde{u}_1 \\ \tilde{u}_2 \\ \tilde{u}_3 \\ \tilde{u}_4 \\ \tilde{u}_5 \end{Bmatrix} + \begin{Bmatrix} 0 \\ -\beta(\tilde{u}_4 - \tilde{u}_2)^3 \\ 0 \\ \beta(\tilde{u}_4 - \tilde{u}_2)^3 \\ 0 \end{Bmatrix} = 0 \qquad (4.28)$$

Where, $m, k,$ and c are the mass, stiffness and damping of the system respectively. β is the nonlinear stiffness of the system which is connected between Masses 2 and 4. Nonlinear response vectors at the physical coordinate system are obtained through numerical simulation. The parameters used for the simulation are $m = 1$kg, $c = 4.8$ Ns/m, $k = 4 \times 10^3$N/m and $\beta = 5 \times 10^9$Nm^{-3}. The resulting natural frequencies and mode shapes of the system shown in Figure 4.3 is obtained by solving the undamped system equations which is tabulated in Table 4.1. Transformation of Equation (4.28) into a modal space by using the mode shapes matrix will yield a system of equations of the form,

$$\ddot{\tilde{q}}_1 + 0.4103\dot{\tilde{q}}_1 + 0.3419 \times 10^3\tilde{q}_1 - 0.0670 \times 5 \times 10^9(\tilde{u}_4 - \tilde{u}_2)^3 = 0 \qquad (4.29)$$

$$\ddot{\tilde{q}}_2 + 1.6192\dot{\tilde{q}}_2 + 1.3494 \times 10^3\tilde{q}_2 + 0.4435 \times 5 \times 10^9(\tilde{u}_4 - \tilde{u}_2)^3 = 0 \qquad (4.30)$$

$$\ddot{\tilde{q}}_3 + 3.2\dot{\tilde{q}}_3 + 2.6667 \times 10^3\tilde{q}_3 + 0.6524 \times 5 \times 10^9(\tilde{u}_4 - \tilde{u}_2)^3 = 0 \qquad (4.31)$$

$$\ddot{\tilde{q}}_4 + 5.2280\dot{\tilde{q}}_4 + 0.3419 \times 10^3\tilde{q}_4 + 0.1223 \times 5 \times 10^9(\tilde{u}_4 - \tilde{u}_2)^3 = 0 \qquad (4.32)$$

$$\ddot{\tilde{q}}_5 + 11.4625\dot{\tilde{q}}_5 + 9.5521 \times 10^3\tilde{q}_5 - 0.3288 \times 5 \times 10^9(\tilde{u}_4 - \tilde{u}_2)^3 = 0 \qquad (4.33)$$

Equations (4.29-4.33) show that all the modes are coupled to each other in the nonlinear modal space. If the nonlinear terms are expressed in modal space then Equations (4.29-4.33) becomes,

$$\ddot{\tilde{q}}_1 + 0.4103\dot{\tilde{q}}_1 + 0.3419 \times 10^3\tilde{q}_1 - 0.0670 \times 5 \times 10^9(-0.0670\tilde{q}_1 + 0.4435\tilde{q}_2 + 0.6524\tilde{q}_3 +$$
$$0.1223\tilde{q}_4 - 0.3288\tilde{q}_5)^3 = 0 \qquad (4.34)$$

$$\ddot{\tilde{q}}_2 + 1.6192\dot{\tilde{q}}_2 + 1.3494 \times 10^3\tilde{q}_2 + 0.4435 \times 5 \times 10^9(-0.0670\tilde{q}_1 + 0.4435\tilde{q}_2 + 0.6524\tilde{q}_3 +$$
$$0.1223\tilde{q}_4 - 0.3288\tilde{q}_5)^3 = 0 \qquad (4.35)$$

$$\ddot{\tilde{q}}_3 + 3.2\dot{\tilde{q}}_3 + 2.6667 \times 10^3\tilde{q}_3 + 0.6524 \times 5 \times 10^9(-0.0670\tilde{q}_1 + 0.4435\tilde{q}_2 + 0.6524\tilde{q}_3 +$$
$$0.1223\tilde{q}_4 - 0.3288\tilde{q}_5)^3 \qquad (4.36)$$

$$\ddot{\tilde{q}}_4 + 5.2280\dot{\tilde{q}}_4 + 0.3419 \times 10^3\tilde{q}_4 + 0.1223 \times 5 \times 10^9(-0.0670\tilde{q}_1 + 0.4435\tilde{q}_2 + 0.6524\tilde{q}_3 +$$
$$0.1223\tilde{q}_4 - 0.3288\tilde{q}_5)^3 = 0 \qquad (4.37)$$

$$\ddot{\tilde{q}}_5 + 11.4625\dot{\tilde{q}}_5 + 9.5521 \times 10^3\tilde{q}_5 - 0.3288 \times 5 \times 10^9(-0.0670\tilde{q}_1 + 0.4435\tilde{q}_2 +$$
$$0.6524\tilde{q}_3 + 0.1223\tilde{q}_4 - 0.3288\tilde{q}_5)^3 = 0 \qquad (4.38)$$

Table 4.1: Frequencies and Mode Shapes of 5DOF Undamped System

Modal frequencies (Hz)	Mode shapes				
	1	2	3	4	5
2.9429	-0.1258	-0.2076	-0.2447	-0.3511	-0.8706
5.8464	-0.2409	-0.3452	-0.3262	-0.3198	0.3378
8.2187	-0.3147	-0.2499	0.0272	0.4081	-0.0672
10.5050	-0.3079	0.0983	0.3262	-0.1975	0.0090
15.5550	-0.1958	0.3139	-0.2447	0.0573	-0.0009

As the implementation of the nonlinear system identification shown in Figure 4.2 works in three stages, each stage is implemented sequentially to find out the nonlinear parameters. In stage I, the system is excited with low base acceleration of magnitude 0.1m/sec^2 which ensures that the nonlinearities are not excited. Exciting the system with low acceleration, the pseudo excited force vector at the measured DOFs is obtained by using Equation 3.16. The results of the pseudo excited force vector are shown in Figure 4.4. In stage II, the system is excited with the high base acceleration of magnitude 4 m/sec^2 such that the nonlinearities are excited. As nonlinear parameters are independent to the mass distribution of the structure, the pseudo excited force vector corresponding to the acceleration 4 m/sec^2 is obtained by using Equation (3.16). Figure 4.5 shows the obtained pseudo excited force vector at the measured DOFs using the base acceleration of 4m/sec^2. Comparing Figures 4.4 and 4.5 it can be seen that the pseudo excited force at high base acceleration is exactly 40 times higher than the low base acceleration which is true as the input acceleration is scaled from low level acceleration magnitude of 0.1m/sec^2 to high level acceleration magnitude of 4 m/sec^2. Once the pseudo excited force vector
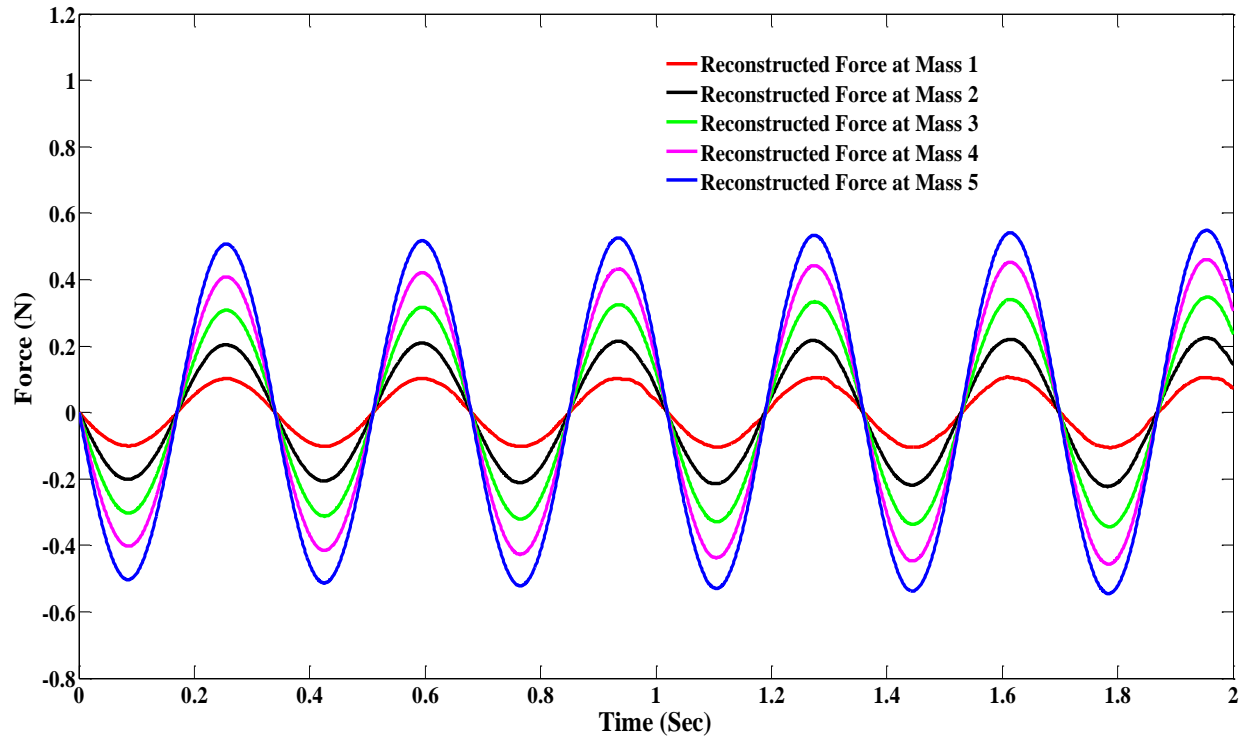
Figure 4.4: Reconstructed Force Vector at Low Base Acceleration
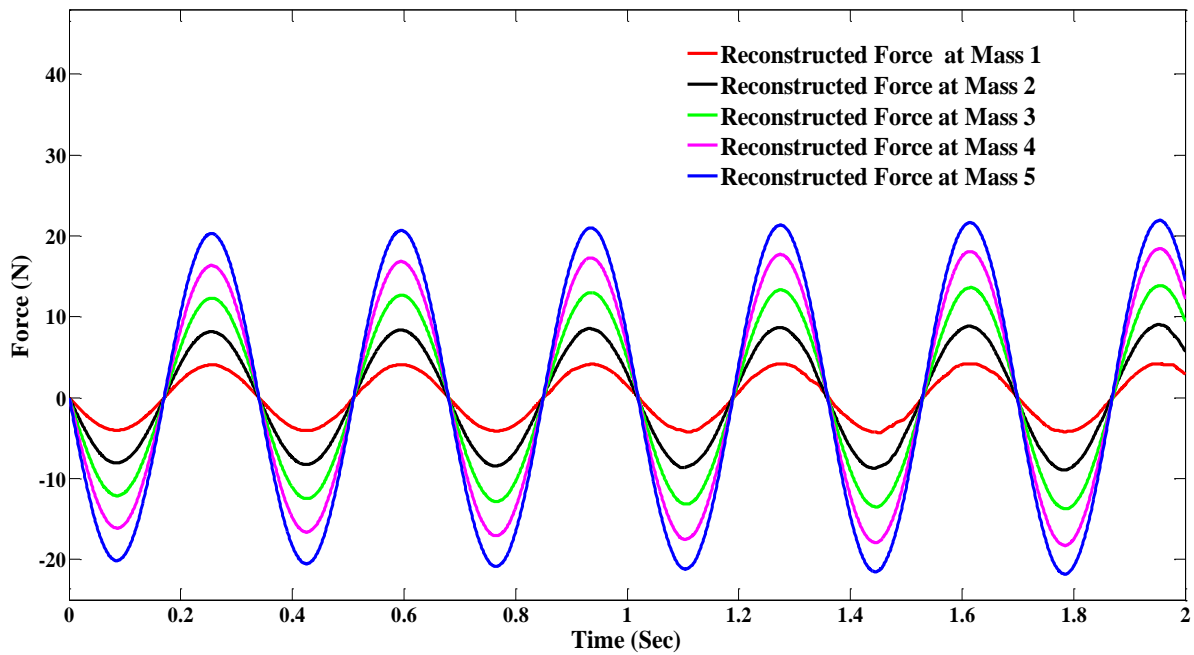
Figure 4.5: Reconstructed Force Vector at High Base Acceleration

corresponding to the high base acceleration is obtained, the nonlinear restoring force at the measured DOFs is recovered by using Equation (4.17). The nonlinear restoring force vector obtained in such a way is transformed to the nonlinear modal space by using mode shapes matrix. In stage III, the nonlinear parameters are obtained by performing multilinear least square regression in a modal space using Equations (4.25-4.27). For the first mode excitation, Figure 4.6 shows the measured and the fitted modal restoring force in a time domain. The Goodness-of-fit in terms of mean square error change is over 99%. The true and the least square fitted modal stiffness coefficient are compared and are tabulated in Table 4.2. The true nonlinear coefficients are the stiffness coefficients given by Equation (4.34) whereas the least square fitted coefficients are the coefficients obtained from using Equation (4.25).
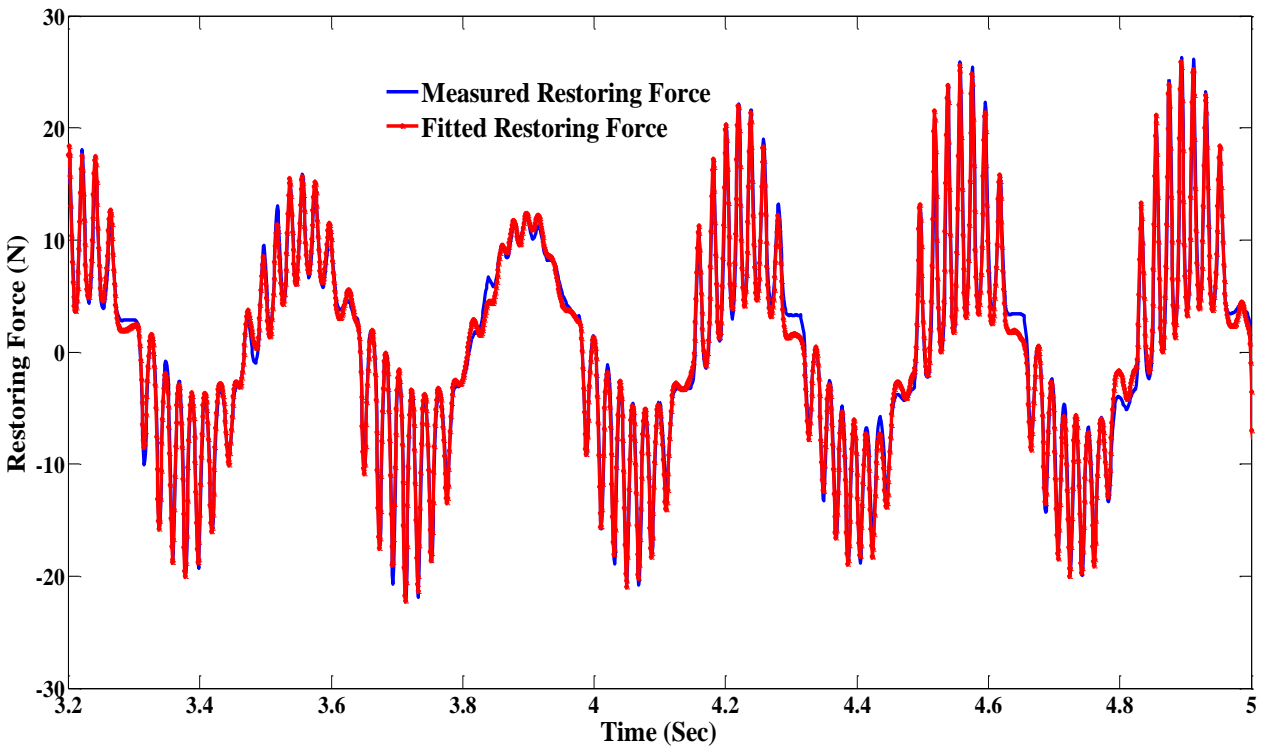
Figure 4.6: Measured and Fitted Mode1 Nonlinear Restoring Force

As shown in Table 4.2, the direct stiffness coefficient for Mode 1 is accurate with the percentage error being less than 0.1%. However, the cross-couplings stiffness terms with Mode 1 are not accurate. The major cause of inaccuracy is due to the imperfect excitation which is shown in Figure 4.7. As shown in Figure 4.7, the excitation is made on Mode 1 with the base acceleration of $4 \, \text{m/sec}^2$, however there are forces in Mode 2, Mode 3, Mode 4 and Mode 5, respectively. These forces indicate that the mode 1 is not clearly isolated. Since Mode 1 is not isolated, the responses in Mode 2, Mode 3, Mode 4 and Mode 5 are due to: (i) cross-coupling response between the modes and (ii) due to the force in each mode. The presence of force in Mode 2, Mode 3, Mode 4 and Mode 5 perhaps causes some linear response in the corresponding modes and which affect the accuracy of the identified cross-coupling coefficients. However, the presence of forces in other modes doesn't affect the direct nonlinear stiffness coefficient associated with the excited mode.

Table 4. 2: Nonlinear Stiffness Coefficients Corresponding to Mode 1 Excitation

Parameters	Exact Stiffness ($\frac{N}{m^3}$)	Identified Stiffness ($\frac{N}{m^3}$)
$q_1{}^3$	1.0075×10^5	1.0058×10^5
$q_2{}^3$	-2.9223×10^7	-3.45022×10^7
$q_3{}^3$	-9.3022×10^7	-7.3014×10^7
$q_4{}^3$	-6.12807×10^5	8.3859×10^5
$q_5{}^3$	1.1908×10^7	5.127989×10^7
$q_1{}^2 q_2$	-2.000825×10^6	-1.7629×10^6
$q_1{}^2 q_3$	-2.94326×10^6	-3.4022×10^6
$q_1{}^2 q_4$	-5.51749×10^6	-2.1032×10^6
$q_1{}^2 q_5$	1.483363×10^6	2.2817×10^6
$q_2{}^2 q_1$	1.3244272×10^7	0.9954×10^7
$q_2{}^2 q_3$	-1.28963634×10^8	-2.2945×10^8
$q_2{}^2 q_4$	-2.4175739×10^7	-0.886815×10^7
$q_2{}^2 q_5$	6.4995773×10^7	3.0268×10^8
$q_3{}^2 q_1$	2.86595×10^7	3.3582×10^7
$q_3{}^2 q_2$	-1.8970×10^8	-0.90388×10^8
$q_3{}^2 q_4$	-5.2314×10^7	-3.0833×10^8
$q_3{}^2 q_5$	1.40645×10^8	4.6687×10^8
$q_4{}^2 q_1$	1.0071×10^6	2.94×10^7
$q_4{}^2 q_2$	-6.666725×10^6	-2.035×10^6
$q_4{}^2 q_3$	-9.8069×10^6	-2.1173×10^6
$q_4{}^2 q_5$	4.942546×10^6	7.8929×10^6
$q_5{}^2 q_1$	7.279549×10^6	3.523×10^7
$q_5{}^2 q_2$	-4.8186269×10^7	-7.8639×10^8
$q_5{}^2 q_3$	-7.0883251×10^8	-3.4015×10^8
$q_5{}^2 q_4$	-1.3287893×10^7	-1.2279×10^8
$q_1 q_2 q_3$	3.8965336×10^7	4.0469×10^7
$q_1 q_2 q_4$	7.304507×10^6	4.4485×10^7
$q_1 q_2 q_5$	-1.9637956×10^7	-5.6969×10^7
$q_1 q_3 q_4$	1.0745119×10^7	1.6238×10^7
$q_1 q_3 q_5$	-2.8887943×10^7	-4.0376×10^7
$q_1 q_4 q_5$	-5.415382×10^6	-2.6970×10^6
$q_2 q_3 q_4$	-7.1126×10^7	-1.0141×10^7
$q_2 q_3 q_5$	1.9122×10^8	5.8849×10^7
$q_2 q_4 q_5$	3.5846598×10^7	4.6606×10^7
$q_3 q_4 q_5$	5.273125×10^7	2.46049×10^7
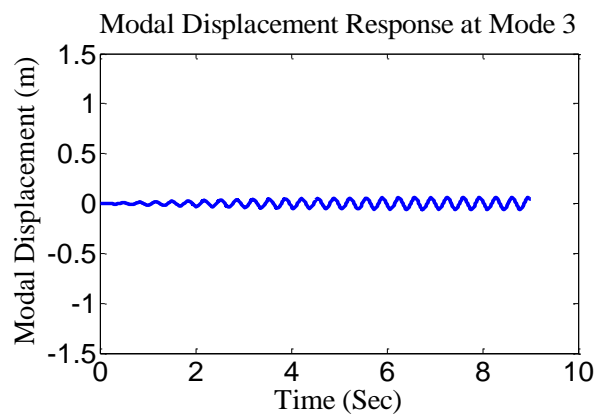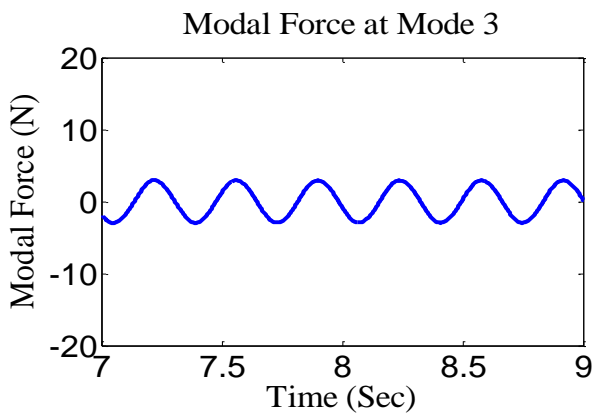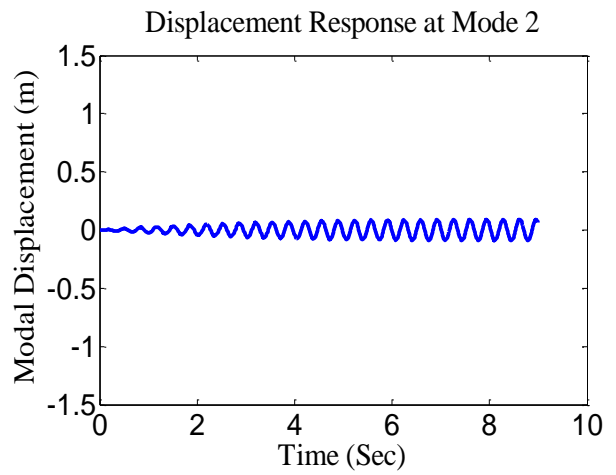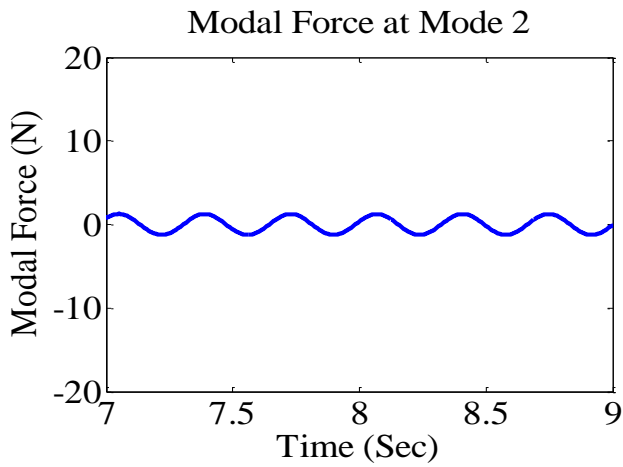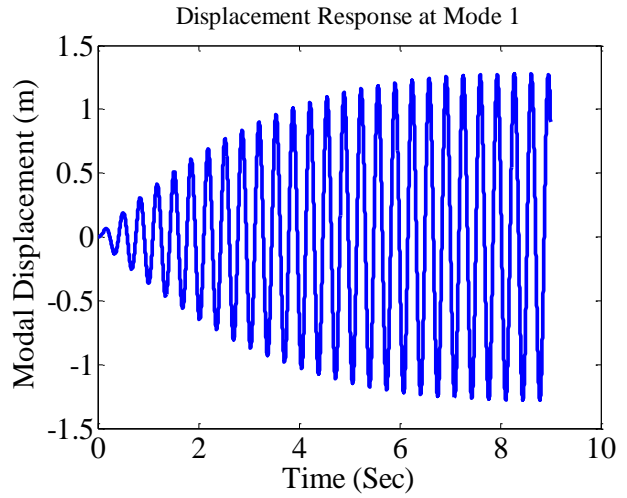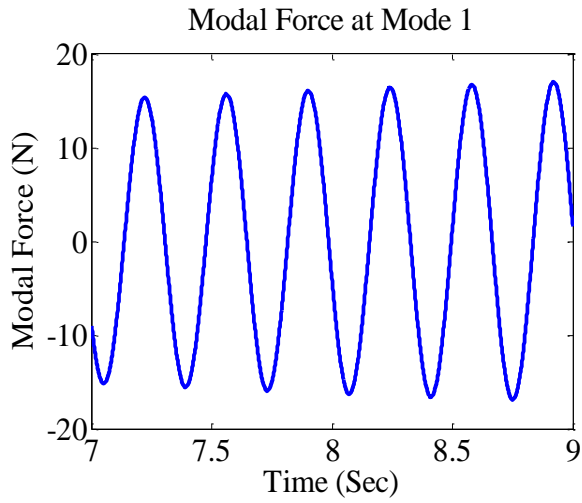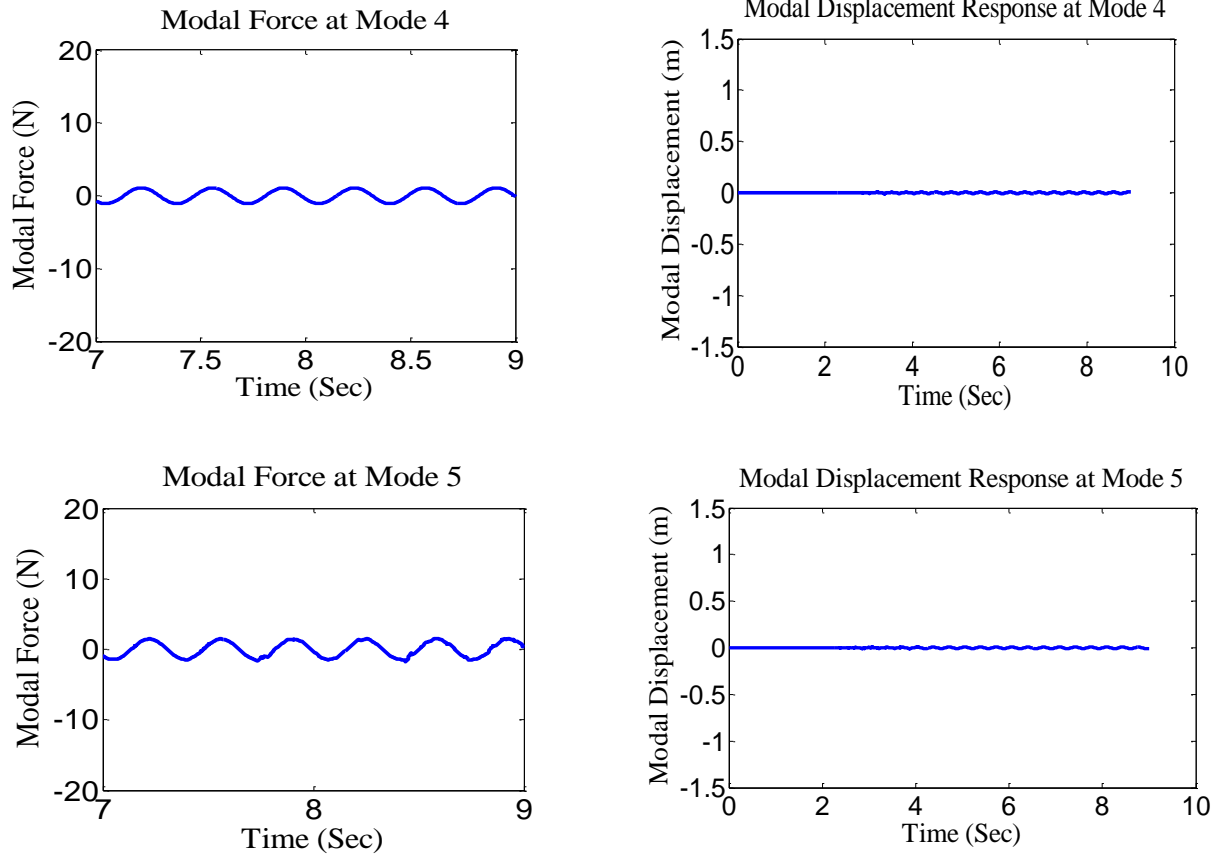
Figure 4.7: Modal Force and Response at each Mode Resulting from the Base Acceleration of 4 m/sec2

In order to identify the stiffness coefficients associated with Mode 2, 3, 4 and 5, each stage of the methodology shown in Figure 4.2 is applied at each modal frequency. Figure 4.8 shows the measured and the fitted nonlinear restoring force for Mode 2 excitation in a 3D surface. The measured Restoring force is the force obtained by using Equation (4.17) whereas the fitted restoring force is the force obtained by performing least square regression including all the modes to Mode 2. Figure 4.8 clearly shows the cross-coupling stiffness terms. Since the cross-coupling terms are not accurate, they are removed by subtracting from the measured nonlinear restoring force given by Equation (4.17). This results in the direct stiffness term for Mode 2. The RFS for the Mode 2 with direct stiffness term is shown in Figure 4.9A. Figure 4.9 B shows the slice view of the Figure 4.9 A in XZ plane. Figure 4.9 B clearly shows the cubic stiffness

nonlinearity associated with the Mode 2. Figure 4.9B indicates that, even the modes are cross-coupled to each other, this method can accurately identify the true direct stiffness nonlinearity associated with the excited mode.
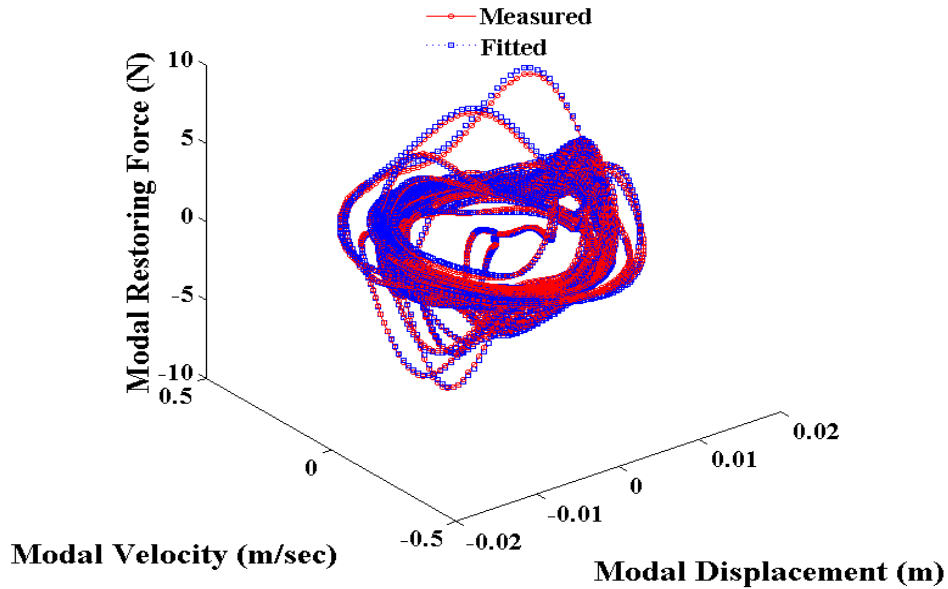
Figure 4.8: Measure and Fitted Modal Restoring Force (Mode 2 Excitation)
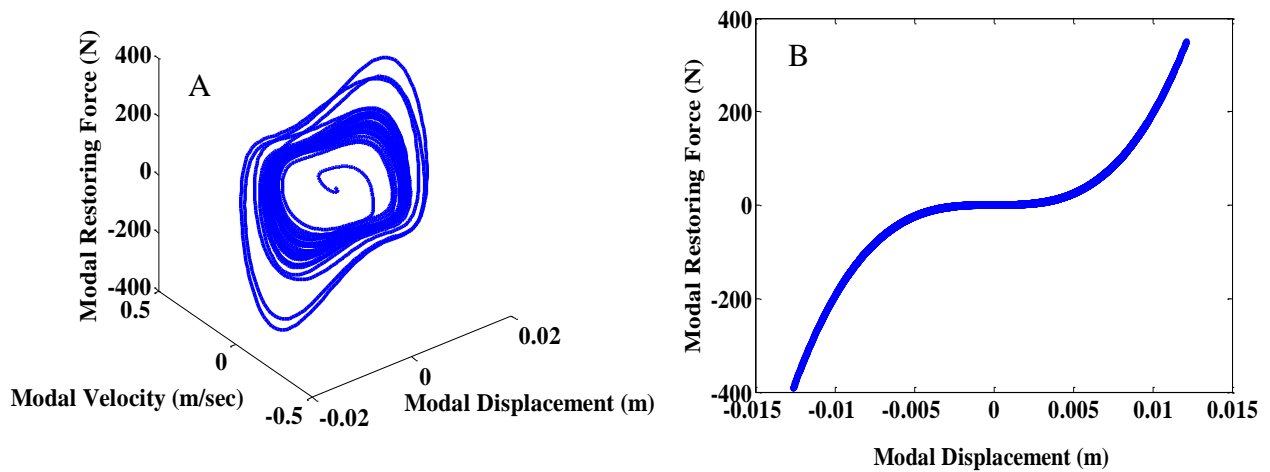
Figure 4.9: Restoring Force Surface Obtained from Least Square Regression for Mode 2 with Direct Stiffness Term (A: RFS B: Stiffness Projection)

The nonlinear modal restoring force for Mode 3, Mode 4 and Mode 5 are shown in time series form in Figures (4.10-4.12) respectively. All of the figures show the direct nonlinear terms as

58

well as the cross-coupling terms. The direct stiffness terms obtained for each mode from regression is tabulated in Table 4.3.
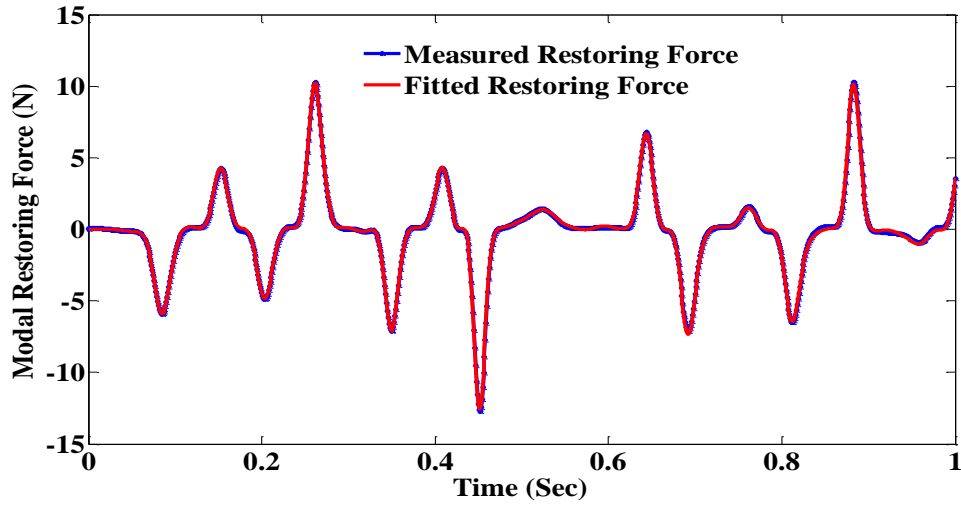
Figure 4.10: Measured and Fitted Modal Restoring Force (Mode 3 Excitation)
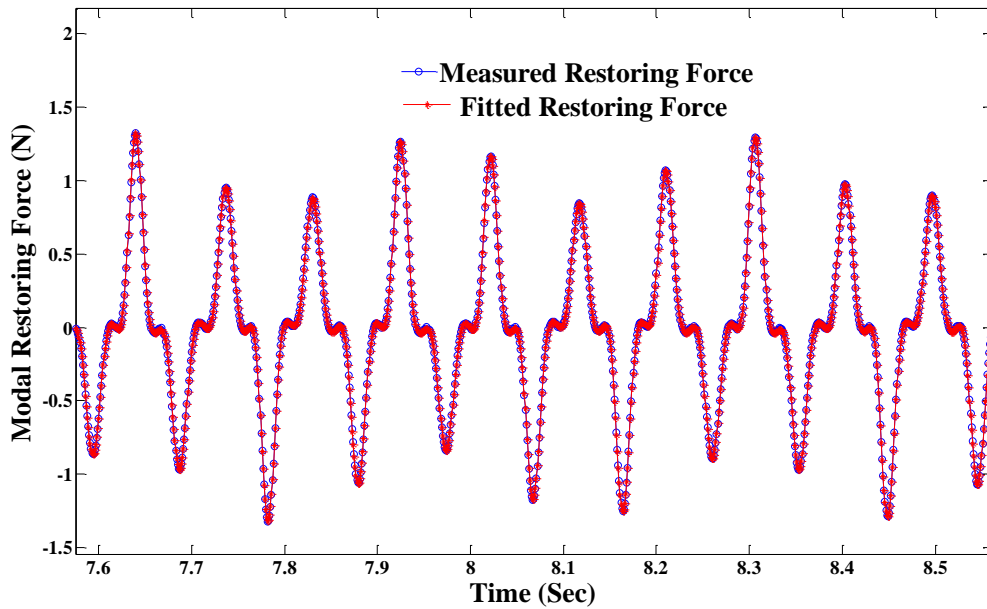
Figure 4.11: Measured and Fitted Modal Restoring Force (Mode 4 Excitation)
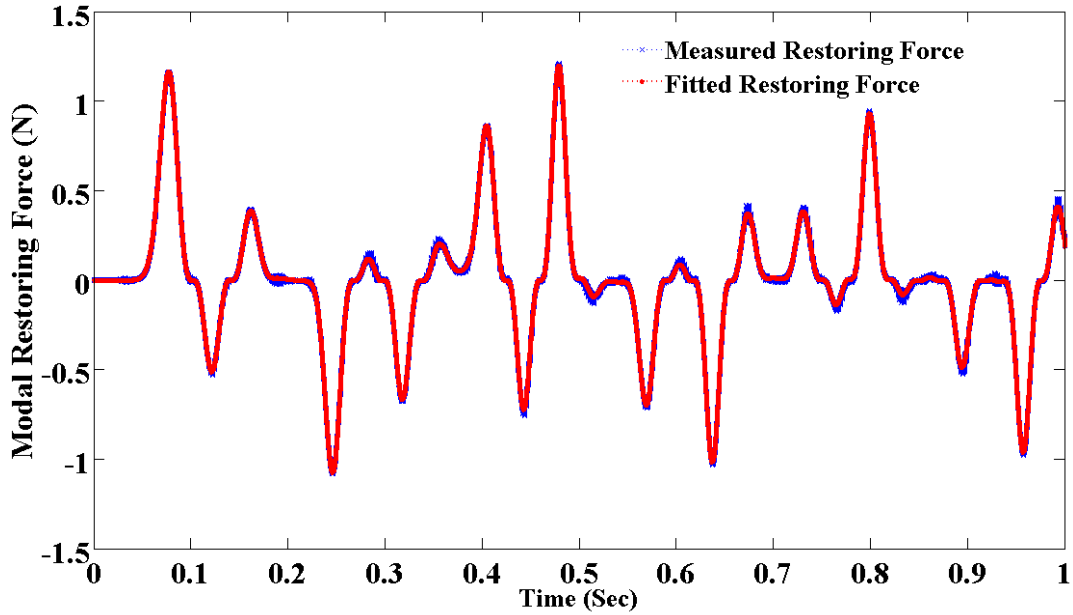
Figure 4.12: Measured and Fitted Modal Restoring Force (Mode 5 Excitation)

Table 4.3: Exact and Identified Direct Stiffness for Each Mode

Mode No	Exact Stiffness	Identified Stiffness	Percentage Error
Mode 1	1.0075×10^5	1.0058×10^5	0.16%
Mode 2	1.9344×10^8	1.924×10^8	0.537%
Mode 3	9.0579×10^8	9.3616×10^8	3.35%
Mode 4	1.1186×10^6	1.112×10^6	0.59%
Mode 5	5.8438×10^7	5.617×10^7	3.88%

4.3   Summary

Two methodologies are proposed for the identification of large multi-degree-of-freedom nonlinear systems where the excitation comes from the moving base. The first methodology works on the frequency domain data and extracts the parameters in a physical coordinate system. In the first methodology, the theoretical formulation of the pseudo force vector and the nonlinear

restoring force vector is presented, which is applicable to base excited structure. The formulation is based on presenting the system equation in the mixed (physical/modal) model form. Presenting the system into the mixed model form has been previously applied for a multi force excited structure [12, 34]. However, this concept has never been used in a base excited structure. In the second methodology, the same formulated concept is used for the reconstruction of force vector. However, the analysis is presented in a modal space. As compared to first method, the second method has several advantages. For example, the advantages are: the method does not need the location and the functional form of the nonlinearity. The excitation is done at the particular mode so it has the potential to show whether the mode is coupled or not. The most promising advantage is that it aids in studying the structural stability analysis problems in the modal domain. Both methodologies presented in this chapter are applicable to base excited structure using experimentally measured data. Since closed form expressions are presented for the extraction of the nonlinear restoring force and the pseudo force vector, the methodologies are not restricted to the test component used in the following chapter.

Chapter 5

Experiment for Nonlinear System Identification

The methodologies developed for identification of nonlinear systems, discussed in Chapter 4, aim at real-world engineering applications and are based on measured testing data. Thus, experimental demonstration of the proposed methods is essential. Since such test facility was not available at the University of Manitoba, a test facility was designed and erected which has the same configuration as the industrial test rig, but with a lower power range. This chapter is divided into three sections. Section 5.1 presents the details of test set- up and requirements for vibration testing of a structure using a mechanical shaker, Section 5.2 presents the demonstration of force reconstruction technique using the base excitation as an input and Section 5.3 presents the demonstration of the nonlinear system identification in base excited structure.

5.1 Experimental Set-up for Nonlinear System Identification

In the field of nonlinear system identification, the interaction between the structure being tested and the testing facility is a critical issue. This is particularly true when testing massive structures (e.g. engine components). The reason is that due to the design and manufacturing limitations, the frequencies of the testing facility often overlap, at least partially, with those of the test specimen. The key issues affecting the table performance include the shaker table which should not vibrate into resonance with the input signal and should have high stiffness with moderate mass. Also, the motion of the table should not be in the unwanted degrees of freedom. These issues were addressed while designing the table. This chapter presents the innovative guidelines for designing the table platform, its assembly and the investigations to provide insight into its response characteristics.

The shaker table is an essential testing facility for conducting durability tests in the laboratory. The shaker table is a platform driven by servo-hydraulic actuators to simulate different types of periodic and random motions, such as artificial ground motions and other dynamic testing signal of interest. In a typical durability test, the testing is often carried out by exciting the shaker table in multiaxial directions. Developing such a shaker table is complex and costly. Moreover, to interpret the results from the multiaxial table is more complex. A single-axis table is the simplest form of the durability test simulator, which is not only useful for many investigations but also simplifies subsequent interpretation of the results. For a similar reason, a single axis shaker table has been chosen for the large outdoor facility developed under the NEES program at University of California, Sandiego [75]. A smaller sized shaker table is also better suited for the small scale model analysis. In addition, it avoids high operational costs, but is versatile enough in the case of dynamic experiments for instrumental and research purposes. However, like every system, the single axis table also has certain limitations. The rest of the chapter discusses the construction, waveform replication and performance analysis of a single axis simulation table.

5.1.1   Shaker Table Assembly

The shaker table developed for the purpose of nonlinear system identification is uniaxial (horizontal) and servo-hydraulic operated. It was constructed with the in-house knowledge and the fabrication capability. The shaker table system comprises of the table platform, servo-hydraulic actuator with controls, ball bushing bearing support systems (linear mechanism) and the reaction mass. A full view of the installed shaker table is shown in Figure 5.1. The overall characteristics of the system as well as individual components are summarized in Table 5.1.

The criteria that were set to design the table were high stiffness, high natural frequencies and low mass. To minimize the mass of the table, the table was designed to build from several
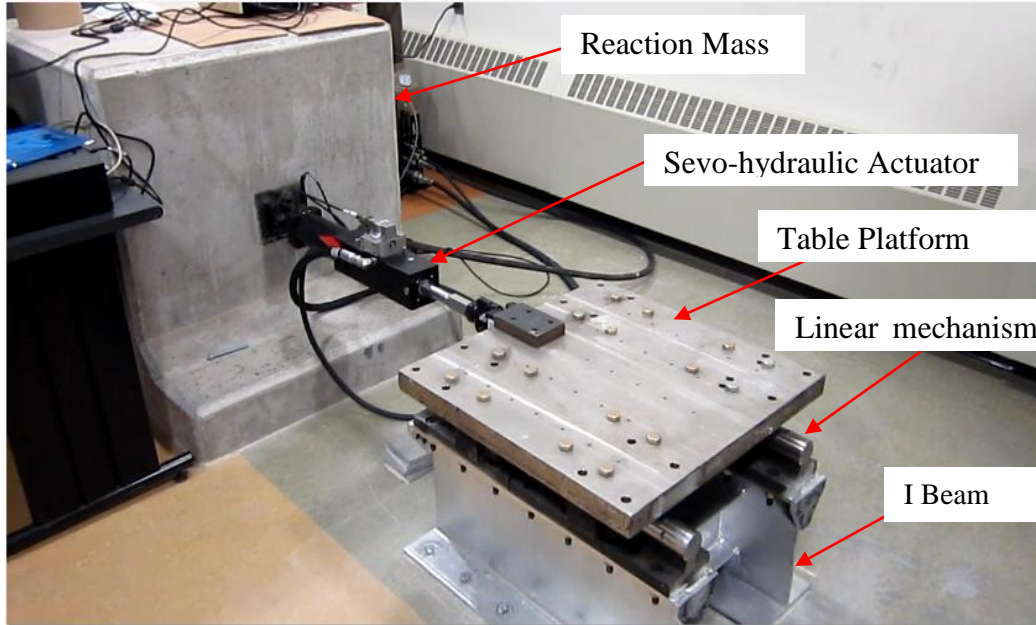
Figure 5.1: Installed View of the Shaker Table

Table 5.1: Specification of the Installed Shaker Table

Table Size	0.6× 0.6 m
Weight of the table	0.60kN
Maximum pay load	5kN
Maximum displacement	±75mm
Maximum acceleration	3g
Frequency range	0.1-80Hz
Actuator Specifications	
Actuator model	MTS 242.02
Thrust	10kN
Stroke length	150mm
Servo valve	Two stage four- way
Specification of supports	
Ball bearing	Thomson,USA(model:XPBO-32-OPN)
Linear system	Thomson, USA (model:XSR-32), extra rigid
Shaft diameter	2.54 cm
Travel life	50 km

components. The design process consists of several steps. They are: selecting the material, setting the initial dimensions for each component of the table, developing a geometrical model and implementing this geometrical model into the FEA software to perform the modal analysis. Mild steel and stainless steel were selected as the material of the shaker table. Stainless steel was used because it has high stiffness and high resistance to corrosion as well as wear and tear.

Selecting the dimensions of the table is one of the important steps for the table design. The length and the width of the table depend on the type of the mechanism used to provide the linear motion to the table and the power of the actuator used to impart motion to the table. On the basis of the specifications of the actuator and the linear mechanism, the overall length and the width of the table were calculated as $0.6m$ and $0.6m$ respectively. To find out the dimensions of the individual components, an iterative approach was carried out by changing the dimensions of each component until the first natural frequency of the shaker table is at least three times higher than the operating frequency range (0.1-80) Hz [75-77].

To determine the natural frequencies of the table, modal analysis was carried out using ANSYS Workbench. The first natural frequency of 350 Hz was obtained for the table with restrained translations (Figure 5.2) of the supports. Thus, the lowest frequency of the table is sufficiently higher than the operating frequency range (0.1–80 Hz) for which the table was designed.

First Mode vibration   Second Mode vibration
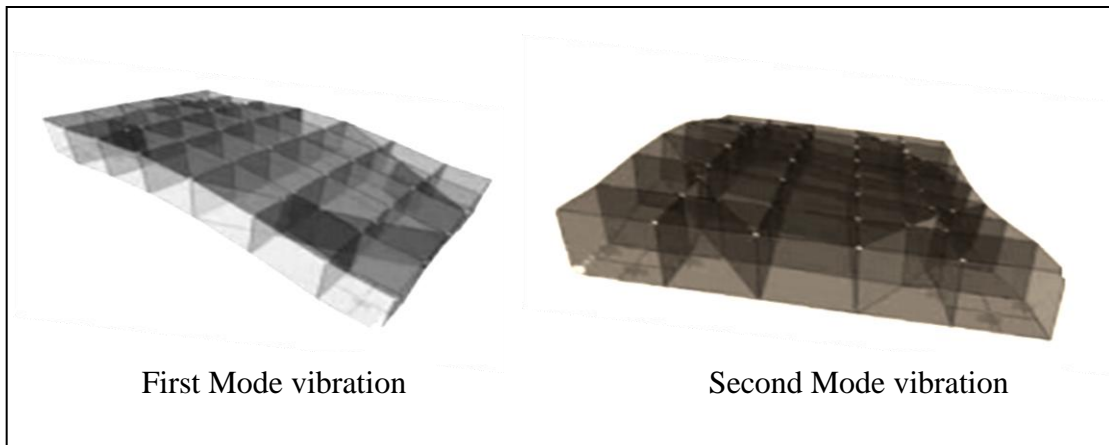
Figure 5.2: Deflection of Table in First Two Modes

The table platform was assembled by welding plates of stainless steel and mild steel (Figure 5.3). The top plate and the side plates are made of stainless steel, while the inner plates are made of mild steel. Threaded holes in the top surface of the table were made for mounting the test structure. Provisions were also made to extend the table to accommodate larger-sized specimens. Figure 5.4 shows the complete table with holes drilled at the desired locations.
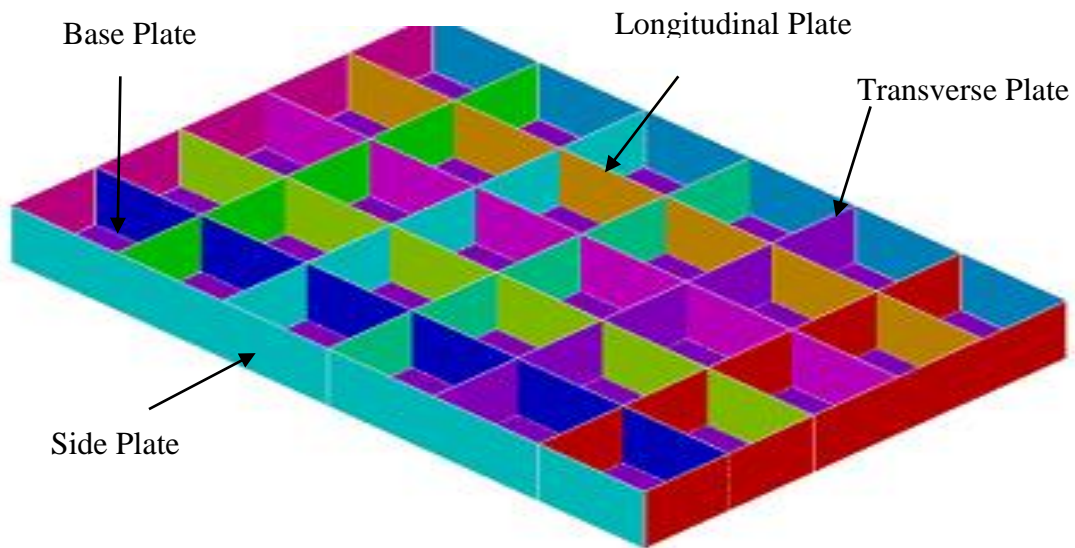
Figure 5.3: Longitudinal and Transverse Plate Welded to the Base Plate
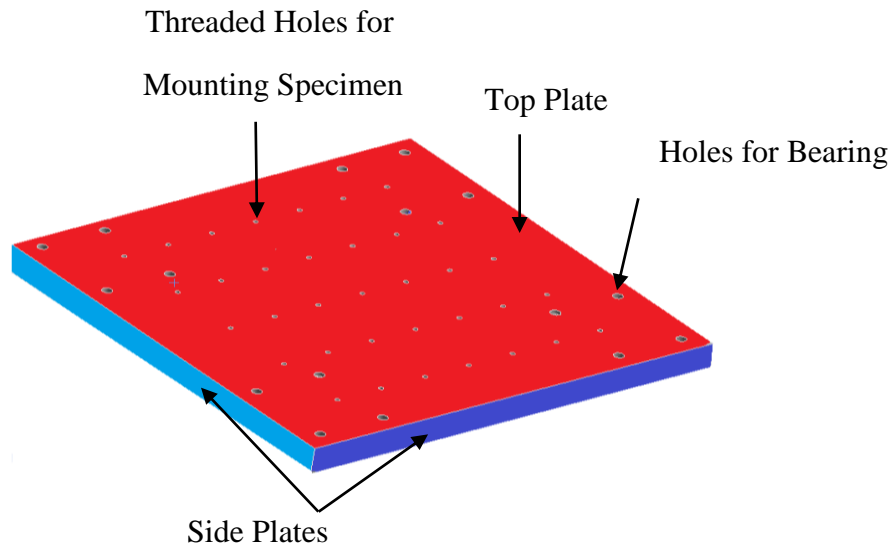
Figure 5.4: Complete Table with Holes at Desired Location

The servo-hydraulic actuator (MTS, USA) is responsible for creating the movement of the table. A full view of the actuator and its specification is shown in Figure 5.5. The actuator has the same configuration as the actuator used in industry but with a lower power range.

Actuator Model	242.02 MTS
Stroke Length	6 inch
Actuator Maximum Force	9.8kN
Servo valve	Two stage, four way
Pump flow rate	26.5 l/min
Sound pressure level	58dB(A)
Hydraulic Fluid	160 liters supplied in HPU
Controller	Flex test 40

Figure 5.5: Servo-hydraulic Actuator Detail (http://www.mts.com/en)

The shaker table platform is supported on the ball bush bearing and the linear rail guide system shown in Figure 5.6. The linear rail guide system facilitates the movement of the table in the

horizontal direction and prevents motion in the unwanted degrees of freedom. The low-friction ball bushing bearing (Thomson, USA) utilizes a special 'return ball mechanism' which comprises of a sleeve and a cage mounted on a shaft member, as shown in Figure 5.6. The ball bushing has a number of closed ball paths and the balls are loaded between the sleeve and the shaft. The sleeve has a number of countersunk longitudinal profiles which define internal raceways for the loaded balls. The reason for choosing this kind of linear mechanism is that it is effective in reducing kinetic friction significantly [78].

Bearing (XPBO-32OPN)	Shaft (XSR-32)
Extra rigid	Extra strong 60 linear case
Coefficient of friction(0.001)	Shaft diameter (2inch)
Dynamic load case	Surface finish Ra u in
Travel life 50 km	Hardness 60 HRC
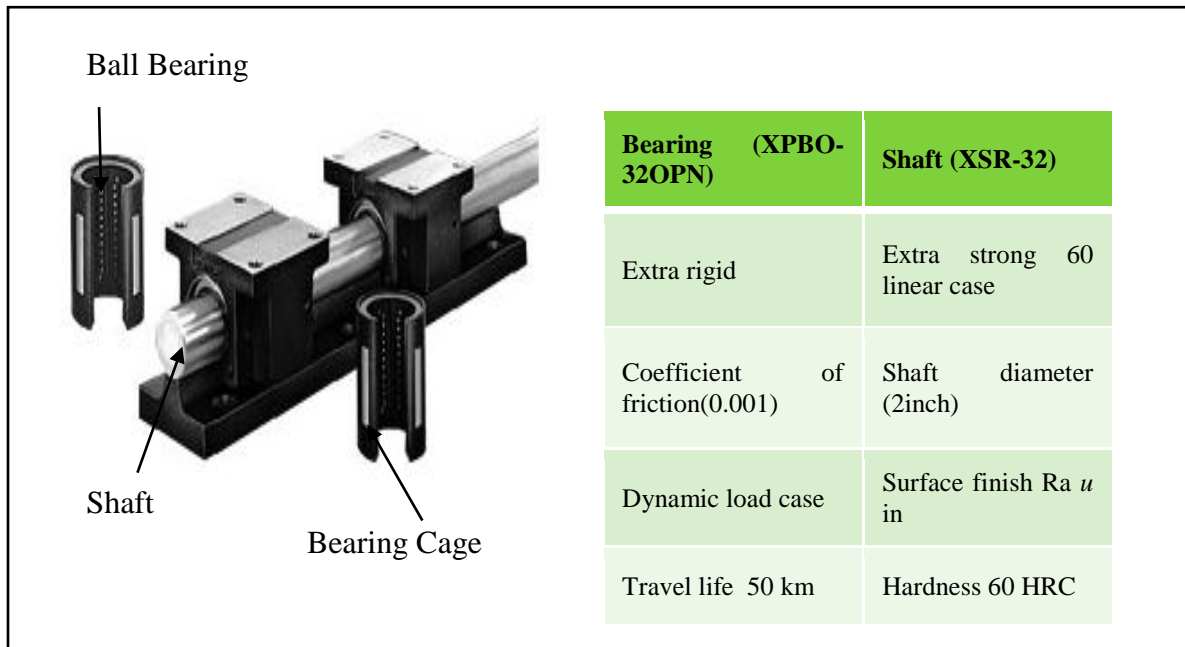
Figure 5.6: Linear Rail Guide Mechanism (http://www.thomsonlinear.com)

5.1.2 Performance Analysis of Shaker Table

The performance of the shaker table was analyzed using a sine wave signal, which provided a considerable amount of information regarding the behavior of the shaker table. Such performance was measured by output only analysis and by comparing the amplitudes of the input and the output at different frequencies of the sine wave signal. Since the developed shaker table is the displacement control table and the sensor used to measure the response is the

accelerometer, comparison of input and output required either differentiation of the input signal or the integration of the output signal. The purpose of output only analysis is to analyze the frequencies content of the signal. This analysis yields the capacity of the shaker table to replicate the input signal and identifies the shaker table frequency performance limitations. Numerous tests at various frequencies were conducted. Two tests reported here are the testing at a frequency of 2.55 Hz, and the testing at a frequency of 17.1Hz. These two frequencies were considered as low and high frequencies in analyzing the shaker table performance. Figure 5.7 shows the amplitudes of the acceleration at the input displacement of 1mm and excitation frequency of 2.55 Hz. As shown in Figure 5.7, the peak magnitude of the acceleration is $0.235 m/sec^2$. As the magnitude of the acceleration is related to the displacement by the square of the excitation frequency, for the accurate replication of the test signal, the peak magnitude of the input acceleration is $0.25 \ m/sec^2$. The accuracy is acceptable for the testing purpose. Moreover, some distortions were observed in the response, as indicated by red circle shown in Figure 5.7. To find out the cause of the distortions, the same response signal is plotted in the frequency domain. Figure 5.8 shows the Auto spectrum density of the response signal. As shown in Figure 5.8, there are two peaks away from the excitation frequency (2.55Hz). The two peaks are at 5Hz and 7.5 Hz. These two peaks represent the higher order harmonics present in the signal. So, the distortions seen in Figure 5.7 are due to the presence of higher order harmonics in the signal. The causes to higher order harmonics are due to the noise from the bearing and the table itself. Similar results are reported in [78] that the cause to distortions is primarily due to the support bearings.
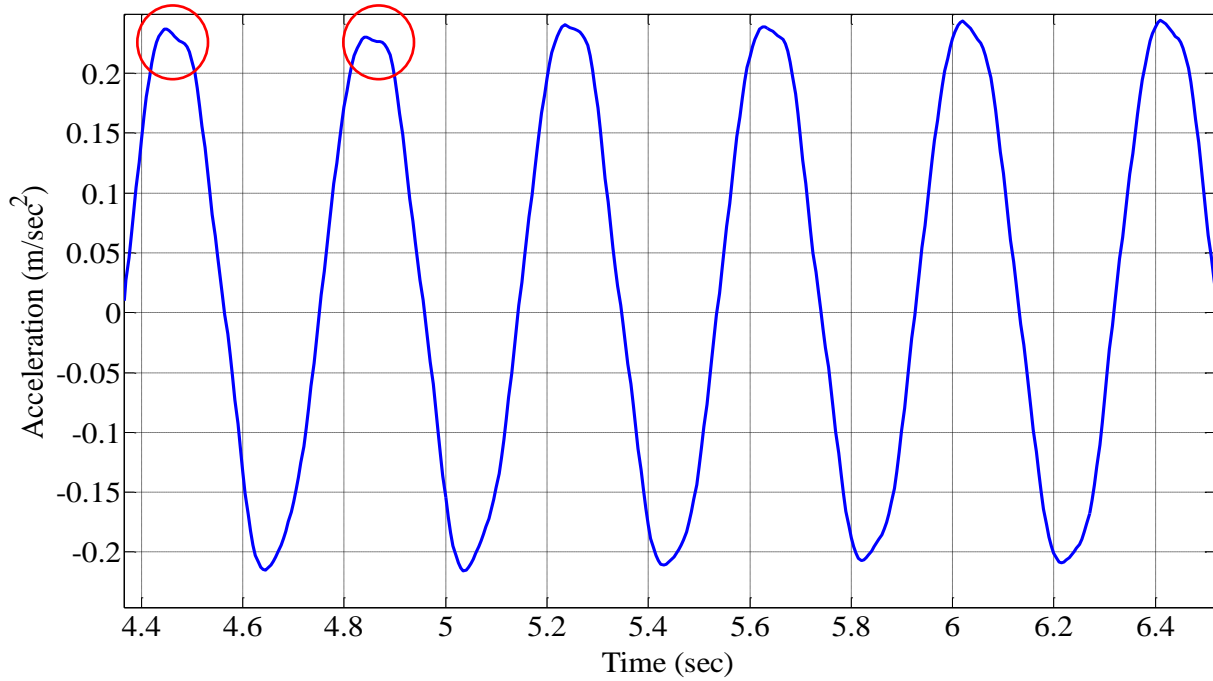
Figure 5.7: Acceleration Response of the Table at excitation Frequency of 2.55Hz (Input Displacement: 1mm
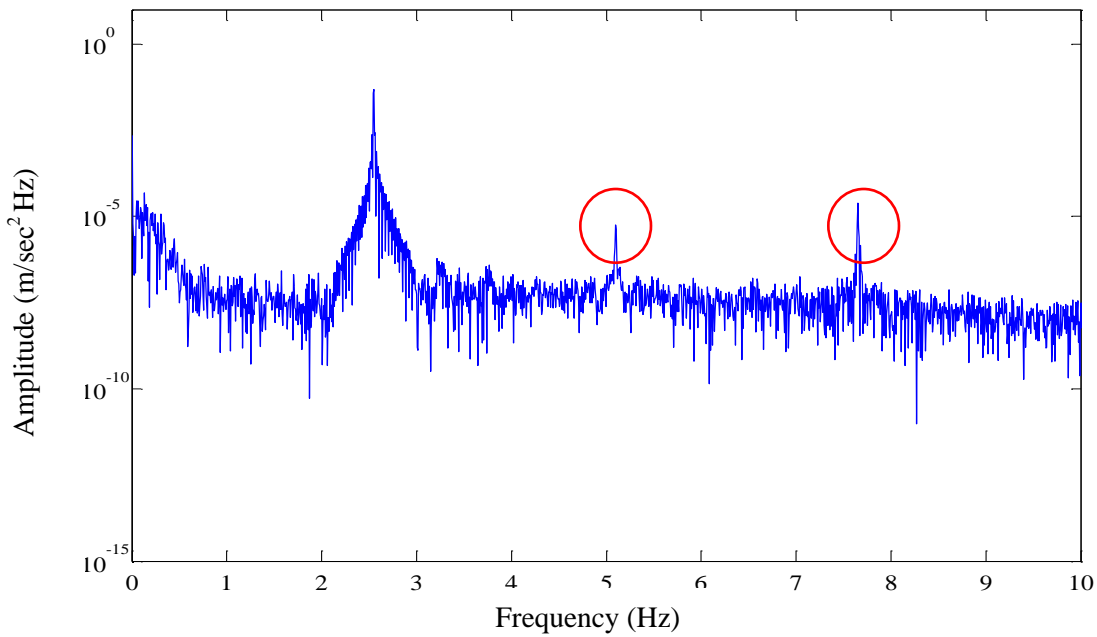
Figure 5.8: Acceleration Auto Spectrum (Excitation Frequency 2.55Hz)

Figure 5.9 shows the acceleration response of the table at the excitation frequency of 17.1 Hz, and the input displacement of 0.1mm. In order to compare the input and the output response of

the table, the input response to the table is integrated to obtain acceleration. The input output

response curve of the table is shown in Figure 5.10. As shown in Figure 5.10, the input and the

response signal matches well. Figure 5.11 shows the test conducted where the response was

measured from the actuator, isolating the response from the table. For this, a sine wave signal at

2.55Hz frequency and 20mm displacement was input to the system. The response was measured

from the actuator and was compared with the input. As shown in Figure 5.11, the input signal is

very close to the output signal. From this test it can be concluded that the distortion seen during

low frequency testing (2.55Hz) is due to the bearing and the table platform itself. As previously

discussed, this testing facility is primarily for the nonlinear system identification, the accuracy in

the produced displacement of the designed shaker table needs to be tested in the wide range of

frequencies. The test was carried out with the load of 2.5kN without the table and with the table.

A load cell was used to measure the force output of the actuator. During the tests, the amplitude

spectra at each excitation frequency were recorded. The frequency of the input loading varied

from 0.1Hz to 100Hz. Figure 5.12 shows the plot of the displacement against the frequency in a

logarithmic scale. As shown in Figure 5.12, there are three curves: blue, green and red. The blue

curve represents the displacement output of the actuator, when the force from the actuator was

maintained at 2.5kN (recorded by load cell) with different frequencies. The green curve

represents the displacement output of the actuator with varying force at different frequencies.

The red curve represents the displacement of the table at different frequencies. As seen in Figure

5.12, the amplitudes of displacement with and without table are fairly close to each other

indicating the effect of the table is negligible. The displacement of the table can be achieved up

to 40mm below 10 Hz. As seen in the literature [63] most of the vehicle components have the

first natural frequency below 10Hz, this test setup is very useful for the nonlinear system identification of the vehicle components.
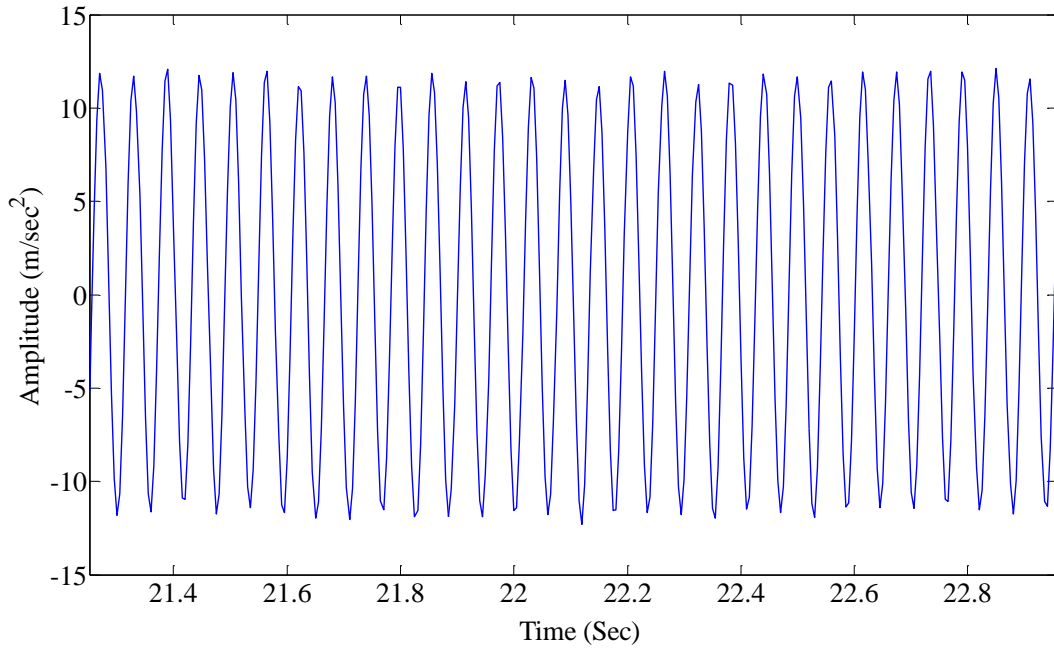
Figure 5.9: Acceleration Response of the Table at the Excitation Frequency of 17.1 Hz
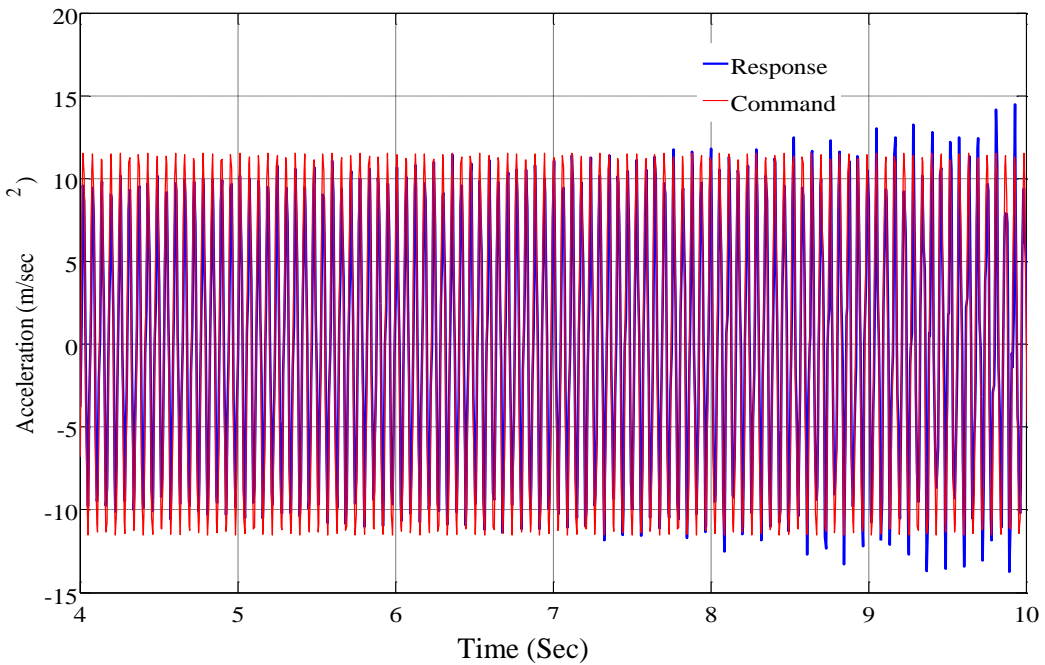
Figure 5.10: Comparison of Acceleration Time Histories of Shaker Table (Acceleration Time Histories with the Excitation Frequency of 17.1Hz)
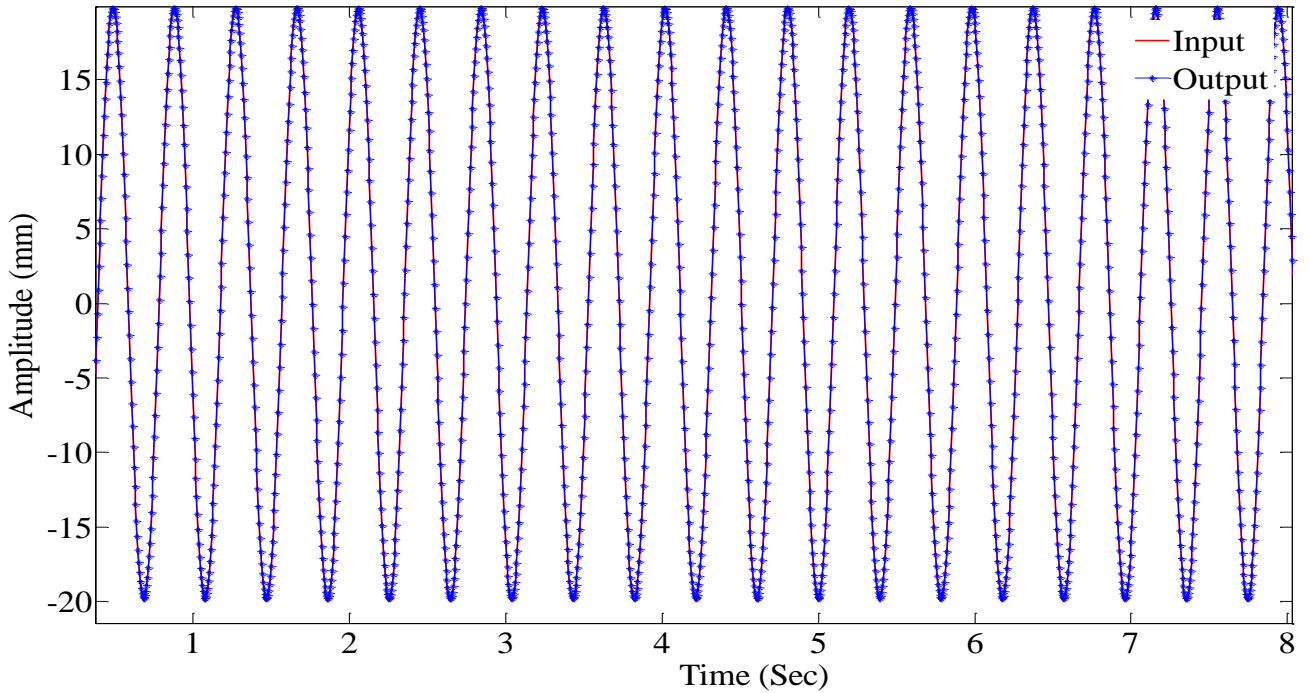
Figure 5.11: Comparison of Command and Response Actuator Time Histories
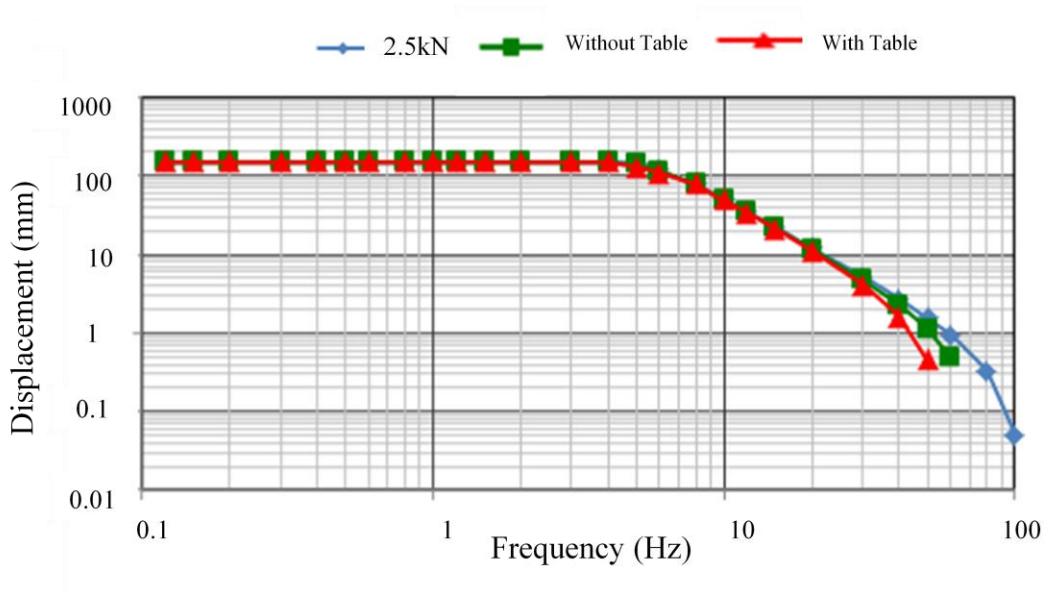
Figure 5.12: Performance Curve of the Shaker Table

5.1.3 Summary

A single axis shaker table for the demonstration of nonlinear system identification was developed and installed at the University of Manitoba. The designed shaker table has the same

configuration and the functions as those used in the industrial setting, but with a lower range of power due to cost. The challenge is to avoid the interactions between the shaker table and the testing specimen; i.e., the natural frequencies of the table should be significantly higher than the operating frequencies. Other design criteria include high stiffness and moderate mass. In this chapter the design and fabrication of the shaker table addressing the above challenges was presented. The key points presented are as follows.

- The fundamental natural frequencies of the table are well above the frequency range of operation, which indicates that the stiffness of the table is significantly high.

- The tests using harmonic signals showed that the displacement, as well as the acceleration time histories for the input and the response matches well. However, some errors are noticed at the low frequencies.

- The distortion seen in the waveform is due to the low cost support bearings and the table itself.

5.2 Demonstration of Force Reconstruction Technique in a Cantilever Beam

The force reconstruction technique using the base excitation as an input proposed in Chapter 3 was implemented in the experimental settings. A cantilever beam was used for the demonstration. As vibration motion is always along the excitation DOFs, there is no scientific relevance/significance of testing the complex structure. So, the transverse vibration of the beam is a good example for the analysis and for interpretation of the results. This section provides the detailed testing setup, test procedure, data acquisition and processing, and the results obtained from the experiments.

5.2.1 Test Setup

The test setup consists of a shaker table platform excited with servo-hydraulic actuators to simulate different types of periodic and random motions, such as artificial ground motions and other dynamic testing signal of interest in the laboratory. The details of the test setup are shown in Figure 5.13. It consists of a hydraulic pump, actuator, shaker table, beam, data acquisition board, and a computer. The hydraulic systems are marketed by MTS Systems Corporation. The shaker table is the uniaxial (horizontal) table constructed with in-house knowledge and fabrication capability. It consists of a table platform, ball bearing with the rail guide and the reaction mass. The test beam is made of Aluminum T6061, which has the following dimensions: length: 0.97m; width: 0.0254m; and, thickness: 0.003175m. The dimensions were chosen to make the beam flexible so as to excite the maximum number of modes resulting from the base motion. Typically base motion varies from 0.1 to 60Hz. The thin cross-section of the beam made it possible to easily excite the first three modes of the beam. One end of the beam is fixed to the shaker table with the fixture and the other end remains free. A four channel data acquisition board "DT9837" from Data Translation [78] is used which is connected to the computer through

a USB cable. For the purpose of response measurements from the shaker table and the beam, PCB accelerometers from Dalimar Instruments Inc. are used. A multipurpose test suit is used for running the hydraulic system while the "VIB Point 2.0" software is used to extract the response data from the beam. Three accelerometers are mounted on the beam and one accelerometer is mounted on the table. The accelerometers are mounted at the tip, 0.67m, and 0.3m measured from the fixed end.
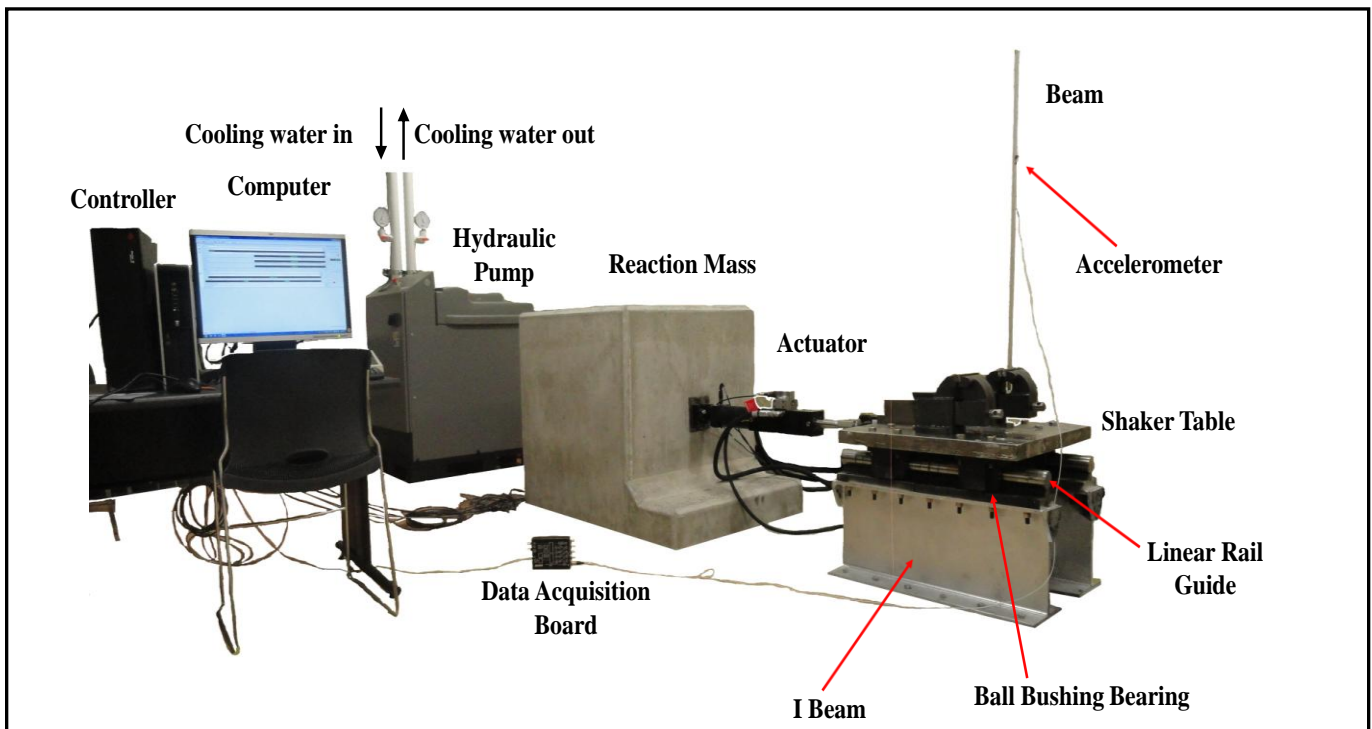
Figure 5.13: Experimental Set-up for Vibration Testing

5.2.2   Test Procedure

This section describes the modal analysis procedure, types of loading used and the results obtained in each stage of the proposed methodology. In chapter 3 a modal based method for the force reconstruction was presented. In this section the demonstration of this method is presented using the experimental data.

As shown by Equation (3.16) in Chapter 3 of this thesis, the force reconstruction procedure has three parts. Part I: conventional modal analysis based on the system Equation (3.1), Part II: measurement of the acceleration response vector at different locations of the beam and Part III: extraction of the pseudo excited force vector. For the implementation of Part I, the guidelines presented for the modal analysis in a base excited structure [39-40] is followed. The conventional modal analysis on system matrices shown in Equation (3.1) yields modal damping ratios, natural frequencies, mode shapes and modal mass of the system. To perform the modal analysis, two types of loadings are applied: (a) sweep sine and (b) random vibration impulse input. The sweep test is used to find out the modal damping ratios and natural frequencies of the beam, whereas the random vibration impulse input is used to extract the mode shapes. Homogeneity and reciprocity are verified with the above mentioned loadings. To estimate the natural frequencies and the modal damping ratios, a swept sine wave starting from 0.1Hz and ending at 50 Hz at an octave rating of 0.1octaves/min is applied. Three natural frequencies of the beam are observed at 2.52 Hz, 16.0, and 42.2 Hz respectively. The observed natural frequencies of the beam are close to the theoretically derived natural frequencies, which show that the beam is lightly damped. The modal damping ratio is estimated using the half power bandwidth method. The half power bandwidth methods yields the modal damping ratios of 0.028, 0.008 and 0.0065 at first, second and third mode respectively.

Part II presents the measurements of the acceleration vector at low base displacement for the extraction of the pseudo force vector. In this part, a sinusoidal loading profile with a base displacement of 0.1mm at the frequency of 16Hz is applied. Figures (5.14-5.16) show the absolute value of acceleration response data obtained by exciting the beam with a base displacement of 0.1mm. The response of the table measured by the accelerometer is shown in

Figure 5.17. As seen from Figures (5.14-5.16) the steady state acceleration response of the beam starts after 5 sec.
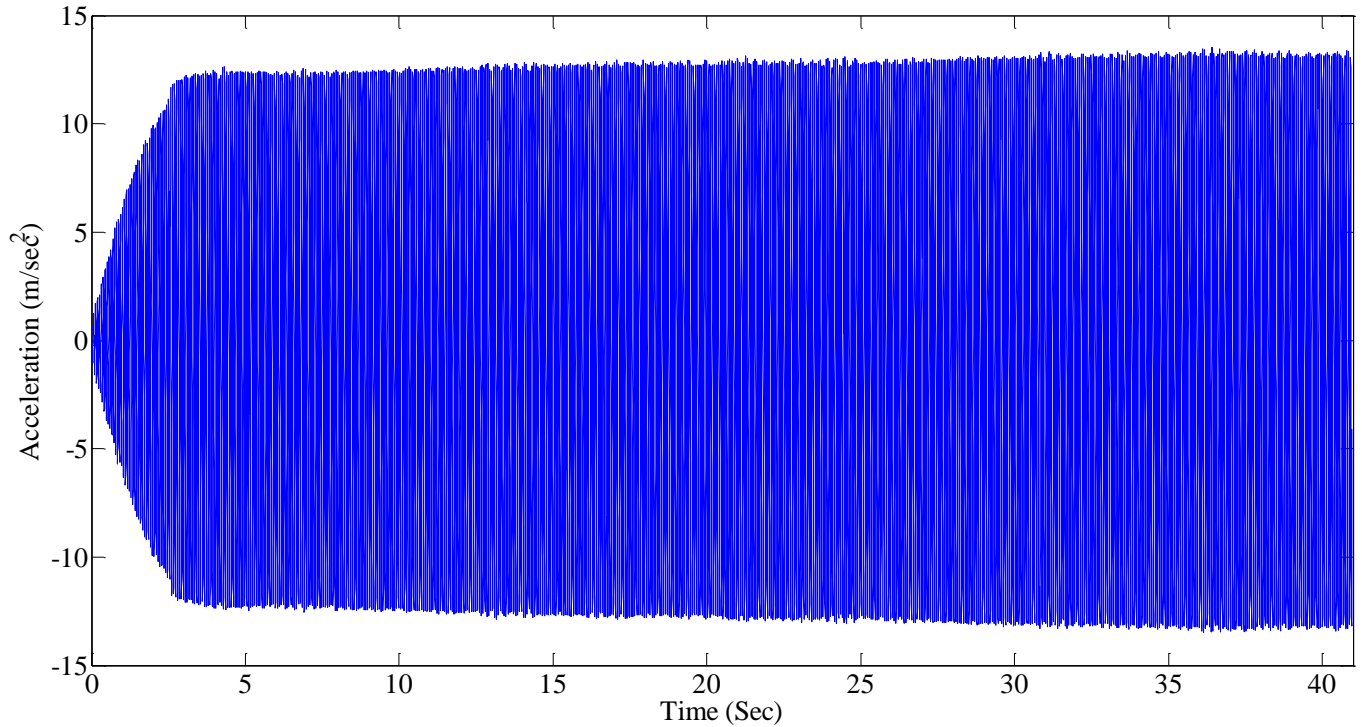
Figure 5.14: Absolute Value of Acceleration Measured at the Tip of the Beam

In order to use Equation (3.16) to reconstruct the force, relative acceleration, velocity and the displacement vector of the beam are needed. To calculate the relative acceleration vector at each DOF, the table acceleration response vector is subtracted from the absolute acceleration response vector at each DOF. Having acceleration response vector at each DOF, the steady state relative velocity and displacement vector can be obtained by using Equations (3.33-3.35), which shows the analytical integration in the measured acceleration response data. The use of Equation (3.33) requires multilinear least square regression at each successive time interval. A multilinear least square regression algorithm is applied to the steady state measured relative acceleration data at each DOF in order to approximate the coefficients of the measured acceleration data given by
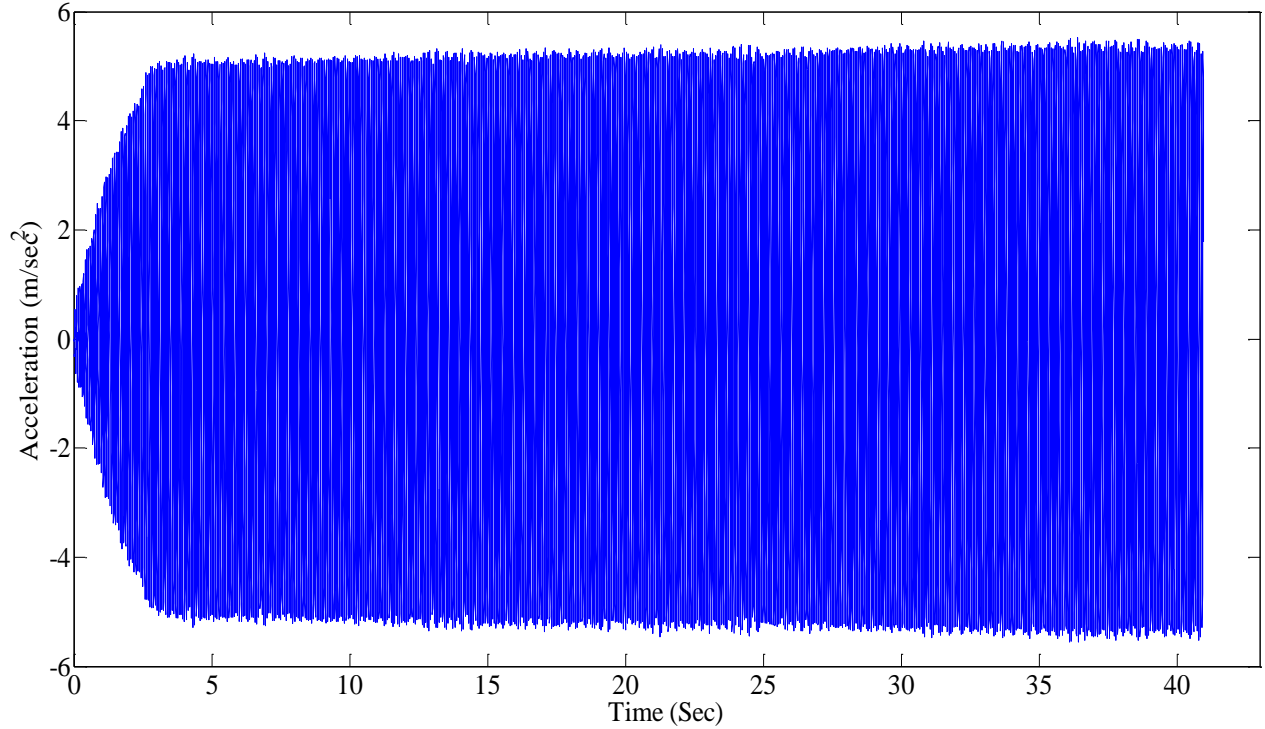
Figure 5.15: Absolute Value of Acceleration Measured at the Distance of 0.67m from the Fixed

End
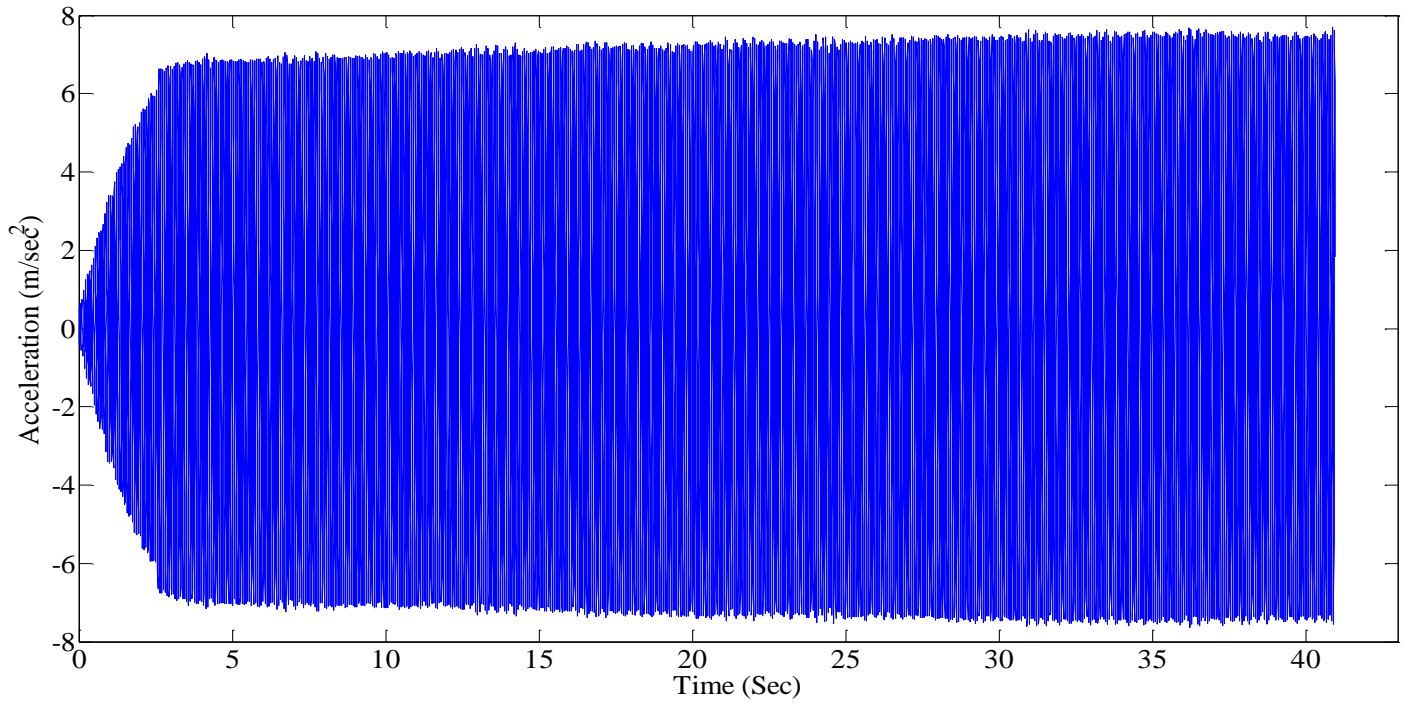
Figure 5.16: Absolute Value of Acceleration Measured at the Distance of 0.3m from the Fixed

End

79
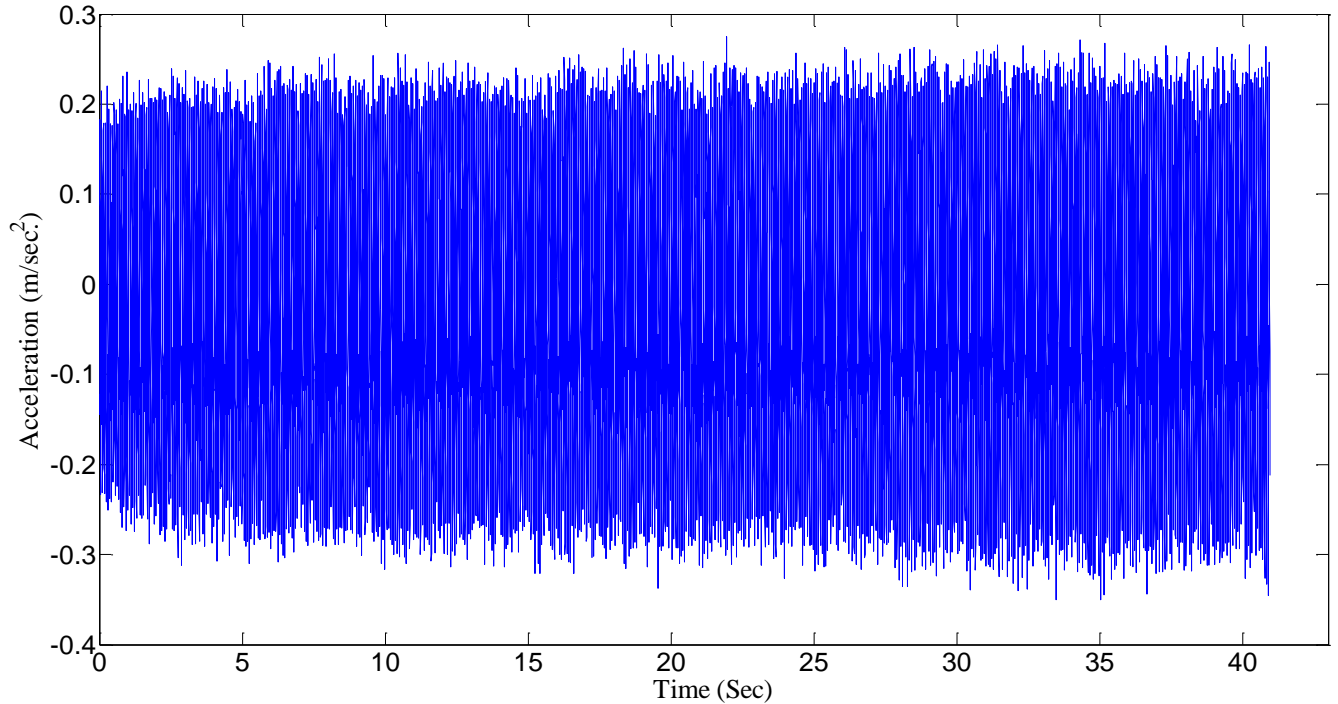
Figure 5.17: Acceleration Response of the Table

Equation (3.33). The measured and fitted steady state acceleration responses at each DOF are shown in Figures (5.18-5.20). Once the coefficients of the steady state acceleration at each DOF are obtained, the velocity and displacement at each DOF are obtained by using Equations (3.34-3.35). Once these parameters are obtained along with the mode shape matrix, Equation (3.16) is used to reconstruct the force. Figures (5.21 -5.23) show the reconstructed force at each DOF. These reconstructed force vector shown in Figures (5.21-5.23) has the effect of unmeasured DOFs and unidentified modes projected at the measured DOFs. Since the objective in this research study is to explore the effect of unmeasured DOFs and unidentified modes, the force vectors are reconstructed at each DOF by exciting the system in a frequency band around the natural frequencies of the system. For a first mode test, the system is excited with a step sine test varying around the first natural frequency of the system.
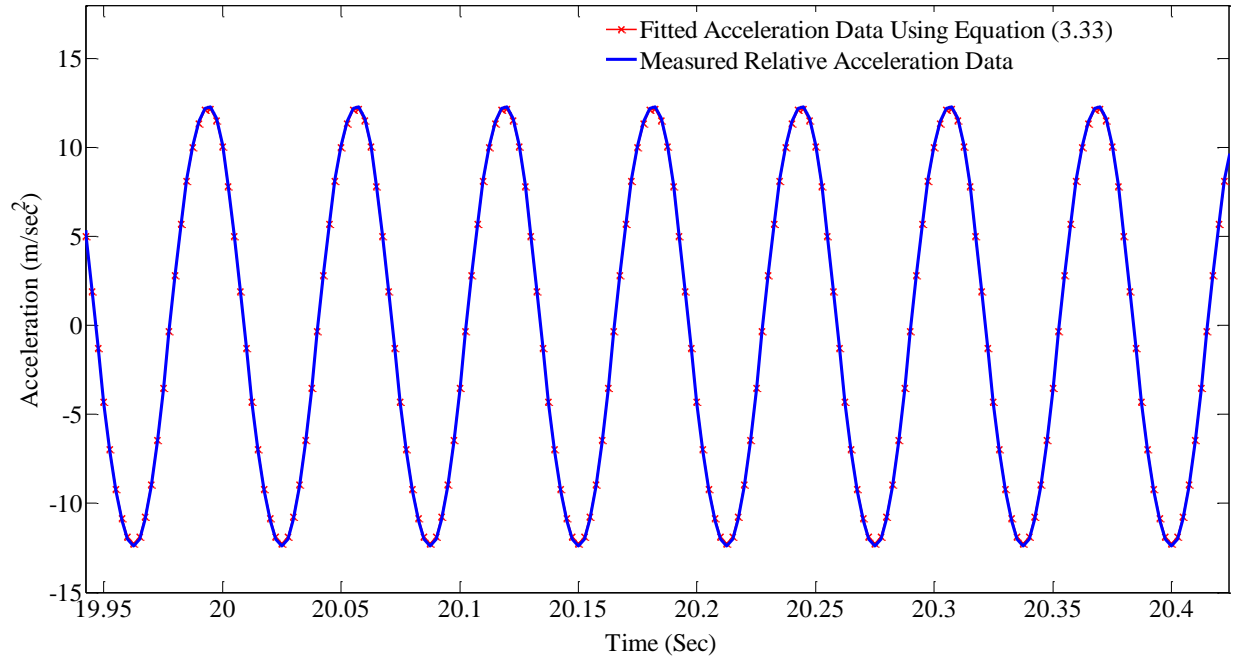
Figure 5.18: Measured and Fitted Steady State Acceleration Data at the Tip of the Beam
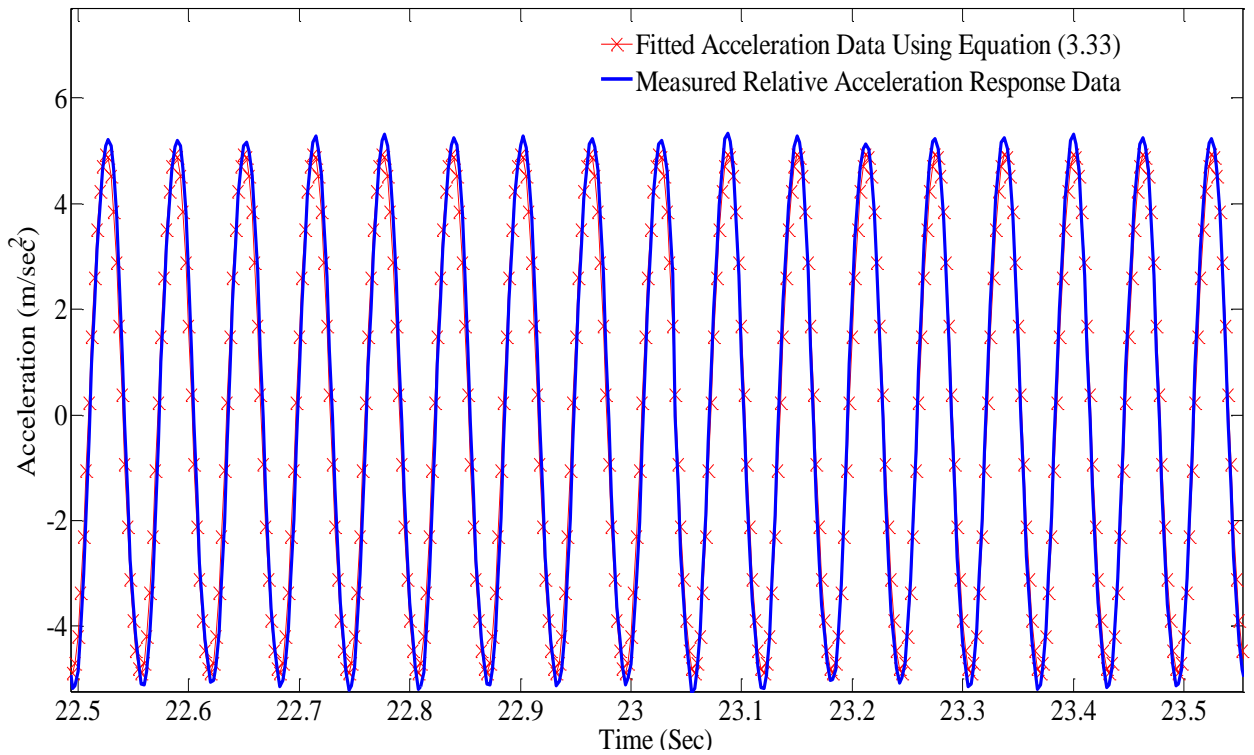
Figure 5.19: Measured and Fitted Steady State Acceleration Data at the Distance of 0.67m from
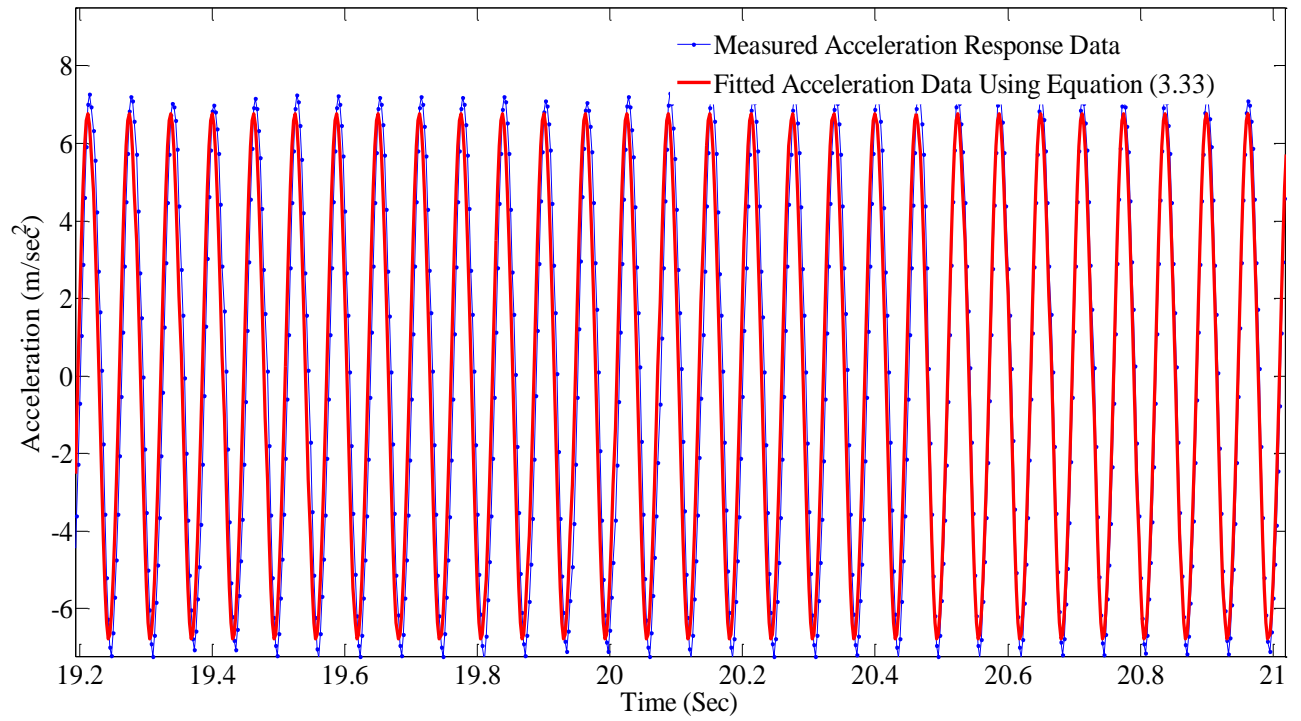
the Fixed End

Figure 5.20: Measured and Fitted Steady State Acceleration Data at the Distance of 0.3m from
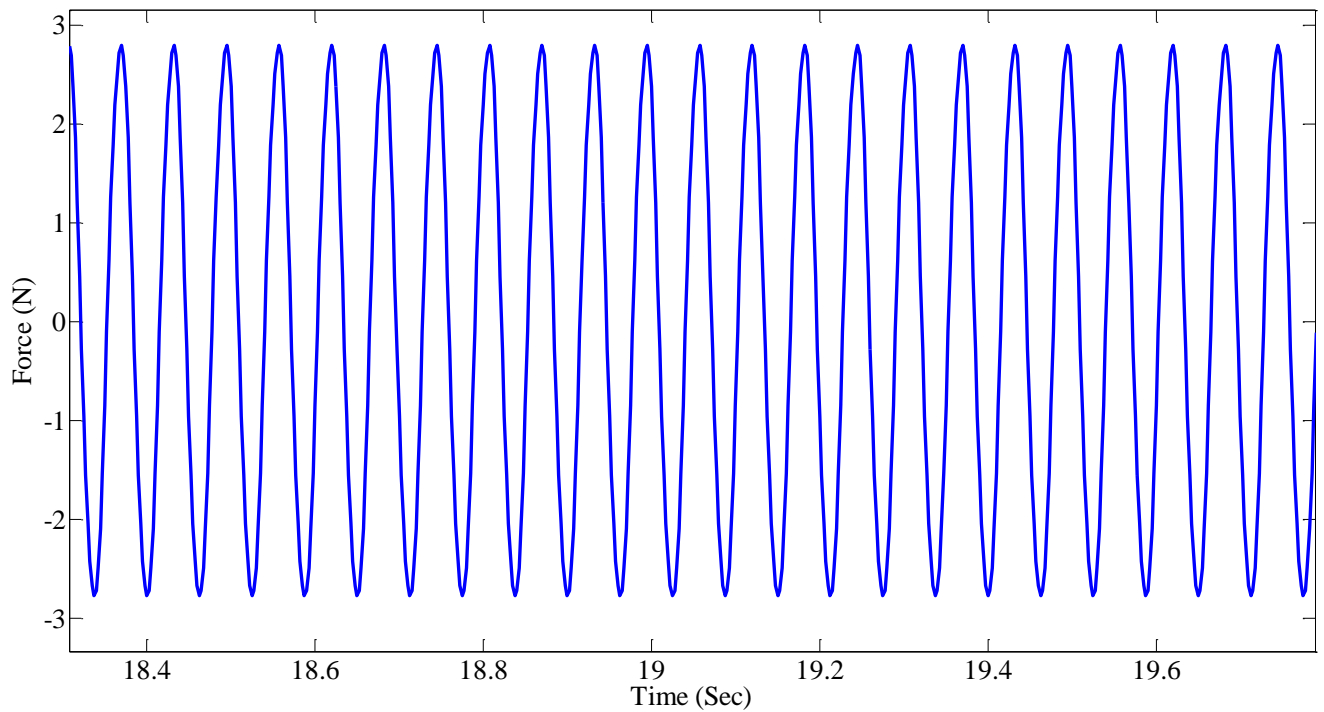
the Fixed End

Figure 5.21: Reconstructed Force at the Tip of the Beam
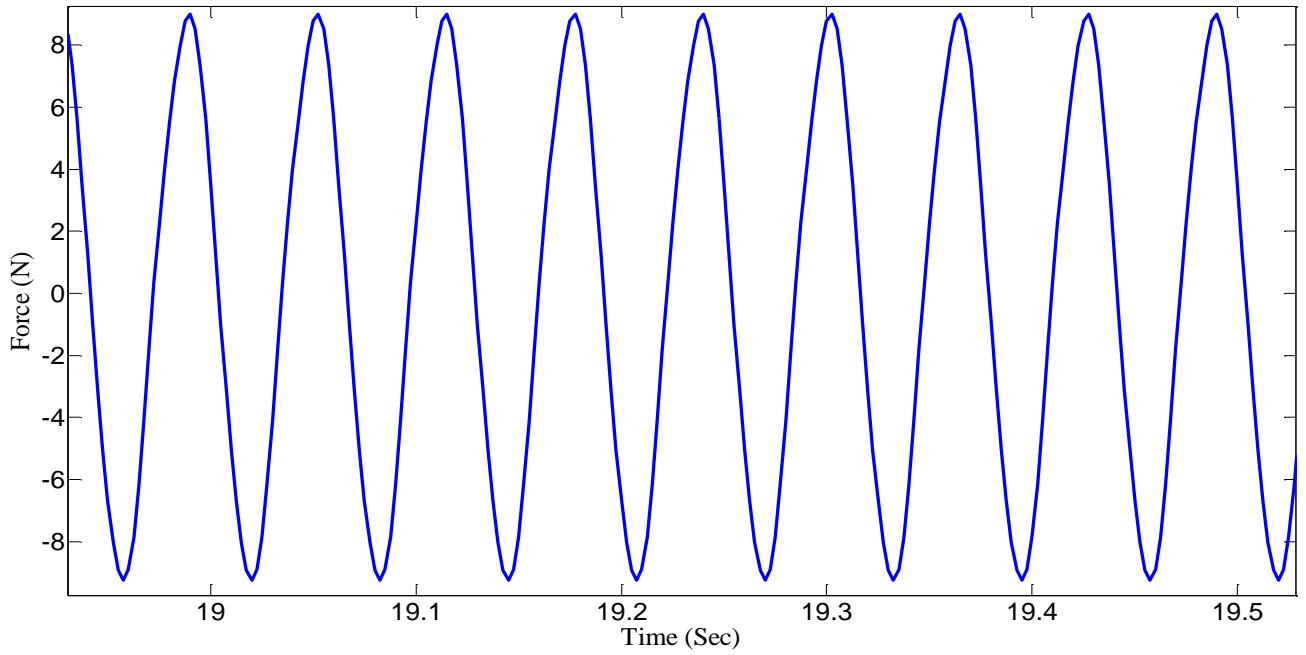
Figure 5.22: Reconstructed Force at the distance of 0.67m from the Fixed End
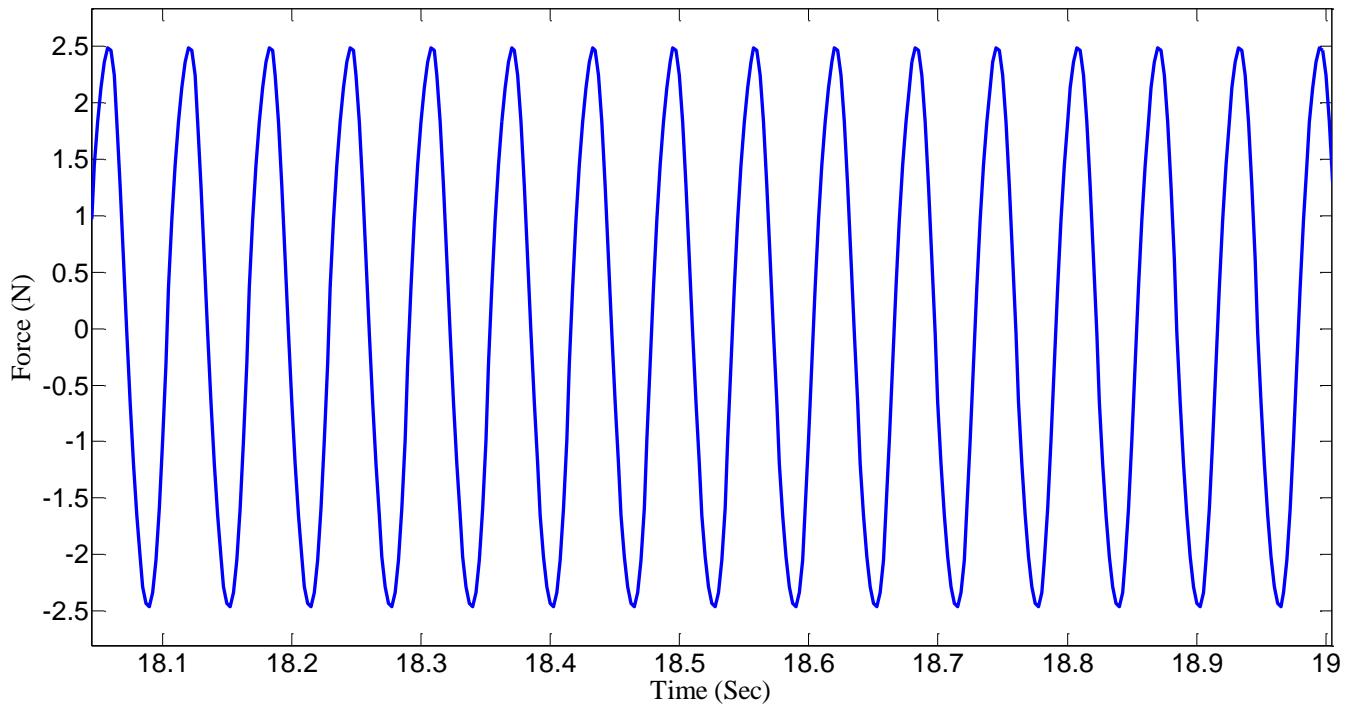
Figure 5.23: Reconstructed Force at the distance of 0.3mfrom the Fixed End

The reconstructed force given by Equation (3.16) is then compared with the equivalent excitation

force vector given by Equation (3.2). Figures (5.24-5.26) shows the plot between the

reconstructed force vector and the equivalent excitation force vector along the excitation frequency range. As shown in Figures (5.24-5.26), the equivalent excitation force vectors at the measured DOFs are varying as a quadratic function of the excitation frequencies. However, the reconstructed force vectors are not varying as a quadratic function of the excitation frequencies. This is due to the effect of the unmeasured DOFs and unidentified modes at the measured DOFs. This effect near the resonance is small as compared to the response away and below from the resonance which seems reasonable as, at resonance the response seems heavily from the excited mode only. As nonlinear system identification is heavily dependent upon the magnitude of the input force vector, this reconstruction of input force vector technique is the most valuable tool for nonlinear system identification.
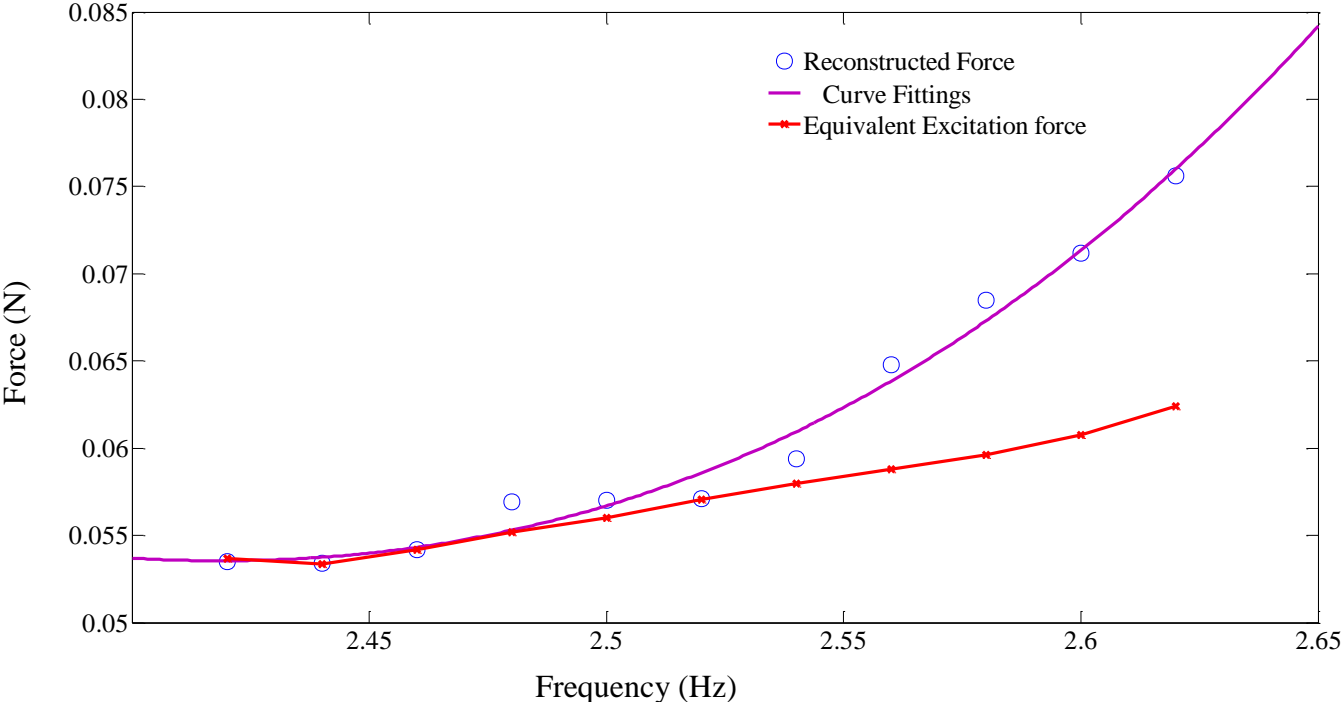
Figure 5.24: Comparison of Equivalent Excitation Force and Reconstructed Force at the Tip of the Beam
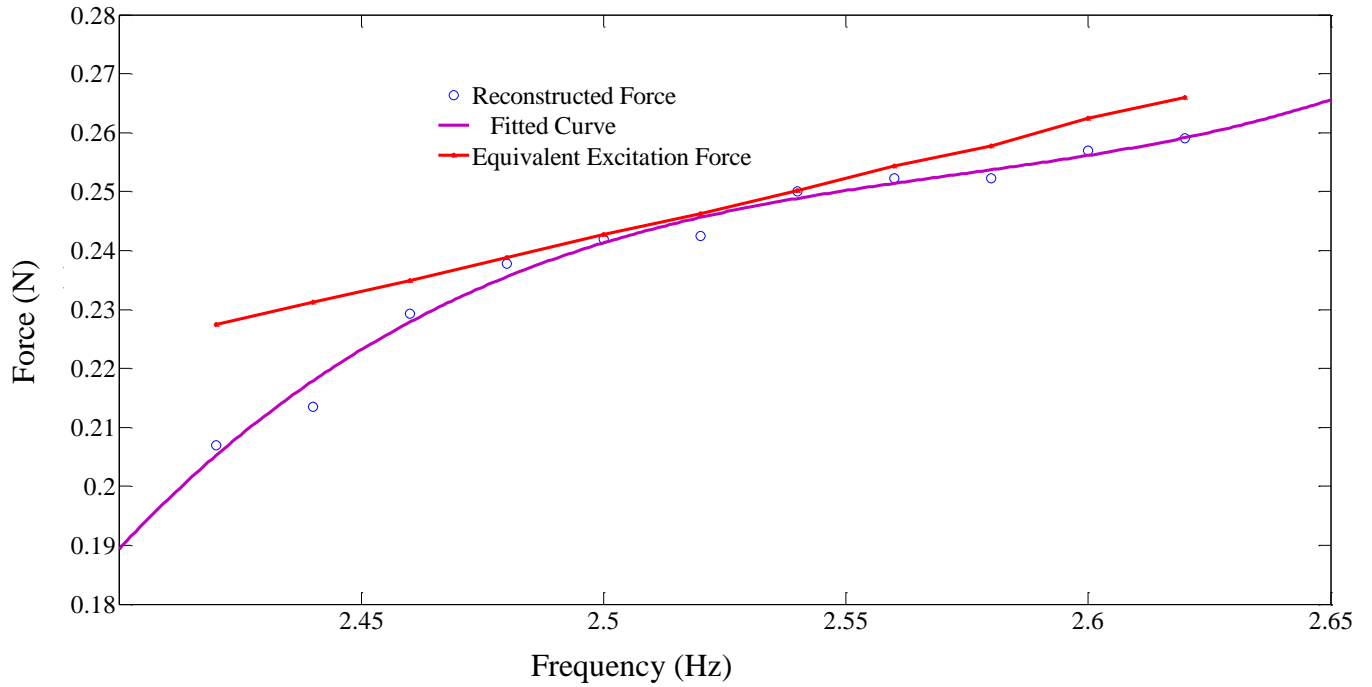
Figure 5.25: Comparison of Equivalent Excitation Force and Reconstructed Force at the Distance of 0.67m from the Fixed End
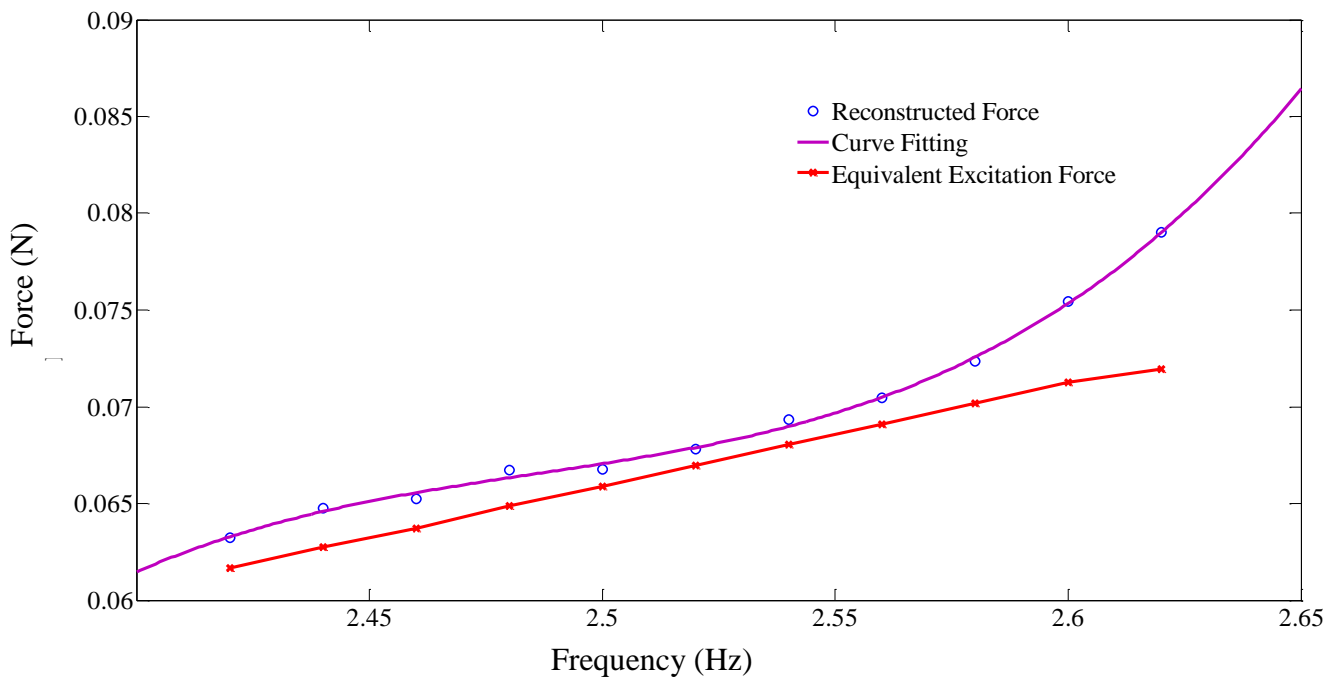
Figure 5.26: Comparison of Equivalent Excitation Force and Reconstructed Force at the Distance of 0.3m from the Fixed End

5.2.3 Summary

This Section demonstrates the force reconstruction technique using the base excitation as an input. This technique is demonstrated by using a cantilever beam as an example. The demonstration approach follows three steps: (a) conventional linear modal analysis with random excitation; (b) measuring the acceleration response vector with single sinusoidal/step sine test; and (c) reconstruction of force vector from the measured dynamics. Several experimental results are shown to demonstrate the methodology. This approach mimics the conditions of incomplete measurements for a continuous system and concludes that it is possible to obtain the excitation force at the measured DOFs only.

5.3   Nonlinear System Identification in Base Excited Structure

Two new methodologies for nonlinear system identification in base excited structure are proposed in Chapter 4. Both methods are based on the approach that combines force reconstruction, base excitation and nonlinear system identification. The first methodology identifies the system parameters in a physical coordinate system, while the second method works in the modal space. The proposed methods are intended to be implemented in an experimental setting. In chapter 4 the second method was shown in a flow chart (Figure 4.2) and was illustrated by a simulated example of 5 DOF model. The simulated results show that the proposed method is robust in estimating the nonlinearity even the modes are highly coupled. The same method is used for demonstration propose, using a cantilever beam as an example. This section presents the detail of the implementation of the method shown in Figure 4.2. Note that since the Section 5.1 and 5.2 of this chapter presents details about the test set-up and data acquisition, the implementation of this method and the results obtained from the experiments are presented in this section. As described in Section 5.2, three accelerometers are used to reconstruct the force vector. As nonlinear parameters are dependent upon the boundary conditions, to demonstrate the nonlinearity four accelerometers are used.

5.3.1   Test Description

A cantilever beam made of Aluminum T6061 is used for the demonstration purpose. The beam has the following dimensions: length: 1.05m; width; 0.0254m; and, thickness; 0.003175m. The dimensions were chosen to make the beam flexible so as to excite the maximum number of modes resulting from the base motion. The accelerometers are mounted at the tip, 0.63m, 0.3m, and 0.03m from the fixed end. The location of the accelerometers is obtained from the FE (finite

element) model so that there is no nodal point and the beam has the maximum vibration motion on those selected locations.

5.3.2: Experimental Implementation of Nonlinear System Identification

The implementation of the nonlinear system identification method, proposed in Figure 4.2, is carried out in three stages: Stage I involves first conventional modal analysis based on the system Equation (3.1); second, measurement of the acceleration response vector at different locations of the beam, and thirdly reconstruction of the force vector. All these three parts follow the same procedure as discussed in Section 5.2. Since the dimension of the beam, the locations of the accelerometers and the number of accelerometers used for analysis are different from Section 5.2, the results obtained in this stage are different such as the natural frequencies changes with respect to the mass of the accelerometer. The number of accelerometers (mass) and the length of the beam change the natural frequency of the beam. Three natural frequencies of the beam are observed at 2.55Hz, 17.1Hz and 47.3Hz respectively. The modal damping ratios obtained are exactly as measured in Section 5.2.

The second part of the stage I presents the measurements of the acceleration vector at low base displacement for the extraction of the pseudo force vector. In this part, a sinusoidal loading profile with a base displacement of 0.1mm at the first natural frequency was applied. The loading was applied for 90 sec in this test, whereas the response data are collected until the beam came to rest. There are two reasons to collect the data until the beam comes to rest. The first reason is that the accelerometers measure acceleration data, while the displacement data are required for using Equation (3.16). Zero initial and final conditions enable to perform leakage free integrations of response data in a frequency domain. The second reason is that there might be possible nonlinearities (normal and cross coupling) during the free decay. Figures (5.27-5.30)

show the relative acceleration response data (beam response data subtracted to the table response data) obtained by exciting the beam with a base displacement of 0.1mm. Some distortions in the response seen in response data were observed, as shown in Figures (5.27-5.30) at 92 sec. These distortions, shown by circles in Figures (5.27-5.30), are especially noticeable at low base motion. They are due to the changes in motion of the bearings from static to dynamic and then again back to static conditions. The distortion is more extreme near the fixed end of the beam as seen in Figure 5.30.
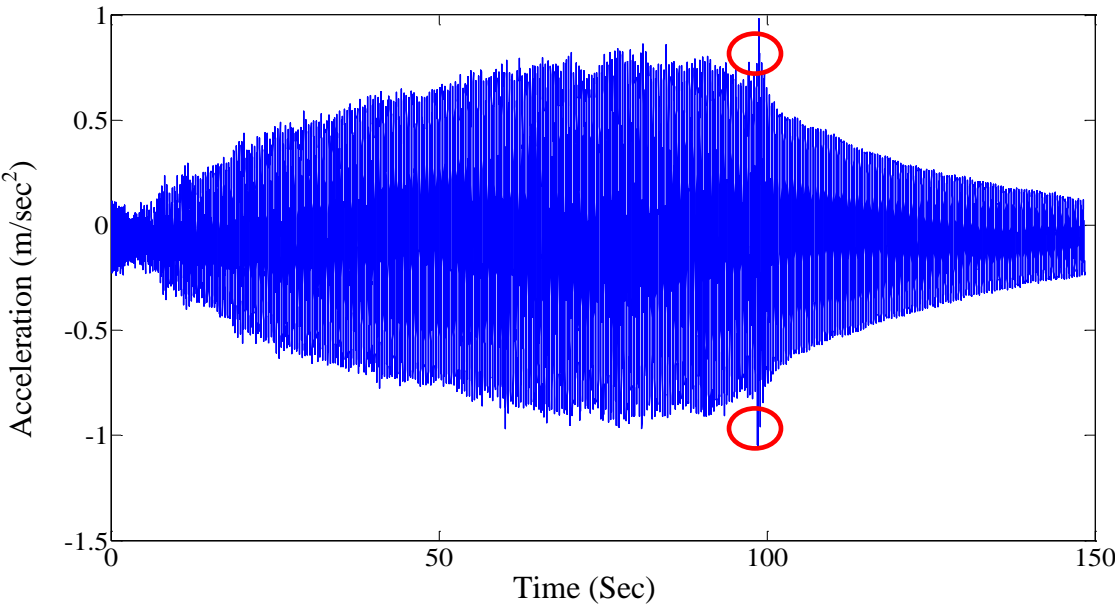
Figure 5.27: Relative Accelerations Vectors at the tip of the Beam
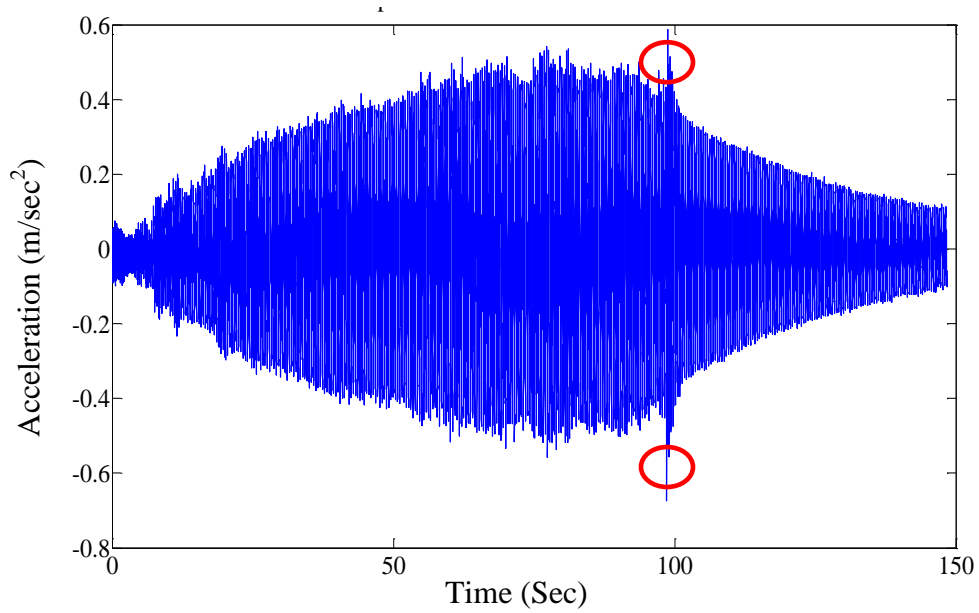
Figure 5.28: Relative Accelerations Vectors at the Distance of 0.63m from the Fixed End
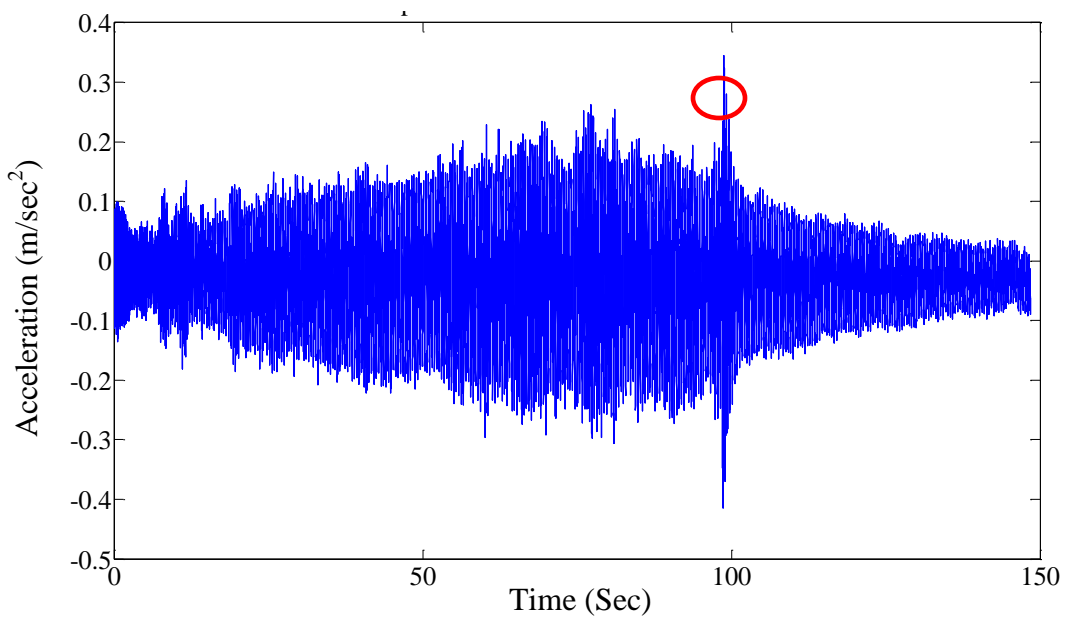
Figure 5.29: Relative Accelerations Vectors at the Distance of 0.3m from the Fixed End

90
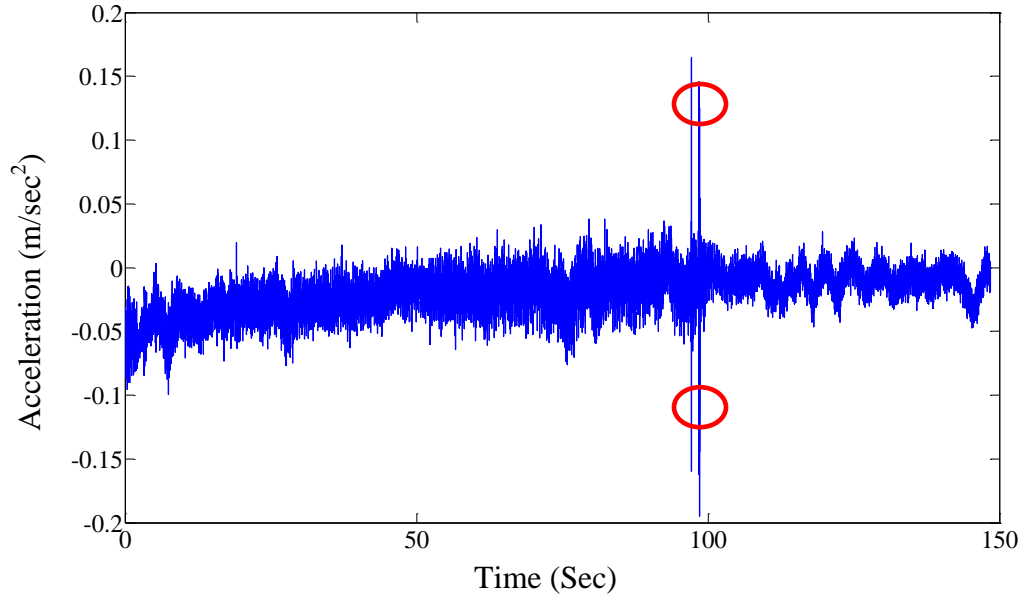
Figure 5.30: Relative Accelerations Vectors at the Distance of 0.03m from the Fixed End

In the third part, the reconstruction of the force vector at the measured degrees of freedom was carried out. The acceleration response data collected in Figures 5.27-5.30 are used to reconstruct the force vector at the measured degrees of freedom. The reconstructed force vector is obtained by using Equation (3.16). Figure 5.31 shows the magnitude of the force plotted against the analysis frequencies. As the excitation is at 2.55Hz, the peak magnitude of the force should be at 2.55Hz, which is clearly seen in Figure 5.31. The obtained force vector has the effect of unmeasured DOFs projected at the measured DOFs.
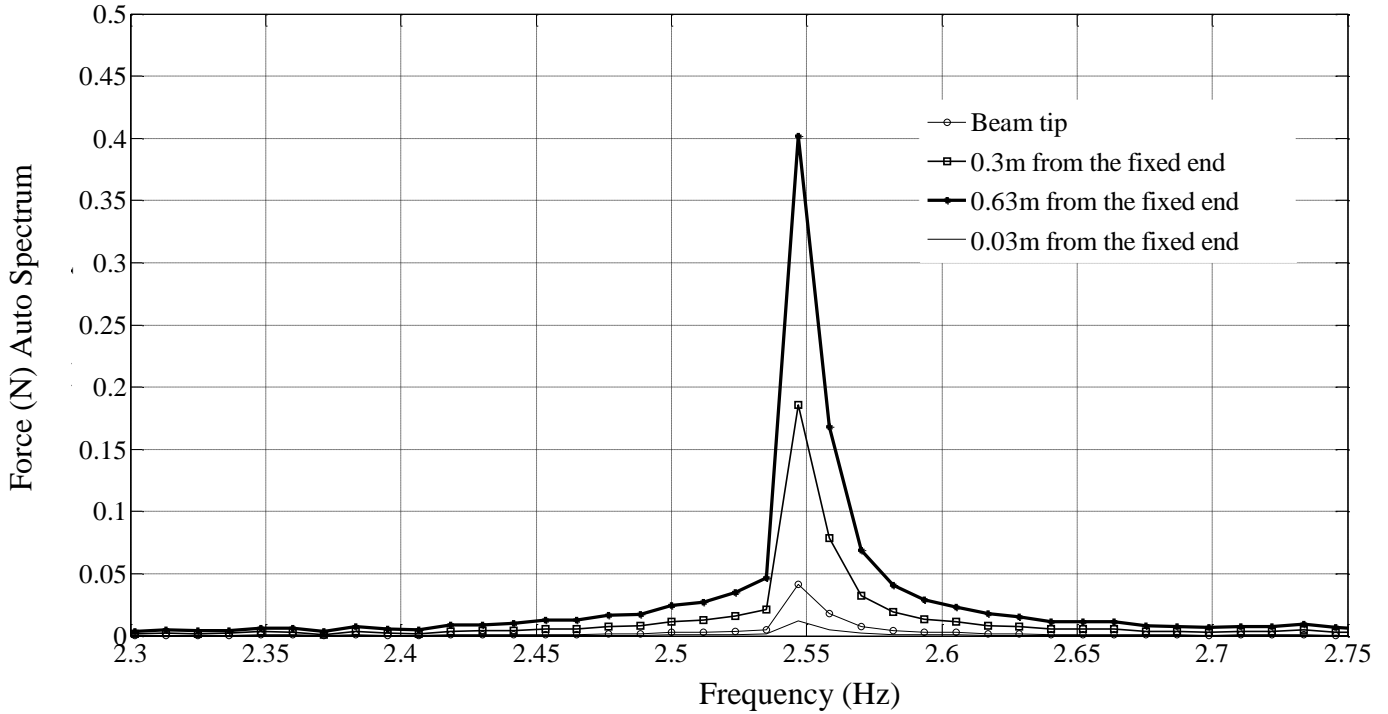
Figure 5.31: Absolute Value of Reconstructed Force Projected at the Measured DOFs Using Low Base Displacement

5.3.2.1 Extraction of the Nonlinear Restoring Force

The Second stage of the methodology (Figure 4.2) consists of exciting the system at high base displacement. There are three parts in stage II: acceleration response measurements at high base displacement, transformation of the response data into the modal space and the nonlinear restoring force extraction in the modal space. In this stage, the system is excited in the first mode frequency but at a higher level of the displacement such that the nonlinearities are excited if present in the system. The nonlinear response data are collected until the vibrating structure comes to rest. The reconstructed force vector for the high base displacement is obtained from Equation (3.16) assuming that the nonlinearity is independent to the mass. The acceleration response data are shown in Figures (5.32-5.35) and the obtained reconstructed force vector is shown in Figure 5.36.
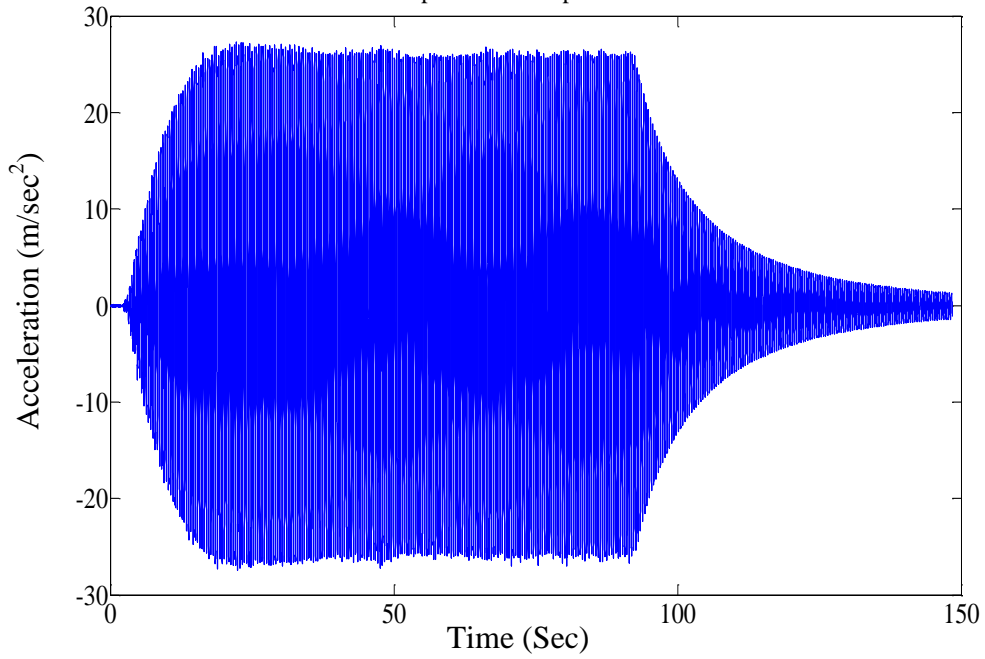
Figure 5.32: Relative Acceleration Vector at the tip of the Beam
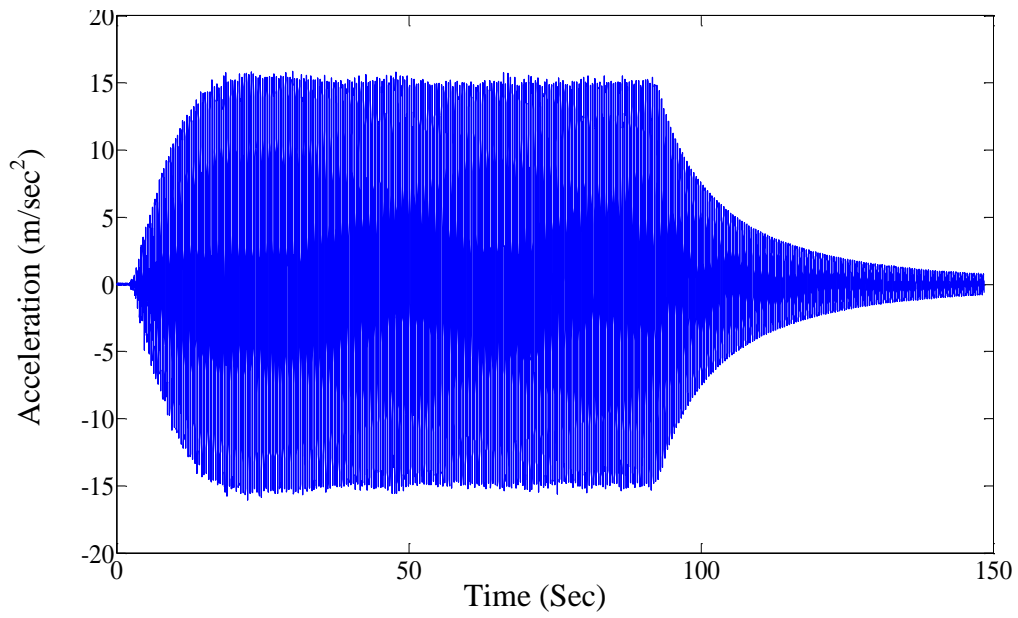
Figure 5.33: Relative Acceleration Vector at the Distance of 0.63m from the Fixed End
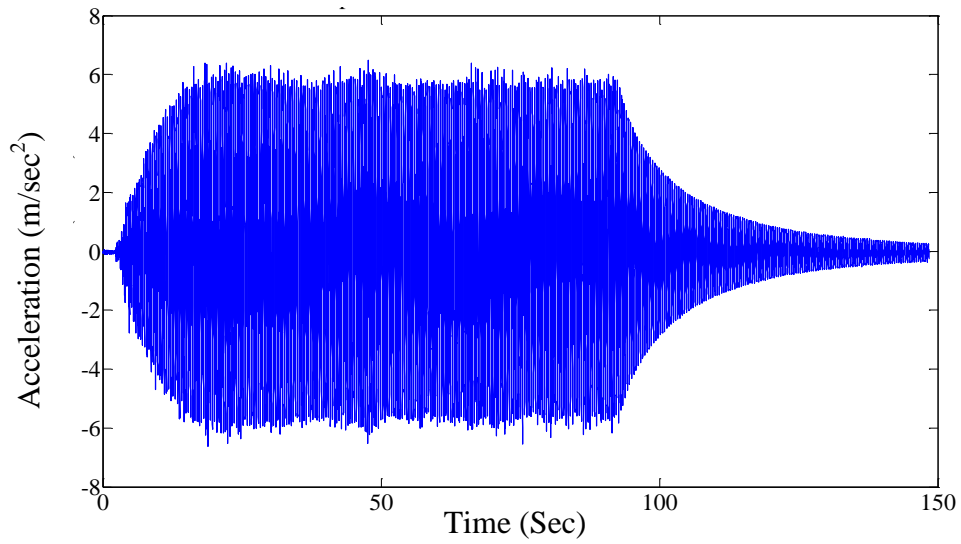
Figure 5.34: Relative Acceleration Vector at the Distance of 0.3m from the Fixed End
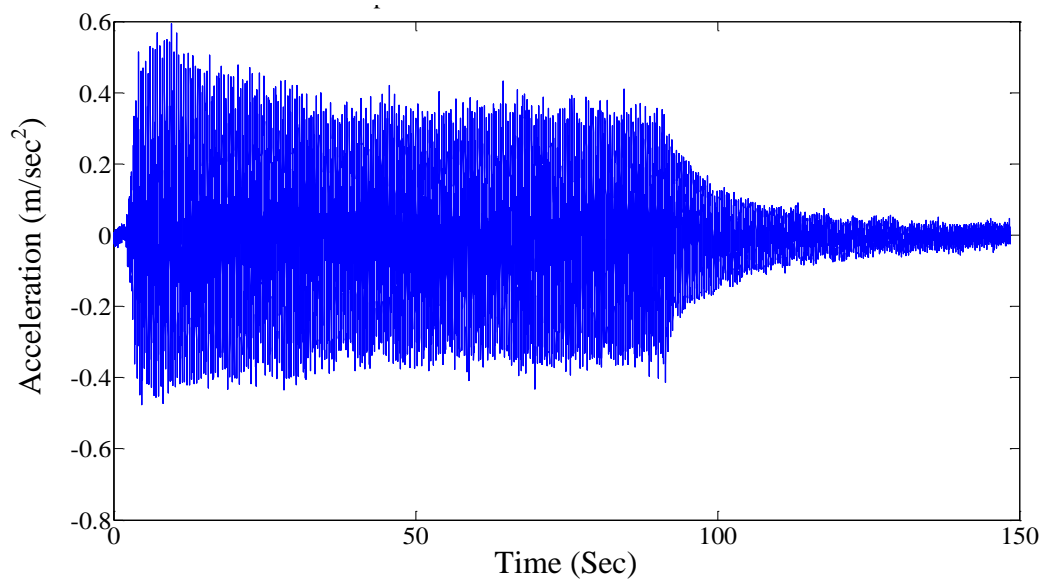
Figure 5.35: Relative Acceleration Vector at the Distance of 0.03m from the Fixed End
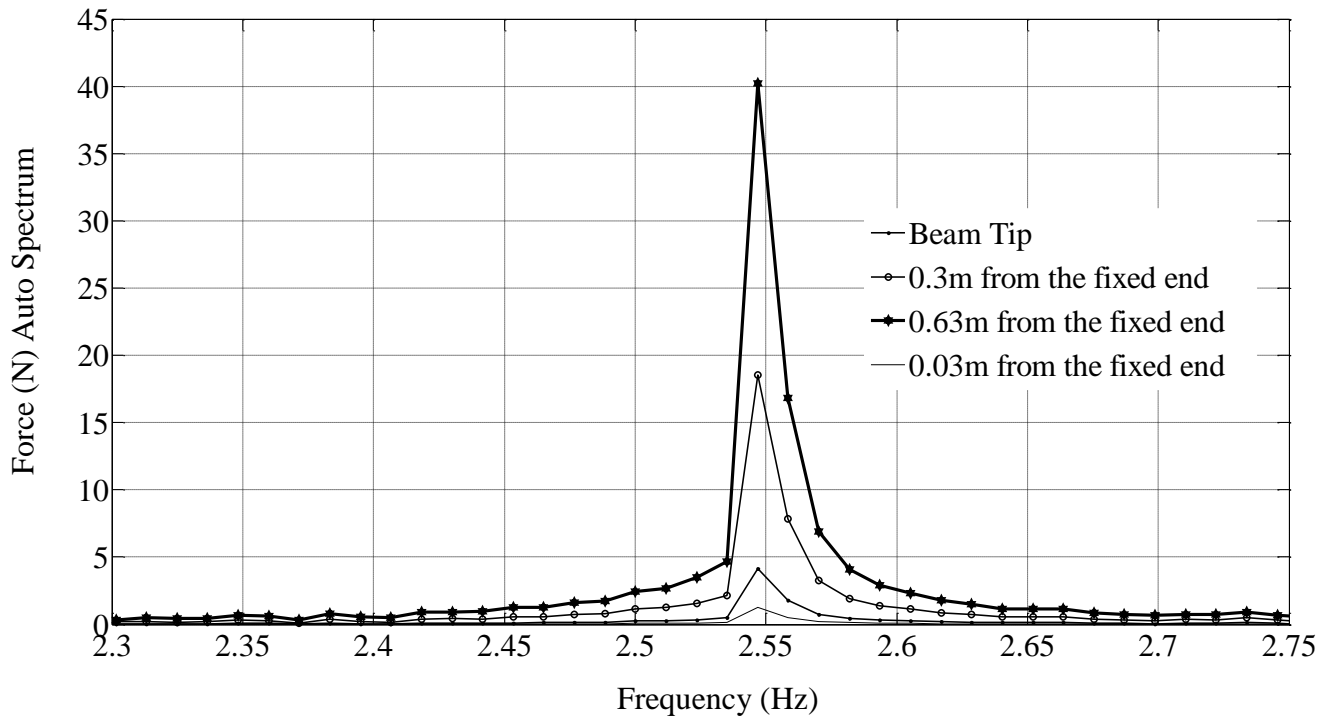
Figure 5.36: Absolute Value of Reconstructed Force Projected at the Measured DOFs Using

High Base Displacement

The second part of the stage two consists of transferring the measured responses and the pseudo force vector into the modal space. Following the theoretical methodology presented in Section 2.3, the response data shown in Figures (5.32-5.35) and the reconstructed force vector (Figure 5.36) are transformed into the modal space. Once the nonlinear response data and the reconstructed force vector are transformed to the modal space, the modal nonlinear restoring force for the excited mode is calculated using Equation (4.17). To calculate the nonlinear modal restoring force, we need the displacement data and the velocity data (using Equation (4.17) in time domain), which are obtained from the measured acceleration response data integrated in the frequency domain. The transformed modal response data for Modes 1, 2 and 3 are shown in Figures (5.37-5.39). Figure 5.37 shows the modal displacement at Mode 1 due to excitation at that mode. The response data, shown in Figure 5.38 and Figure 5.39, show the modal response at

Mode 2 and Mode 3, respectively, due to excitation at mode 1. The small response at Mode 2 and Mode 3 is due to two reasons. The first reason is that the imperfect excitation linear response also comes into modes 2 and 3. The second reason is the cross-coupling nonlinearity between Mode 1 and Mode 2, and Mode 1 and Mode 3.
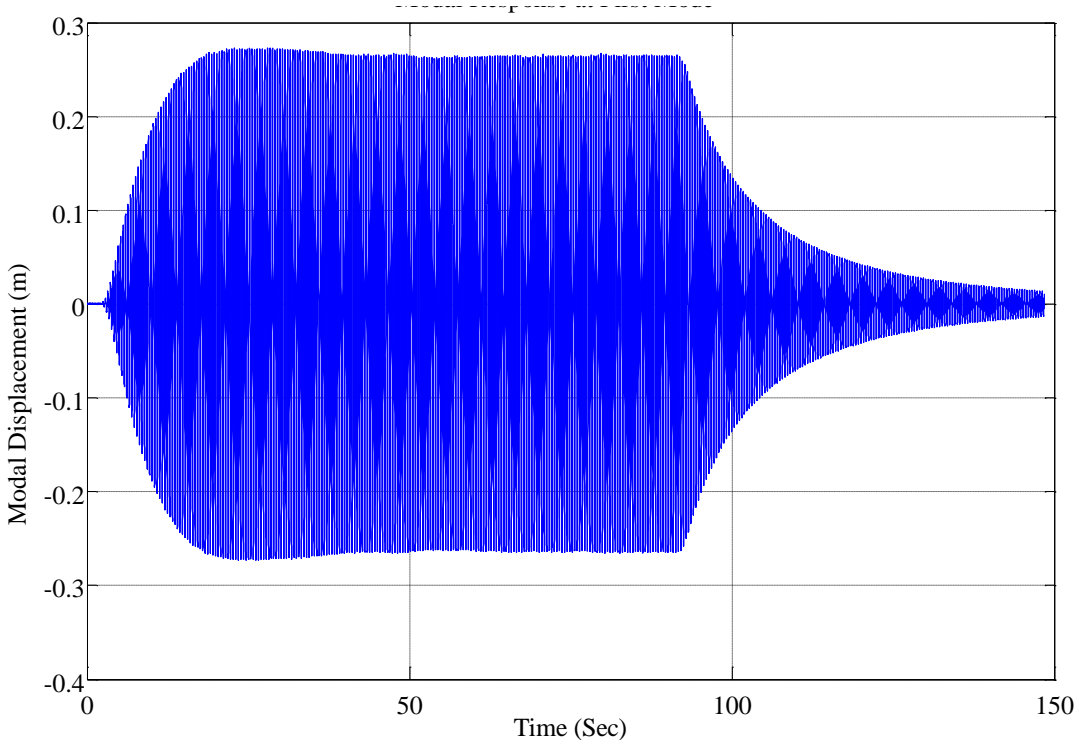
Figure 5.37: Modal Response at First Mode
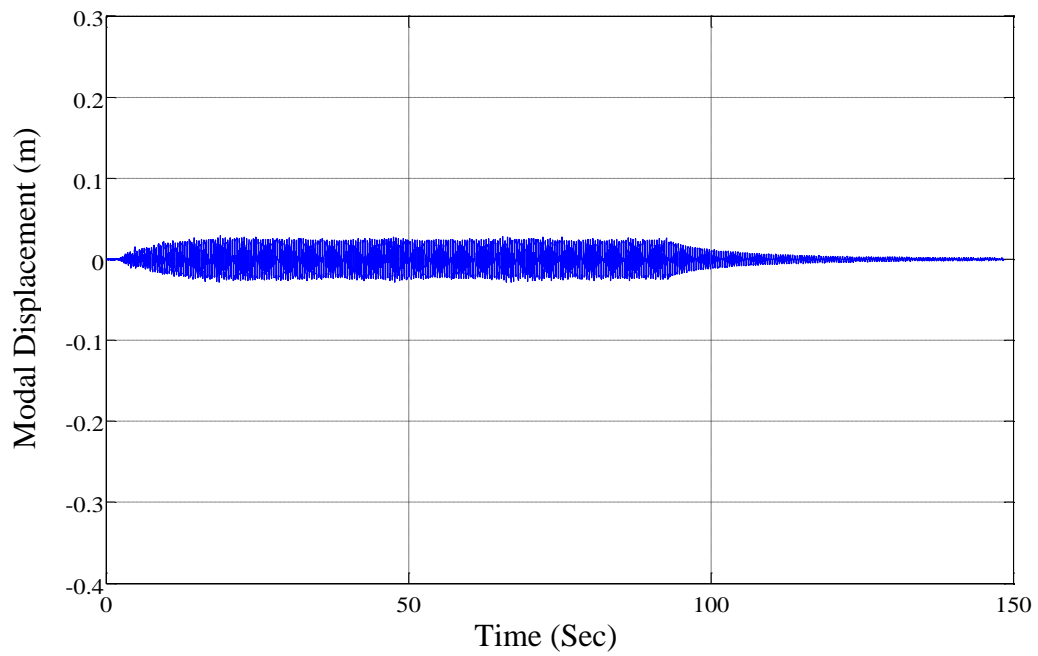
Figure 5.38: Modal Response at Second Mode
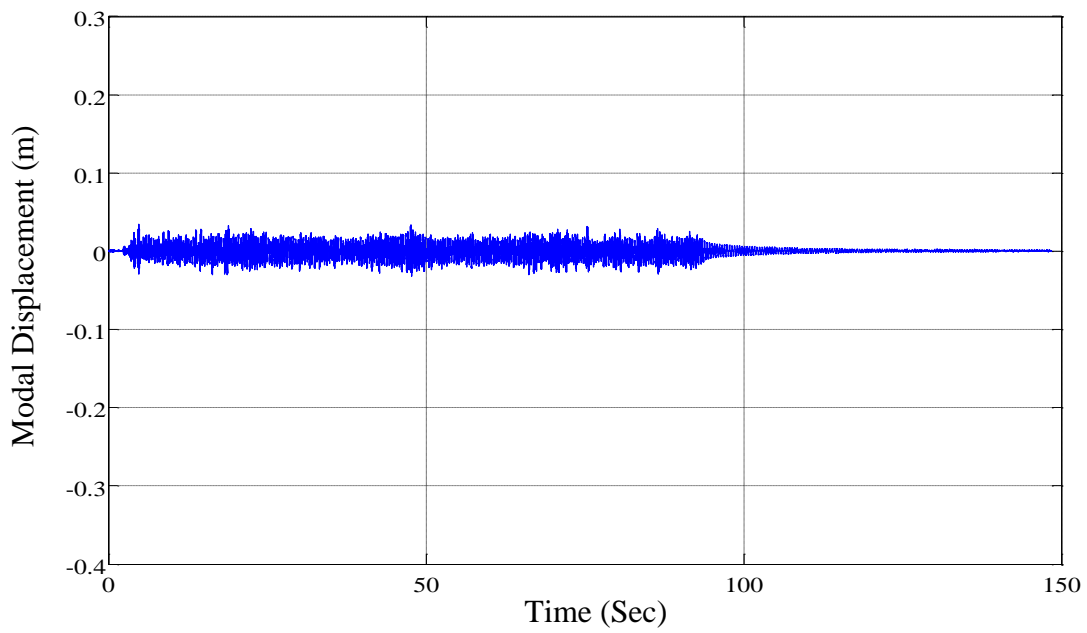
Figure 5.39: Modal Response at Third Mode

5.3.2.2 Estimation of the Nonlinear Parameters

The third stage of the methodology consists of the nonlinear parameter extraction in a modal space. A nonlinear restoring modal force in the form of discrete data for the excited mode is calculated in stage II. This nonlinear restoring modal force is now needed to be fitted, in a least square sense, by using a suitable curve fitting algorithm to identify the nonlinear parameters. A stepwise model building algorithm is chosen, which minimizes the error between the true and fitted nonlinear restoring force in the least square sense [14]. A stepwise model selection method is the simplest data driven model building approach. In this approach nonlinear variables are entered into the model one at a time. At each step, each variable that has not been in the model is tested for inclusion in the model. To determine which terms are significant and which terms can be safely discarded, the significant factor is calculated using Equation (4.27). The procedure is stopped when the mean square error between the fitted and the measured restoring forces is in an acceptable range given by Equation (4.26). The Goodness-of-Fit to the identified model is measured in terms of the minimum mean square error [14].

Figure 5.40 shows the Mode 1 restoring force calculated from the experimental raw data of the modal force and the acceleration in a red color. The identified modal restoring force (RFS) is over plotted at the same modal velocity and the displacement values in a blue color. The Goodness-of-Fit measured in terms of mean square error change was 0.97, which is an acceptable range for curve fittings [37]. The curve fit to Mode 1 showed significant cubic stiffness nonlinearity. When the coupling to Mode 2 and Mode 3 was included, it was found to be insignificant, so Mode 1 is essentially an only mode with direct nonlinearities, i.e., no cross-coupling nonlinear terms with Mode 2 and 3. There are no significant damping nonlinearities at the level of excitation. The nonlinear stiffness of the Mode 1 was found to be $4.97 \times 10^3 \frac{N}{m^3}$.
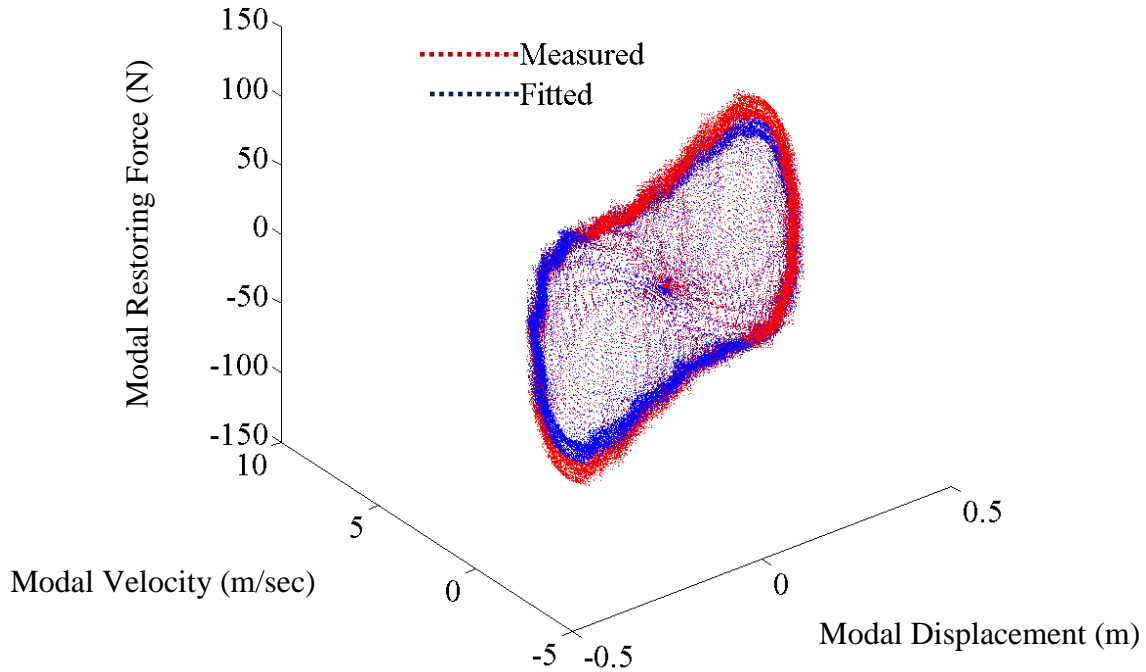
Figure 5.40: Measured Red and Fitted Blue Modal Restoring Force

Figure 5.41 shows the stiffness curve, which is the projection of RFS on XZ plane. Figure 5.41 clearly shows that the modal restoring force is significantly nonlinear. Figure 5.41 clearly indicates there is no nonlinear damping present in a tested cantilever beam. As nonlinear parameters are directly dependent on the excitation amplitude, the base excitation is increased to $1.1\ mm, 1.2\ mm$ and $1.3\ mm$. The above mention procedure for the nonlinear system identification is repeated. RFS for a base excitation of $1.1 mm$ is shown in Figure 5.42. From Figure 5.42, it is clear that there is no any coupling nonlinearity term. The RFS in Figure 5.42 shows the significant stiffness nonlinearity.
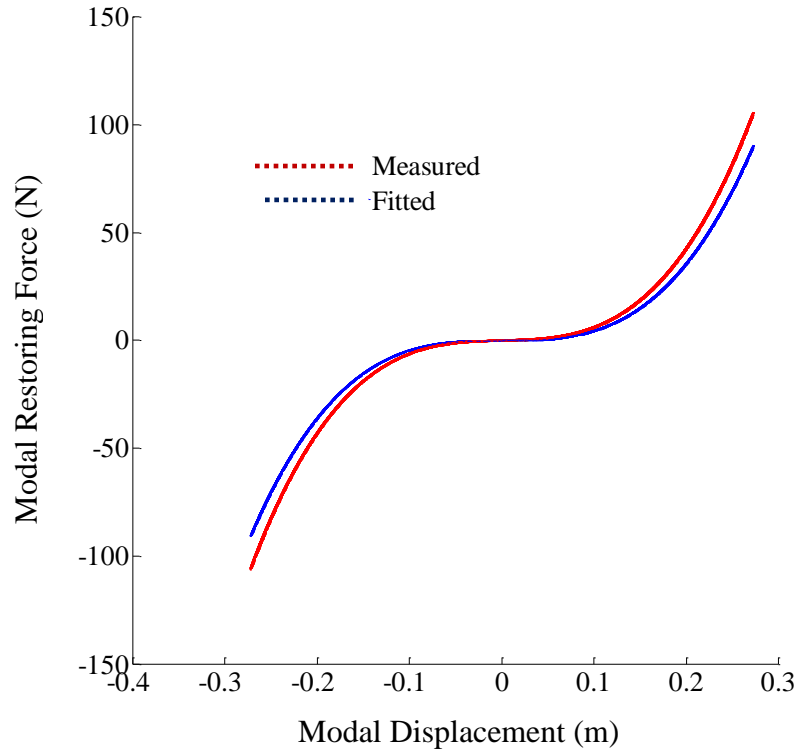
Figure 5.41: Projection of Restoring Force on XZ plane (Stiffness Curve)
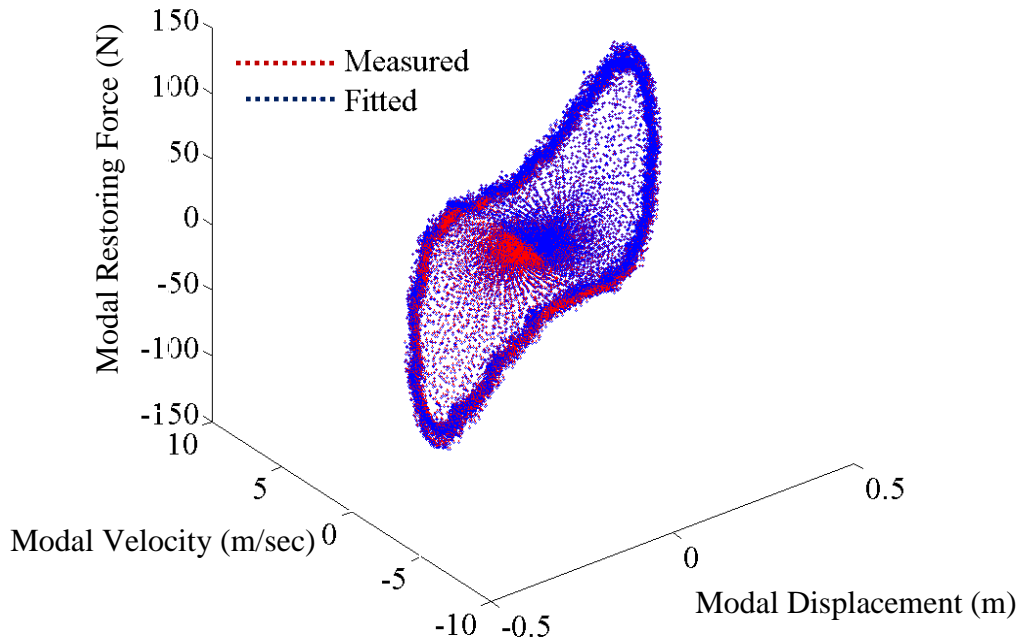
Figure 5.42: Restoring Force Surface for a base excitation of 1.1mm

5.3.2.3 Estimation of Nonlinear Parameters Using the Steady State Vibration Response

The methodology presented in Section 5.3.2 utilizes transient, steady state as well as free decay data for the nonlinear system identification. The use of free decay data is to identify the coupling between the modes, if the modes are nonlinearly coupled. The above mentioned method is accurate theoretically. However, the vibration signal may suffer from phase distortion while integrating the measured data. Moreover a single harmonic assumption has been made while integrating the measured vibration signal, which potentially might be the serious issue when the higher order harmonics are present in the signal. Also it has been observed in the literature that the estimation of damping is 100% inaccurate when there is a phase distortion in an integrated signal [54]. Thus, it is essential to compare the identified parameters obtained in Section 5.3.2.2 by using the analytical integration algorithm in the measured response data shown in Section 5.3.2. The time domain relative acceleration response at the tip of the beam with a base excitation of 1mm is shown in Figure 5.43. As shown in Figure 5.43, the response consists of three parts: (a) transient response from (0-20) sec; (b) steady state response from (20-90) sec; and a free decay from (90-148) sec. The steady state response, as shown by the window in Figure 5.43 has a constant magnitude with mean value zero. Thus, this steady state acceleration response can be approximated by the function shown by Equation (3.33). A multilinear least square regression is carried out to find out the coefficients of the steady state response. Figure 5.44 shows the measured steady state response and the approximated function with known coefficients. The derived coefficients are tabulated in Table 5.2. It can be seen from Table 5.2 that there is a significant contributions from third harmonic components. Knowing these coefficients, the velocity and displacement response are obtained through analytical integration

(Equations 3.34-3.35). The analytically integrated velocity and displacement response at the tip of the beam is shown in Figures (5.45-5.46).
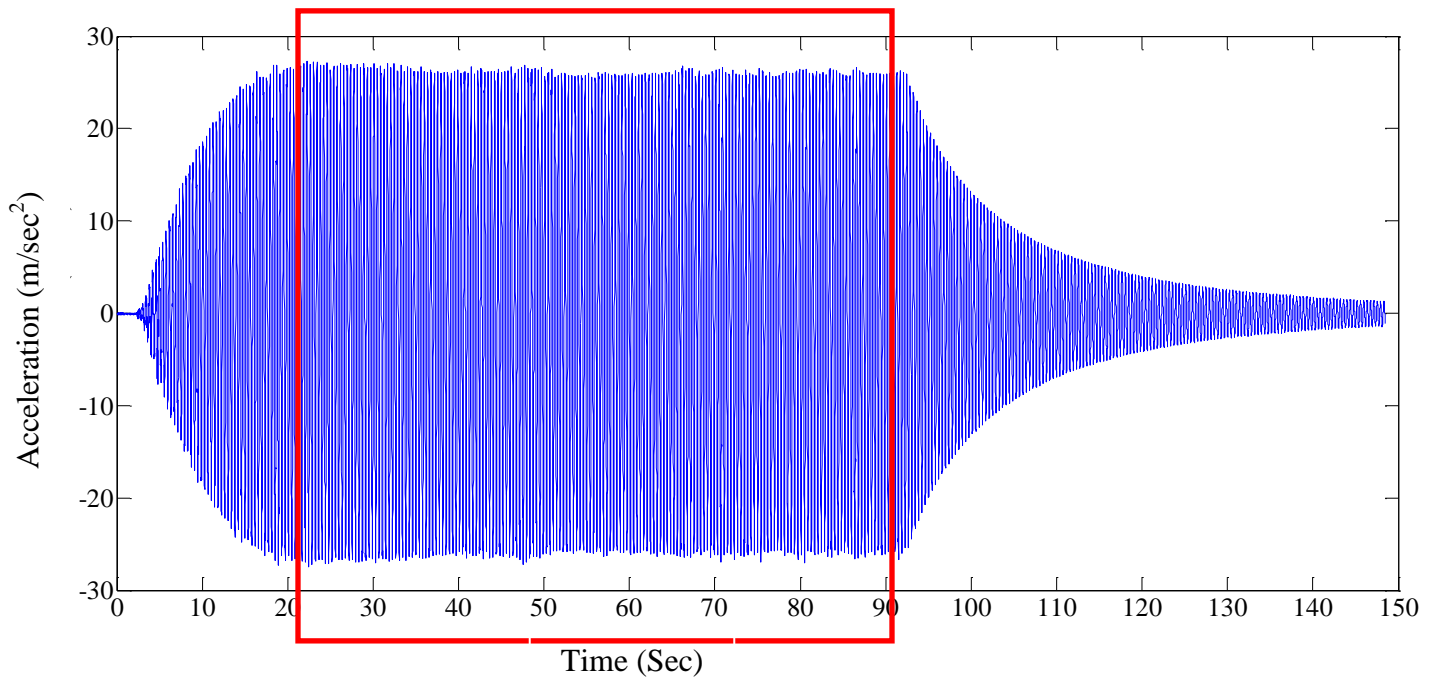
Figure 5.43: Acceleration Response at the Tip of the Beam (Base Excitation 1mm)
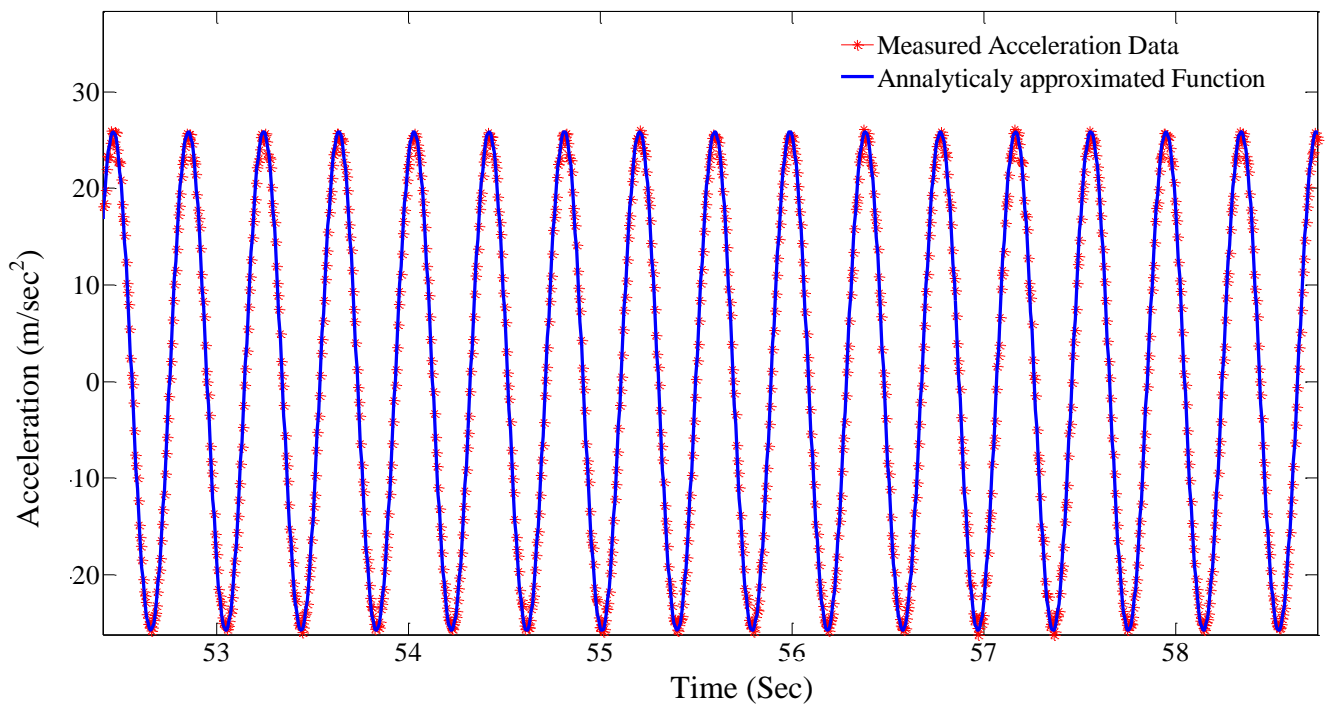
Figure 5.44: Measured and Approximated Steady State Acceleration Response Data (Base Excitation 1mm)

Table 5.2: Coefficients of Harmonics in the Measured Signal

Functions	Harmonic Coefficients			
	First Harmonic	Second Harmonic	Third Harmonic	Fourth Harmonic
Sine	-25.5731	-0.0289	0.0823	0.0105
Cosine	3.3600	-0.0353	-0.0765	-0.0074
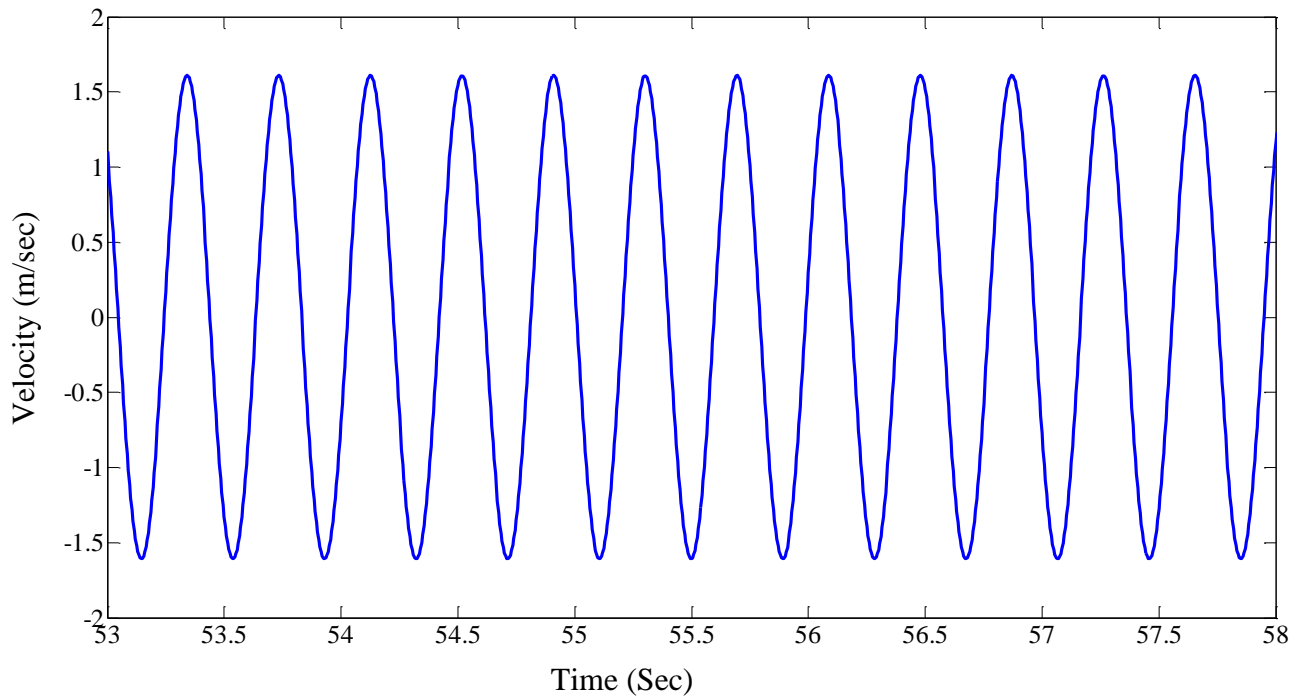
Figure 5.45: Analytically Integrated Velocity Data (Base Excitation 1mm)

The procedure is repeated at all measured DOFs and the restoring force is calculated using Equation (4.17) in time domain. The restoring force thus obtained is transformed to modal space to obtain the modal restoring force. A least square regression algorithm is used to find out the modal parameters. The new restoring force is regenerated based on the obtained modal parameters. Figure 5.47 shows the measured and the regenerated restoring force. The nonlinear stiffness terms obtained at different excitation with two different numerical techniques are tabulated in Table 5.3. The nonlinear stiffness terms obtained are reasonably close with two

103

different integration techniques. The first technique described in section 5.3.2, utilizes the motion to be single harmonic but the response also has significant contributions from third harmonic so the nonlinear stiffness terms obtained from steady state data have higher value as compared to single harmonic integration in frequency domain. The stiffness value increased when the excitation to the base is increased, it shows that the nonlinear parameters are dependent upon the excitation amplitude unlike the linear parameters which are independent to the excitation amplitude. The test for Mode 2 does not yield any significant nonlinearities at the excitation level tested. Hence Mode 1 is essentially the mode behaving nonlinearly, when the excitation to the system is increased.
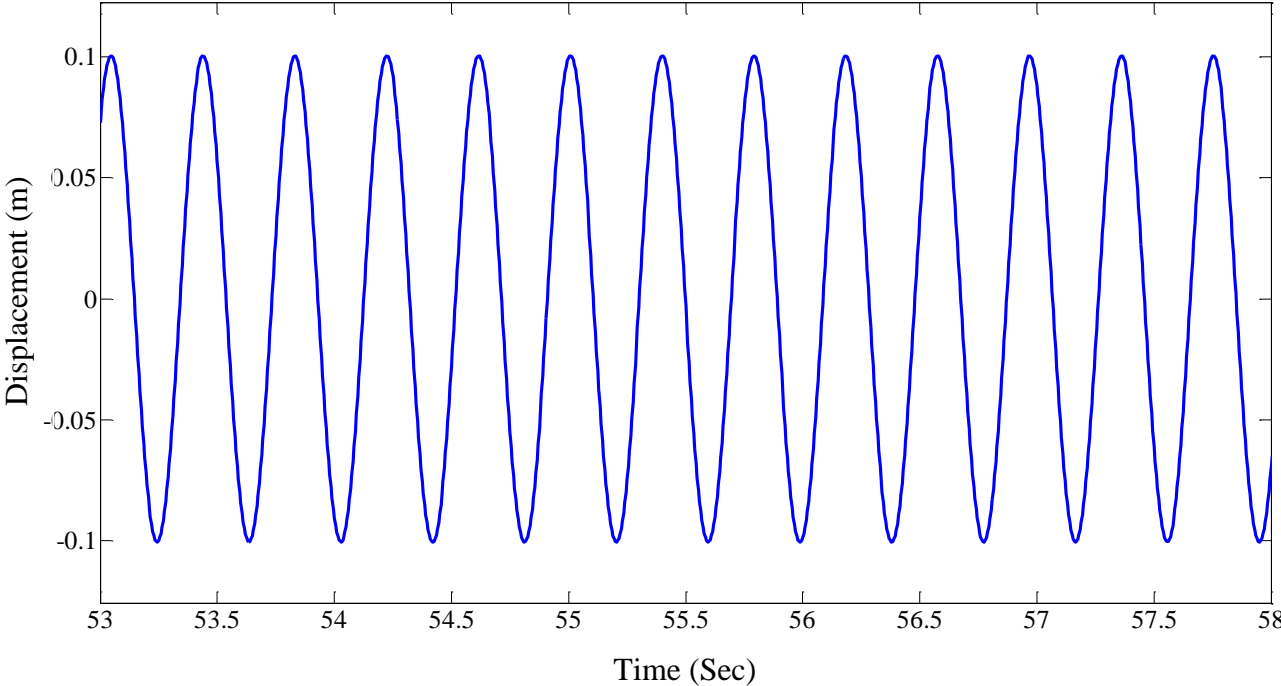
Figure 5.46: Analytically Integrated Displacement Data (Base Excitation 1mm)
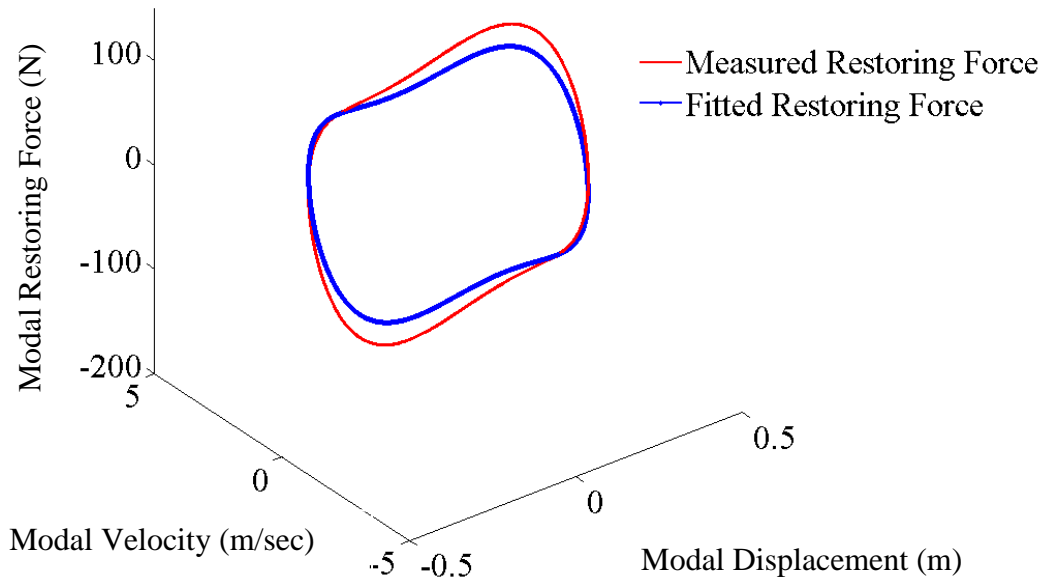
Figure 5.47: Restoring Force Surface (measured and regenerated)

Table 5.3: Nonlinear Stiffness at Different Excitations

Nonlinear Stiffness (N/m^3)		
Base Excitation Amplitude	Transient, Steady State and Free Decay Vibration Response	Steady State Vibration Response
1mm	4.97×10^3	5.07×10^3
1.1mm	5.21×10^3	5.235×10^3
1.2mm	5.35×10^3	5.45×10^3

5.4   Summary

This section demonstrates the nonlinear system identification for base excited structure from experimental measurements directly using the cantilever beam as an example. The identification procedure works in three stages to extract the nonlinear parameters, which have been discussed in detail. All the stages and the identification of the final nonlinear parameters are carried out successfully using only the experimental measurements from the base excited structure.

Although this method is applied in a simple cantilever beam for demonstration, it is equally applicable to a complex practical structure. For this, the exact form of mode shapes and modal mass are required. The measurement of the mode shapes can be done by output only analysis [40] or by a single degree of freedom method [41].In more complex base excited structure, the measured mode shapes may not satisfy the condition of orthogonality. To satisfy this condition, a finite element model defining a mass matrix can be used [41]. The measured mode shapes can be normalized with the mass matrix obtained from the finite element. This can be used as an alternative technique where the modal mass cannot be measured experimentally.

Chapter 6

Nonlinear System Identification of Structures with Bolted Lap Joints

The nonlinear system identification methodologies for structures which contain geometric nonlinearities are demonstrated in Chapter 5 by using the cantilever beam as an example. The results show the presence of a significant cubic stiffness nonlinearity when the input excitation to the base is increased sufficiently. One of the objectives of this research study is to demonstrate the presence of damping nonlinearities and the methodology for the estimating of nonlinear damping and stiffness parameters. It is thus crucial to test a structure which includes both damping and stiffness nonlinearities. Typical engineering structures which include both damping and stiffness nonlinearities are structures with joint connections. In this chapter, the methodology for nonlinearity detection and characterization in a structure with a bolted lap joint is presented. A collection of the frequency response functions (FRFs) for a nonlinear system with different contributions of stiffness and damping nonlinearities are developed. Once the nonlinearities are detected and characterized, the nonlinear parameter identification methodology presented in Chapter 4, which works in the modal space, is used to identify the nonlinear parameters.

The body structure of ground vehicles is joined in some way, by bolting, welding, riveting or by more complicated fastenings such as smart joints[4]. It is known that the added flexibility introduced by the joint to the structure heavily affects its behavior and when subjected to dynamic loading, much of the energy is lost at the joints. Determining the relevant mechanics of each joint is critical to a validated full body model of the structure. The most common failures at joints are frictional slip at micro and macro levels [71-73]. As a force is applied to a joint, small regions of the interface area will break free and begin slipping, these localized motions are

---

[4] The piezoelectric materials embedded between two structures at the critical locations of the joint.

known as microslip. As the level of the force applied to the joint increases, a larger portion of the interface will break free and slip; eventually, the entire contact area will be slipping, which is termed as macroslip. For most joints excited at reasonable force levels, macroslip does not occur but microslip is common. The small and localized motion during microslip results in energy losses at the joint, which is perceived as localized damping of the structure. Neglecting these effects in modeling of joint structure produces error in predictions of the structure responses. So, it is essential to understand the dynamic behavior of the structure due to the bolted joint connection.

Several experimental studies have been carried out in the past using the modal shaker and the hammer providing important new results (nonlinear damping and stiffness) and understanding of bolted joints. Goege et. al. [56] presented a test strategy that can be used to identify and characterize nonlinear structural behavior due to a joint during modal testing. The method assumes a weak nonlinear behavior and operates in modal space. Ma et. al. [71] studied the effects of a lap joint placed between two cantilever beams while the assembly is excited using concentrated force acting parallel to the bolt axis. Their method attempted to compare the overall dynamics of the bolted structure to that of a similar but unbolted one. Experiments were carried out on bolted and unbolted beams using non-contacting laser vibrometry, the identification revealed non-proportional damping and nonlinear softening effects due to micro-impact in the bolted joint. Hartiwigsen et.al. [72] experimentally studied the principle joint effects on the structural dynamics of two structure composed of beam elements. The two structures used were: a simple beam with a joint located at its centre and a rectangular frame with the joint in the centre of one of its longitudinal beams. They concluded with the nonlinear viscous damping as a function of the amplitude of the displacement.

Experimental observations reported in the current literatures [69-73] show that the detailed constitutive models describing the behavior of frictional interfaces are more complicated and that the simple phenomenological models having parameters obtained from the vibration measurements are more preferable. Thus, it is decided in this study to explore the system nonlinearity due to a joint using measured vibration data. In order to detect and characterize the nonlinearity by using measured vibration data, it is essential to know what kind of excitation is to be used (force excitation, base excitation and impulse hammer excitation etc.); what kind of input is to be used for nonlinearity detection (single sinusoidal, swept sine, and step sine etc.); and, what frequency range of the structure is to be tested. As the objective of this study is to identify the nonlinear parameters of a system using the base excitation as an input, for the nonlinearity detection and characterization purpose, the base excitation, step sine test and the frequency range around the first natural frequency of the system is taken as the test parameters.

The rest of this chapter is organized as follows: Section 6.1 presents the numerical example to detect, characterize and identify the nonlinearities due to a joint connection. Following the numerical example, in Section 6.2, an experimental study is carried out on a structure with two beams connected with a bolted joint. An innovative approach using base excitation is developed which can detect and characterize the joint nonlinearities. The approach consists of maintaining the equivalent excitation force constant while changing the base displacement and the excitation frequency simultaneously. It is believed that maintaining the constant equivalent excitation force magnitude will reveal the unique FRF for a nonlinear system measured along each excitation frequency. Finally, in Section 6.3, the parameters associated with joint nonlinearities are obtained using the nonlinear system identification algorithm developed in Chapter 4. The

identified parameters are amplitude dependent damping with nonlinear stiffness which resembles that of the results found in reference [72].

6.1 Nonlinearity Detection Characterization and Identification Methodology (Numerical Example)

In this section, a numerical example for a base excited structure is defined accordingly to the experimental work by Hartwigsen et.al. [72]. The model is simulated (the Forward Approach) for various excitation frequencies in order to study the effect of maximum amplitude of displacement on damping, stiffness and natural frequencies of the structure. Following the numerical simulations, the nonlinear parameters of the defined model are assumed to be unknown and using the nonlinear response data from the simulations, the system identification methodology (the Reversed Approach) described in Chapter 4 is used to obtain the assumed parameters. The identified parameters are then compared with the initially assumed parameters to show the efficacy of the proposed nonlinear parameter identification method described in Chapter 4.

6.1.1 Numerical Example to Demonstrate the Detection and the Characterization of Nonlinearity due to Joint (The Forward Approach)

In order to demonstrate the detection and characterization of the nonlinearity of structure due to the joint connection, a suitable test procedure was developed such that it would be feasible to apply for the experimental implementation. A classical example is presented here to demonstrate the test procedure. A single DOF system represented in a modal coordinate with a softening stiffness k_2 and the nonlinear viscous damping c_{eq} due to joint slip is considered. The governing equation of motion in a modal space for base excited structure can be written as,

$$\ddot{\tilde{q}}(t) + c_{eq}\dot{\tilde{q}}(t) + w^2\tilde{q}(t) - k_2\tilde{q}^3(t) = p^d \qquad (6.1)$$

Where, $\tilde{q}$ is the nonlinear modal response vector, w is the natural frequency and p^d is the reconstructed force vector using the base motion as an input. Equation (6.1) is the extended form of Equation (4.23), where the proportional damping of the structure is replaced by amplitude dependent damping term c_{eq} so as to represent the joint nonlinearity. It should be noted that the base motion can be measured either in the form of displacement or acceleration. The term c_{eq} is dependent on the displacement amplitude of vibration and can be generalized as,

$$c_{eq} = c_0 + c_1 r_{max} + c_2 r^2{}_{max} \dots \dots \qquad (6.2)$$

It has been reported in the current literature that the equivalent damping coefficient for a joint interface is a positive definite function and is dependent as a quadratic function of the maximum amplitude of vibration [72]. According to reference [72], Equation (6.1) can be written as,

$$\ddot{\tilde{q}}(t) + (c_0 + c_1 r_{max} + c_2 r^2{}_{max})\dot{\tilde{q}}(t) + w^2\tilde{q}(t) - k_2\tilde{q}^3(t) = p^d \qquad (6.3)$$

The parameters used for the simulation are: $c_0 = 0.05\ Nm/sec, c_1 = 65Nm/sec, c_2 = 1 \times 10^4 Nm/sec, w = 150 rad/sec = 23.87Hz,\ k_2 = 4 \times 10^7 N/m^3$ and $p^d = 10N$.

It is clear from Equation (6.3) that the nonlinear viscous damping is dependent upon the maximum amplitude of the displacement response rather than the frequency of vibration. The numerical value of the maximum amplitude of displacement r_{max} is initially unknown. An iterative approach is used to determine the value of r_{max} [69]. In order to solve the unknown r_{max}, an initial value is assigned for r_{max} in the first iteration and using such an assigned value the amplitude of vibration response is obtained by integrating Equation (6.3) using the Runge Kutta algorithm. In the second iteration, using the new value of r_{max}, Equation

(6.3) is again integrated. The integration procedure stops after r_{max} converges to the constant value. Figure 6.1 shows the r_{max} in a typical displacement time series data, where the maximum amplitude r_{max} is shown by a circle. The simulation is carried out by assuming the initial value of $r_{max} = 0.001m$. The simulation results converged at the fifth iteration with $r_{max} = 0.009877m$.
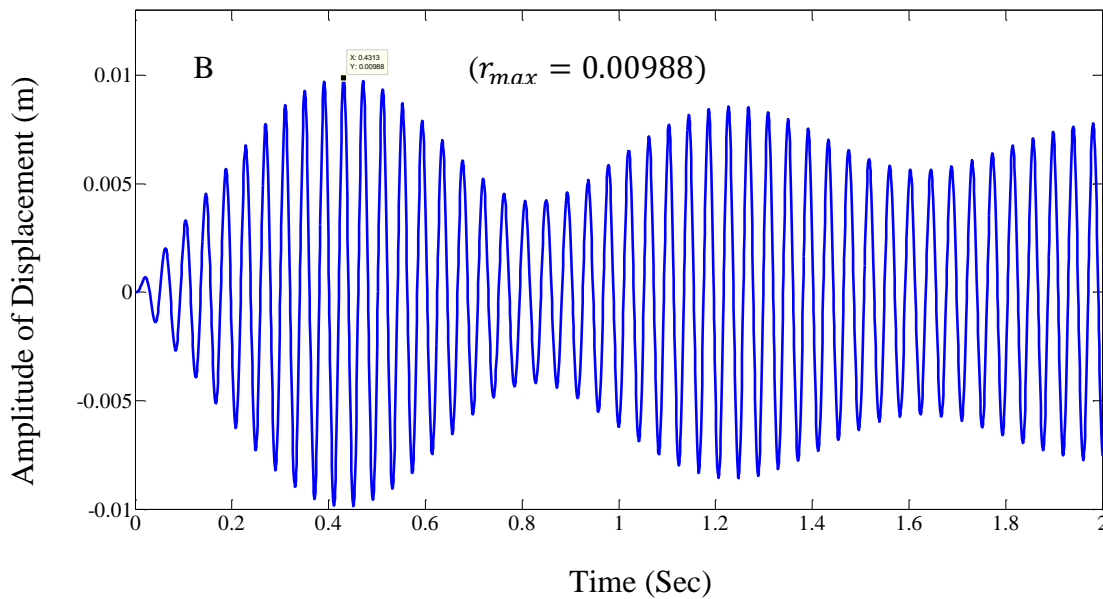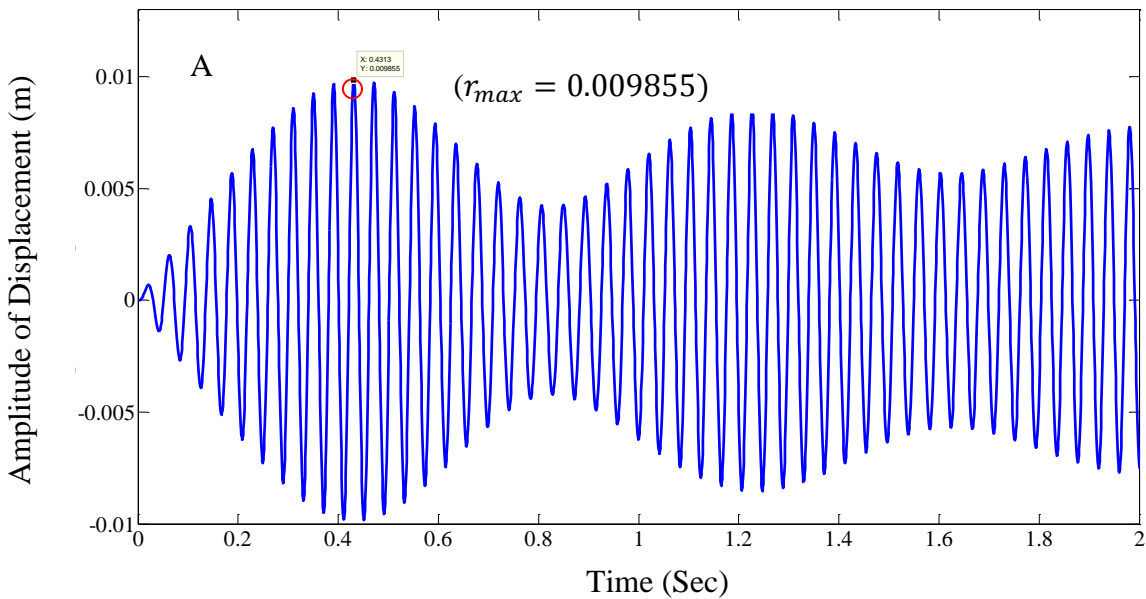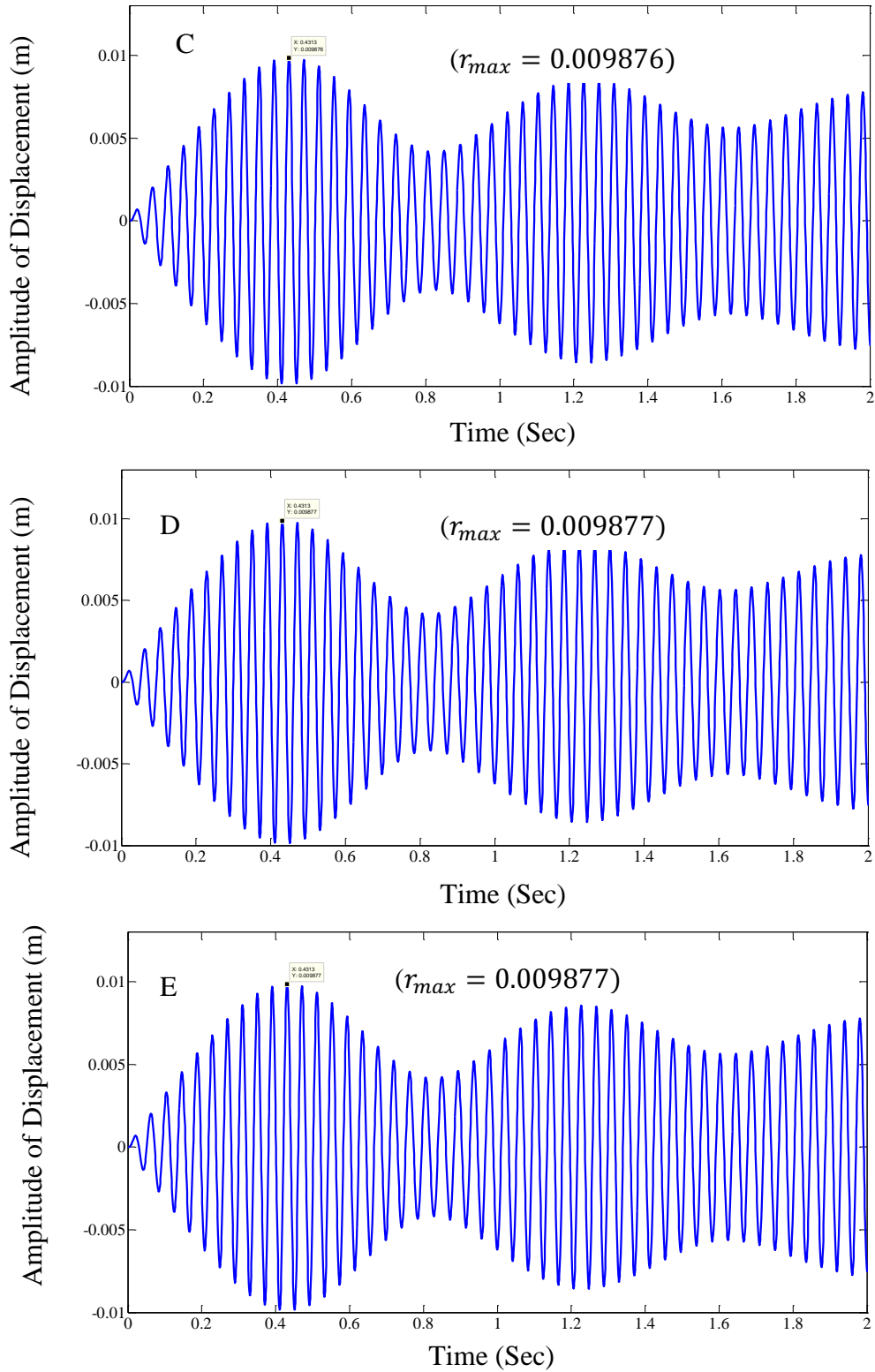
Figure 6.1: Maximum Amplitude of Displacement (A: Ist Iteration, B: 2nd Iteration, C: 3rd Iteration, D: 4th Iteration and E: 5th Iteration)

The excitation frequency is varied around the natural frequency w of the system shown by a model defined by the Equation (6.3). The maximum amplitude of displacement r_{max} along with the time domain responses of acceleration, displacement and velocity are obtained through iterations for each excitation frequency. The nonlinear FRF of the system is obtained by plotting the maximum amplitude of the simulated response at each excitation frequency against the excitation frequencies. The nonlinear FRF plot is shown in Figure 6.2. From Figure 6.2 it is clear that the maximum amplitude of vibration is at the excitation frequency of $23.08Hz$. As the linear natural frequency of the assumed model is at $23.87Hz$, there is a shift in the natural frequency from the linear $23.87\ Hz$ to the nonlinear $23.08Hz$. The shift in the natural frequency is due to the nonlinear softening effect at the joint. The simulation is carried out including nonlinear stiffness and nonlinear damping; nonlinear damping only; and equivalent linear system only (all the nonlinear terms are removed from the assumed model). The comparisons of FRFs for each type of nonlinearity are shown in Figure 6.3. As shown in Figure 6.3, for the equal magnitude of input, the amplitude of displacement is fairly low when the system is nonlinear as compared to the equivalent linear system. As shown by the maximum amplitude of displacement, the shift in the natural frequency is from the linear 23.87Hz to the nonlinear 23.08Hz. The presence of the nonlinear viscous damping reduces the amplitude of displacement however it does not reduce the natural frequency of the system. The significance of the FRFs, shown in Figure 6.3, is that the shift in the natural frequency can be used as a tool to detect and characterize the nonlinearity for a complex structure using the measured vibration data.
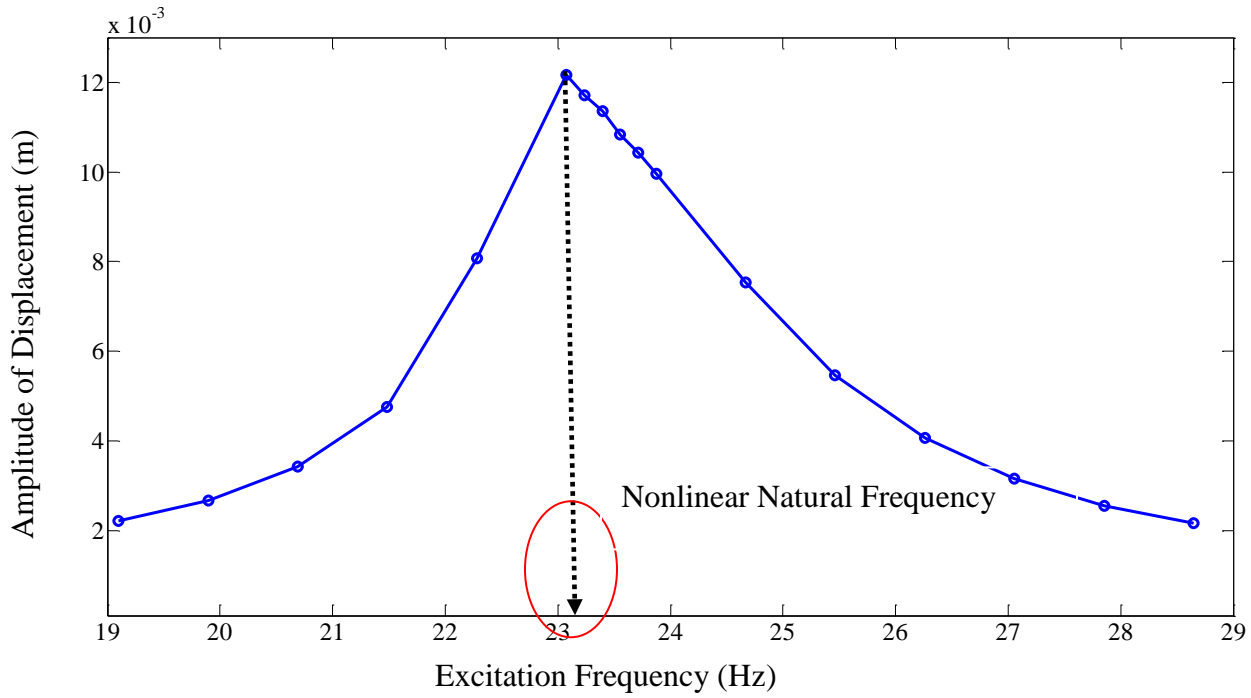
Figure 6.2: FRF of Nonlinear System with Stiffness and Damping Nonlinearities
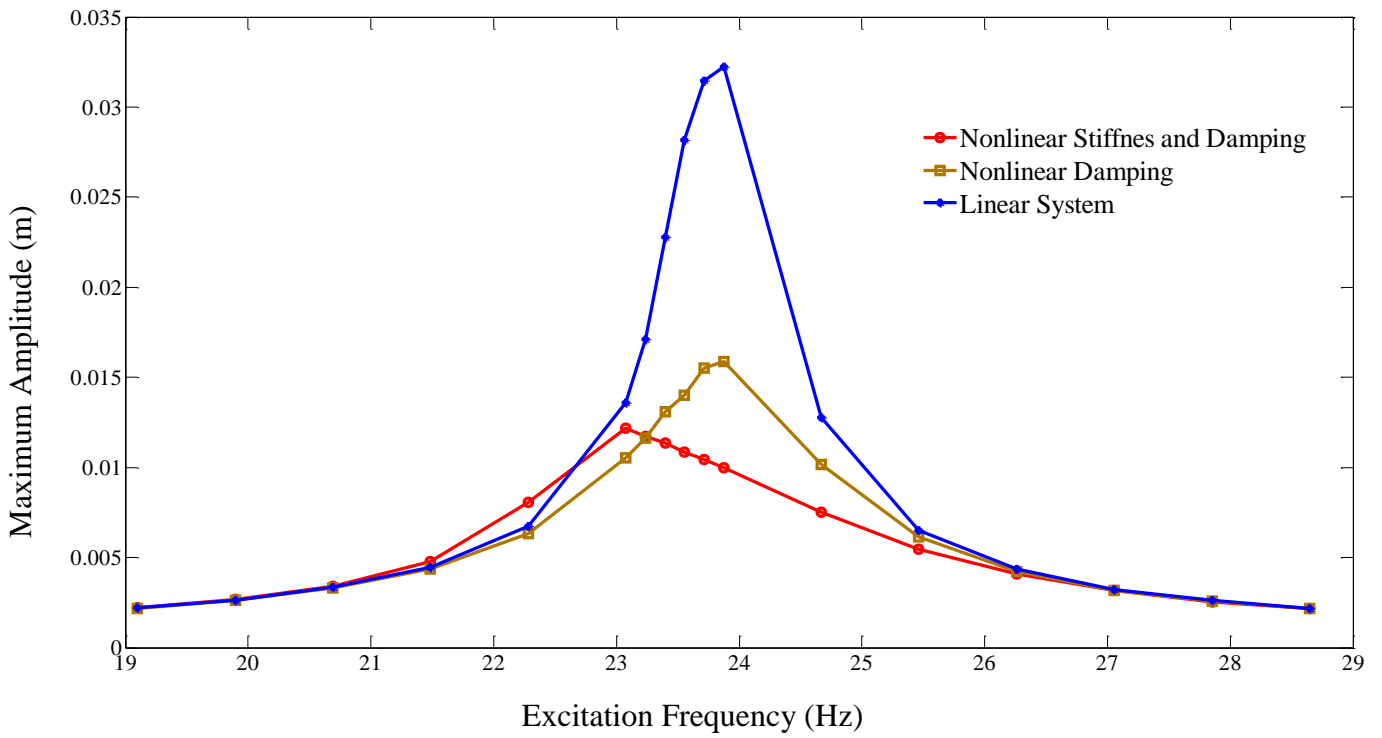
Figure 6.3: FRFs Comparison of Linear and Nonlinear System

115

6.1.2 Identification of Nonlinear Parameters (The Reverse Approach)

In Section 6.1.1, a simulation approach is shown for a system which has the amplitude dependent damping and the stiffness nonlinearity. As this research study focuses on the identification of nonlinear parameters (the Reverse Approach), the parameters used for the simulations are assumed to be unknown and the time series responses of acceleration, displacement and velocity with the known excitation force are taken for further analysis. The values of c_0, c_1, c_2 and k_2 which are assumed to be unknown are obtained by using the theory described in Chapter 4 of this thesis. For a single excited mode Equation (4.23) can be written as,

$$\ddot{\tilde{q}}(t) - w^2 \tilde{q}(t) + G(\tilde{q}, \dot{\tilde{q}}) = p^d \tag{6.4}$$

Where, $G(\tilde{q}, \dot{\tilde{q}})$ is the nonlinear modal restoring force which contains the amplitude dependent damping and the stiffness term due to joint motion. $G(\tilde{q}, \dot{\tilde{q}})$ can be further written as,

$$G(\tilde{q}, \dot{\tilde{q}}) = p^d - \ddot{\tilde{q}}(t) - w^2 \tilde{q}(t) \tag{6.5}$$

As the right hand side of Equation (6.5) is known, $G(\tilde{q}, \dot{\tilde{q}})$ can be computed at each time instant for each excitation frequency by using Equation (6.5). Once $G(\tilde{q}, \dot{\tilde{q}})$ is obtained, a multilinear least square regression algorithm which utilizes Equations (4.24-4.26) described in Chapter 4 is used to determine the stiffness and the nonlinear damping parameters. Figure 6.4 shows the identified nonlinear stiffness coefficient as a function of the excitation frequency. The identified nonlinear stiffness coefficient is constant over the excitation frequencies, which is true as the response data are measured for constant nonlinear stiffness. Similarly, Figure 6.5 shows the identified equivalent damping coefficient c_{eq} for each excitation frequency. The equivalent damping coefficient c_{eq} has the maximum value at the nonlinear natural frequency of the system

23.08Hz. Once the equivalent damping coefficient at each excitation frequency is identified, the next step is to identify the value of c_0, c_1 and c_2 . As previously discussed, c_0, c_1 and c_2 are dependent upon the maximum amplitude of the displacement r_{max}, the least square regression of c_{eq} on r_{max} is carried out to identify the coefficients c_0, c_1 and c_2. Figure 6.6 shows the plot between the maximum amplitude of the displacement r_{max} and the equivalent damping coefficient c_{eq}. Figure 6.6 clearly shows that the equivalent damping coefficient is varying as a quadratic function to the maximum amplitude of displacement r_{max}. The exact and identified parameters are tabulated in Table 6.1. As shown in Table 6.1, the percentage error between the exact and the identified parameters for the equivalent damping coefficients is less than 2%. The identified stiffness coefficient is equal to the exact stiffness coefficient which indicates that the nonlinear parameter identification algorithm described in Chapter 4 can be used for the estimation of the joint nonlinearities.
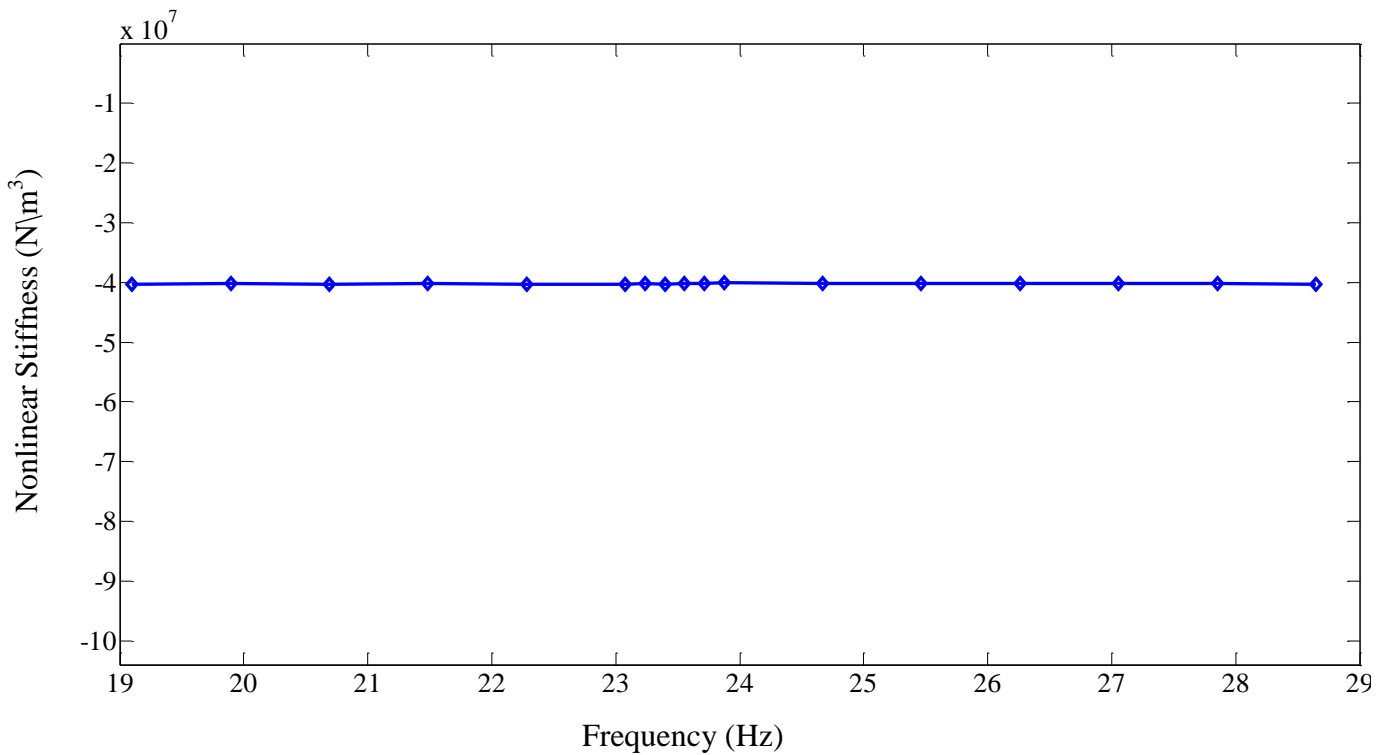
Figure 6.4: Identified Stiffness as a Function of Frequency
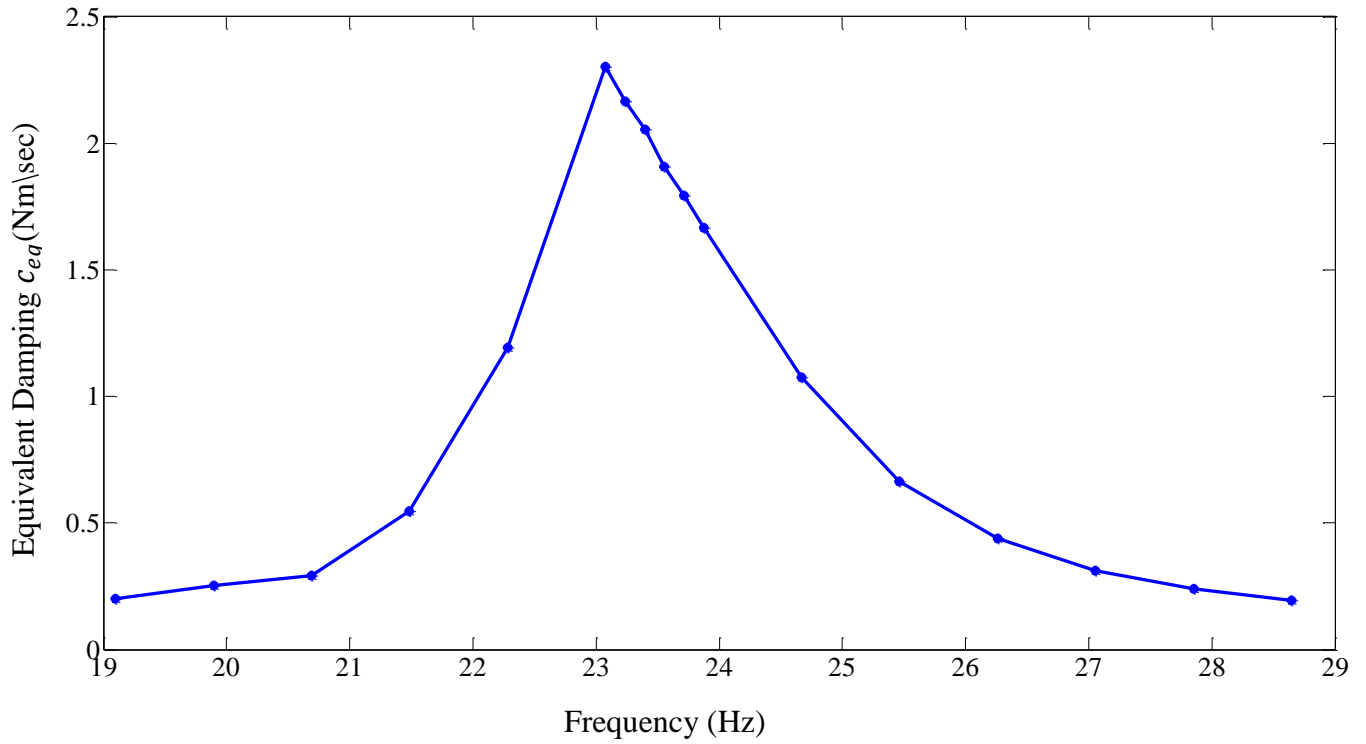
Figure 6.5: Identified Equivalent Damping Coefficient as a Function of Frequency
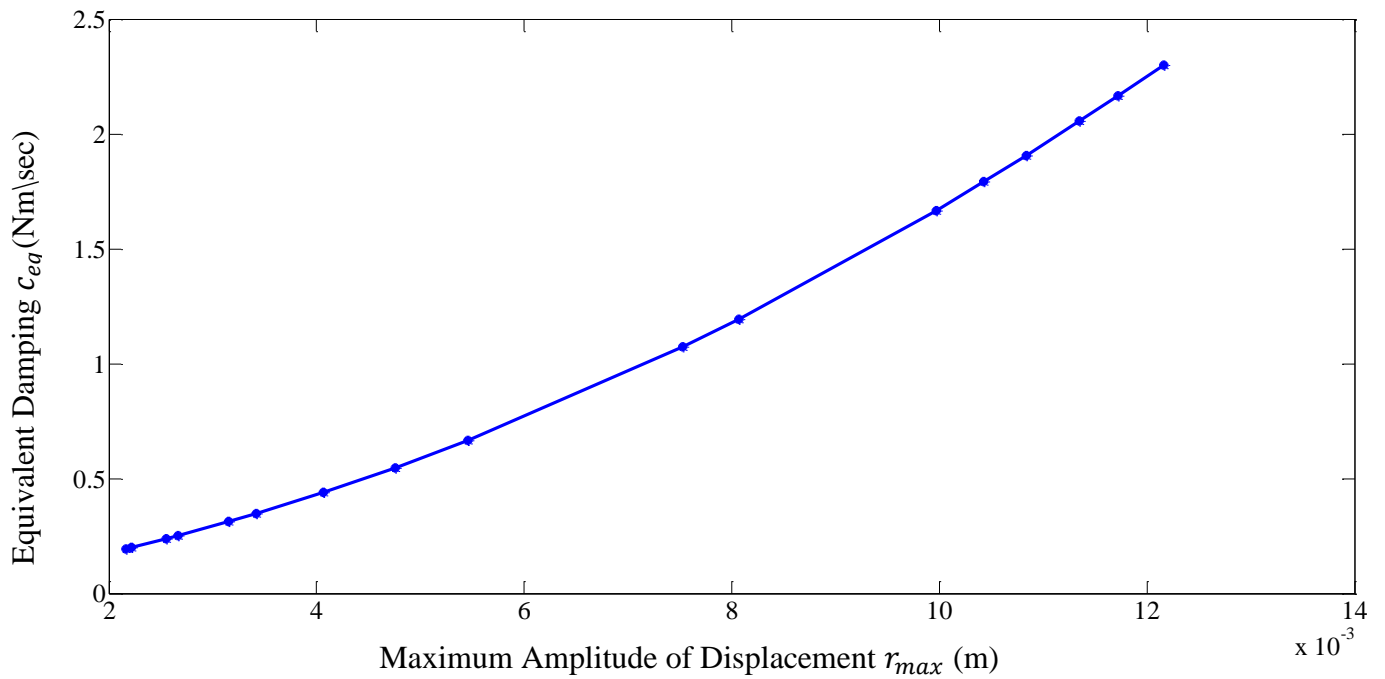
Figure 6.6: Equivalent Damping Coefficient as a Function of Maximum Amplitude of Displacement

118

Table 6. 1: Exact and Identified Nonlinear Parameters

	c_0	c_1	c_2	k_2
Exact	0.05	65	1×10^4	4×10^7
Identified	0.045	66.12	1.01×10^4	4×10^7
Error (%)	0.5	1.69	1	0.0

6.2 Experimental Demonstration of Nonlinear System Identification in a bolted Joint

The objective of this section is to show that the theory presented in Chapter 4 can be applied to structures where nonlinearities arise from the joint connection. In Chapter 4, the nonlinear system identification methodology was divided into three sections: linear system identification, force reconstruction and the nonlinear parameter identification. In order to apply the same theory, this section is divided into four subsections: experimental setup, linear system identification and force reconstruction, nonlinearity detection and characterization and nonlinear parameter identification.

6.2.1 Experimental Set-up

The experimental setup consists of two Aluminum (T6061) beams (Figure 6.7) connected with a bolted joint in a fixed-free boundary condition. As shown in Figure 6.7, the dimensions of the beam are: length = 90cm; width = 2.54 cm; and thickness = 0.625 cm. The bolt material used for fastening the beam is mild steel with the nominal bolt diameter of 0.9525 cm. The technical data for the bolt material along with the tightening torque values to produce corresponding bolt clamping load is provided in Appendix B. The experiments are conducted for three different preloads (different tightening torques): 19.77 Nm, 13.55 Nm and 9.03 Nm.
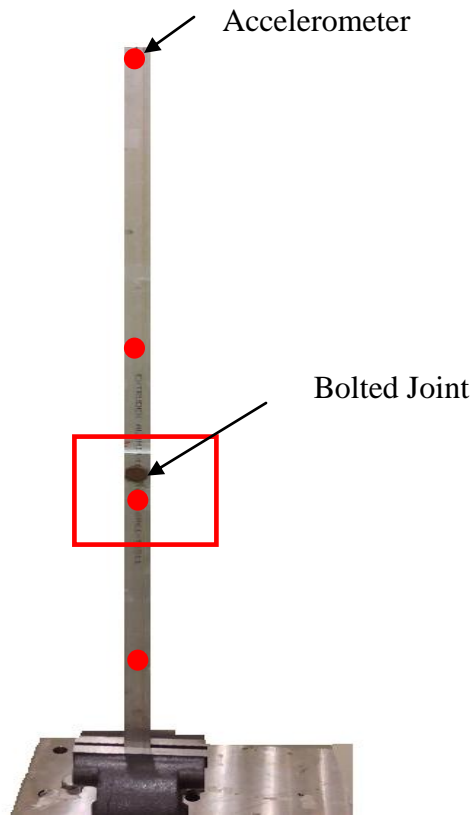
Figure 6.7: Bolted Beam with Fixed-Free Boundary Condition

6.2.2 Linear System Identification

The linear system identification methodology consists of: (a) measuring the linear response data ; (b) identifying the mode shapes matrix (modal vector); and, (c) measuring the natural frequencies of the structure. In order to measure the linear parameters, the bolt was fully tightened with a tightening torque of 19.77 Nm. The fully tightened bolt under a low magnitude of excitation will show clearly the linear behavior, as reported in reference [69-71]. Equation (3.16) was used to reconstruct the force under a low displacement, provided that the mode shapes of the bolted connection are known. One way of identifying the modal matrix (mode shapes) of the structure is usually done by developing the FE model of the structure. However, for a structure with a bolted connection the type of the bolt model that can accurately predict the mode shapes of the structure using the FE approach is still unknown. The alternative technique of

identifying the mode shapes is to measure them experimentally. There are several established methods for mode shape measurements [6-8]. The procedure to normalize the measured mode shapes to unity mass matrix is clearly shown in reference [6]. Having made the decision to measure the mode shapes for a bolted beam, a PCB Piezotronics model hammer (086C03) was used to measure the mode shapes. Both the roving hammer tests and roving accelerometers tests (moving the excitations/sensors at the different locations of the test structure) were carried out such that the mode shapes are accurate and consistent in both tests. Figure 6.8 shows the driving point FRF of the roving hammer test. The three natural frequencies are at 5.9Hz, 33.6 Hz and 105.1 Hz. Similarly, Figure 6.9 shows the FRF at the tip of the beam with roving accelerometers tests. The natural frequencies are in good agreements in both tests. The coherence measured is excellent with more than 95% at resonance. Having measured the mode shapes and the natural frequencies with fully tight bolt conditions, it is possible to construct the equivalent excitation force vector using Equation (3.1) and reconstruct the force vector from the dynamics using Equation (3.16) if the excitation at the base is known.
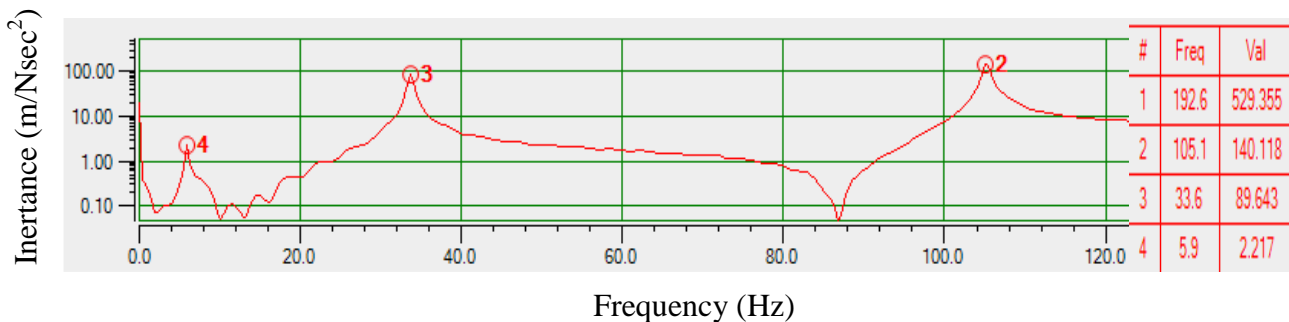
Figure 6.8: Driving Point FRF (Roving Hammer Test)
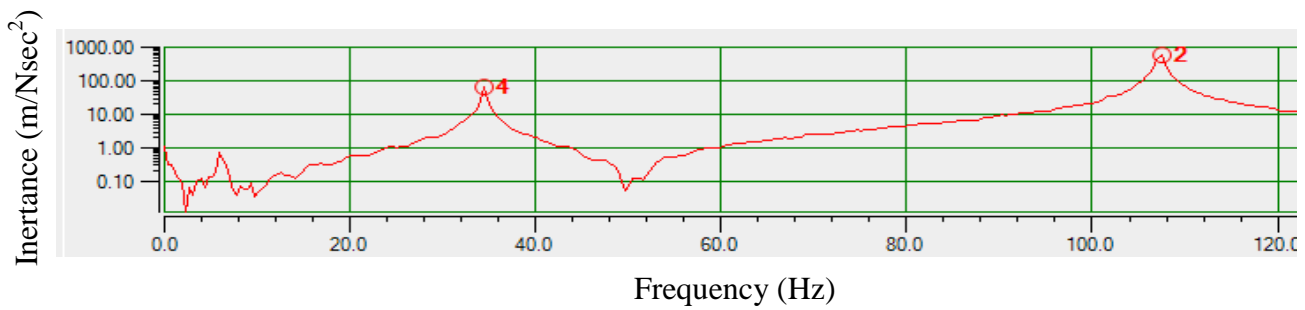
Figure 6.9: FRF at the Tip of the Beam (Roving Sensor)

The equivalent excitation force vector for a base displacement of 0.1mm and an excitation frequency of 5.9 Hz is shown in Figure 6.10. Such forces, shown in Figure 6.10, will vary as a quadratic function of excitation frequencies, if the constant displacement is maintained at the base. As presented in the numerical example in Section 6.1.2, the equivalent force is maintained at constant magnitude, when the excitation frequency is varied around the natural frequency of the system. So, in experiments it is necessary to maintain the magnitude of the equivalent excitation force constant over the excitation frequency range. In order to maintain the constant equivalent excitation force, a scaling factor for a base displacement is calculated. It is believed that the nonlinear stiffness due to the joint will be constant over the excitation frequency range, if the magnitude of the equivalent excitation force with respect to the excitation frequency range can be maintained constant at the base. The input base displacement that can maintain the constant equivalent excitation force over the excitation frequency range is tabulated in Table 6.2. The excitation frequency and the base displacement are now varied with a fully tight bolt condition. The maximum amplitude response at each excitation frequency with four accelerometers (locations shown in Figure 6.7) is recorded. The maximum response for each excitation is now transformed to the modal space using the mode shapes matrix. With the maximum amplitude at each excitation frequency known in the modal space and the equivalent modal force known, it is possible to create a FRF of the system for Mode 1. The FRF in the form

122

of Inertance is shown in Figure 6.11. The FRF in Figure 6.11 indicates the natural frequency at 5.9 Hz showing the system behaving linearly. As the linear FRF is known along with the mode shapes matrix it is possible to reconstruct the force at the measured DOFs only (Equation 3.16).
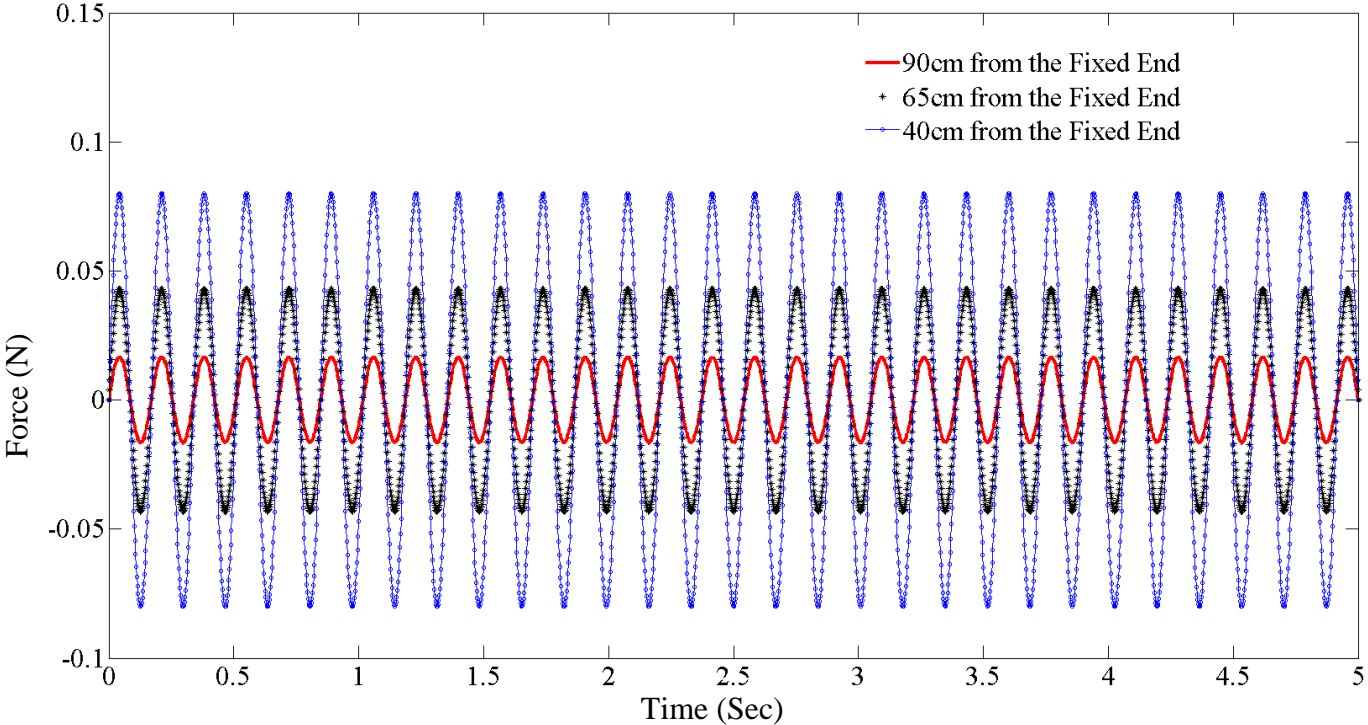
Figure 6.10: Equivalent Force at the Measured DOFs (Excitation Frequency 5.9Hz)

Table 6.2: Input Base Displacement for the Excitation Frequency Range

Excitation Frequency (Hz)	Scaling Factor (SF)	Base Displacement (mm)
5	1	1
5.1	0.9612	0.09612
5.2	0.9246	0.09246
5.3	0.8900	0.08900
5.4	0.8573	0.08573
5.5	0.8264	0.08264
5.6	0.7972	0.07972
5.7	0.7695	0.07695
5.8	0.7432	0.07432
5.81	0.7406	0.07406
5.82	0.7381	0.07381
5.83	0.7355	0.07355
5.84	0.7330	0.07330
5.85	0.7305	0.07305
5.86	0.7280	0.07280
5.87	0.7255	0.07255
5.88	0.7231	0.07231
5.89	0.7206	0.07206
5.90	0.7182	0.07182
5.91	0.7158	0.07158
5.92	0.7133	0.07133
5.93	0.7109	0.07109
5.94	0.7085	0.07085
5.95	0.7062	0.07062
5.96	0.7038	0.07038
5.97	0.7014	0.07014
5.98	0.6991	0.06991
5.99	0.6968	0.06968
6	0.6944	0.06944
6.10	0.6719	0.06719
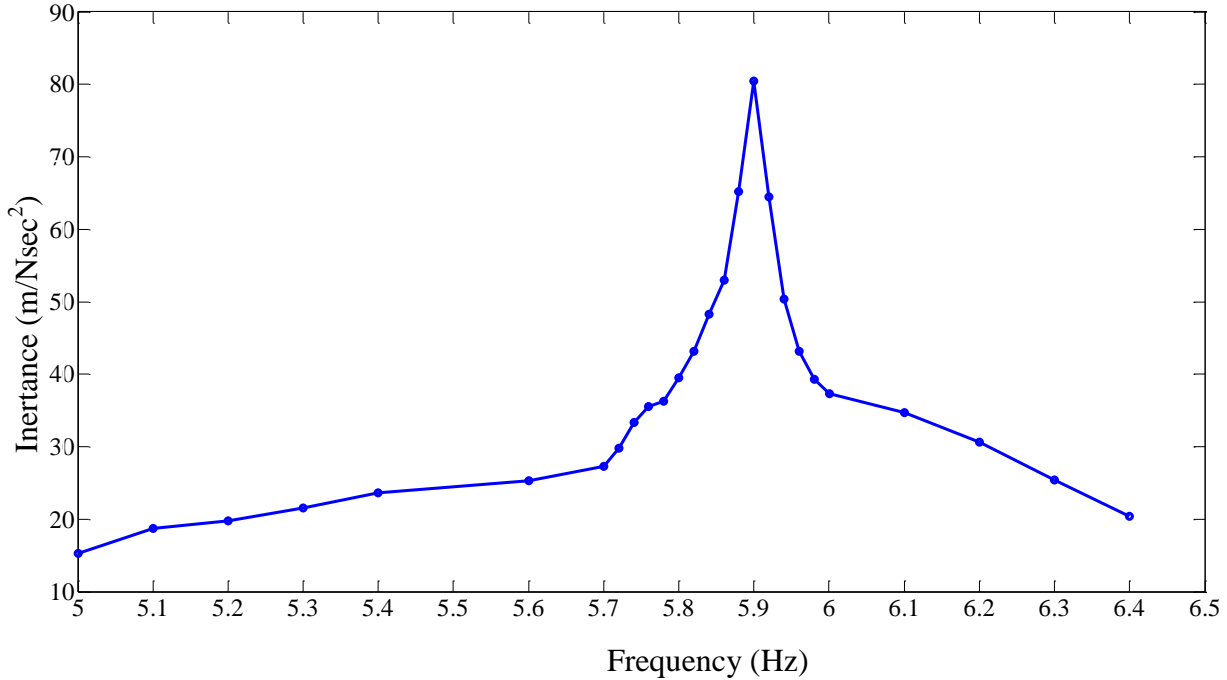
Figure 6.11: Linear FRF Generated from a Step sine Test

6.2.3 Nonlinearity Detection and Characterization (Experimental Approach):

This section presents the procedure to detect and characterize the nonlinearities due to the joint connection. Nonlinearity is present in the structure if the FRFs of the structure at different excitation level are not constant. In order to detect and characterize the nonlinearity, the fully tightened bolt is now loosen using a torque wrench. The test is carried out in two different torques which will generate two different preloads. The tests are carried out at 13.55 Nm and 9.03 Nm such that the bolt is sufficiently loosen to induce damping and stiffness nonlinearities. The magnitude of base excitation shown in Table 6.2 is scaled to the higher value such that it can induce nonlinearity when excited to the structure shown in Figure 6.7. The excitation frequency is varied as shown in Table 6.2. At each excitation frequency the maximum amplitude of acceleration at each DOF is recorded. The recorded magnitude of acceleration at each DOF is then transformed to the modal space using the mode shapes matrix. The equivalent excitation force for the scaled base excitation in the modal space is obtained from Equation (3.1) using the

125

mode shapes matrix. Having the equivalent modal force for Mode 1 and the modal acceleration it is possible to create FRF in the form of inertance (output acceleration/input force). This FRF is plotted across the excitation frequency range to show the nonlinear behavior. Figure 6.12 shows the nonlinear FRFs generated with various scaled base excitation shown in Table 6.2. The scaling up is done 10 times, 12 times and 15 times (sufficient input magnitude to induce nonlinear behavior) to induce different input magnitude. Due to the stiffness and damping nonlinearities, there is a shift in natural frequency as shown in Figure 6.12. Furthermore, the magnitudes of FRFs are not constant at different excitation magnitudes which show that the system is purely nonlinear. Similarly, Figure 6.13 shows the nonlinear FRFs generated when the tightening torque is reduced to 9.03Nm. Comparing Figure 6.12 and 6.13, one can conclude that the bolted joint induces significant nonlinearities when the bolt is loosen.
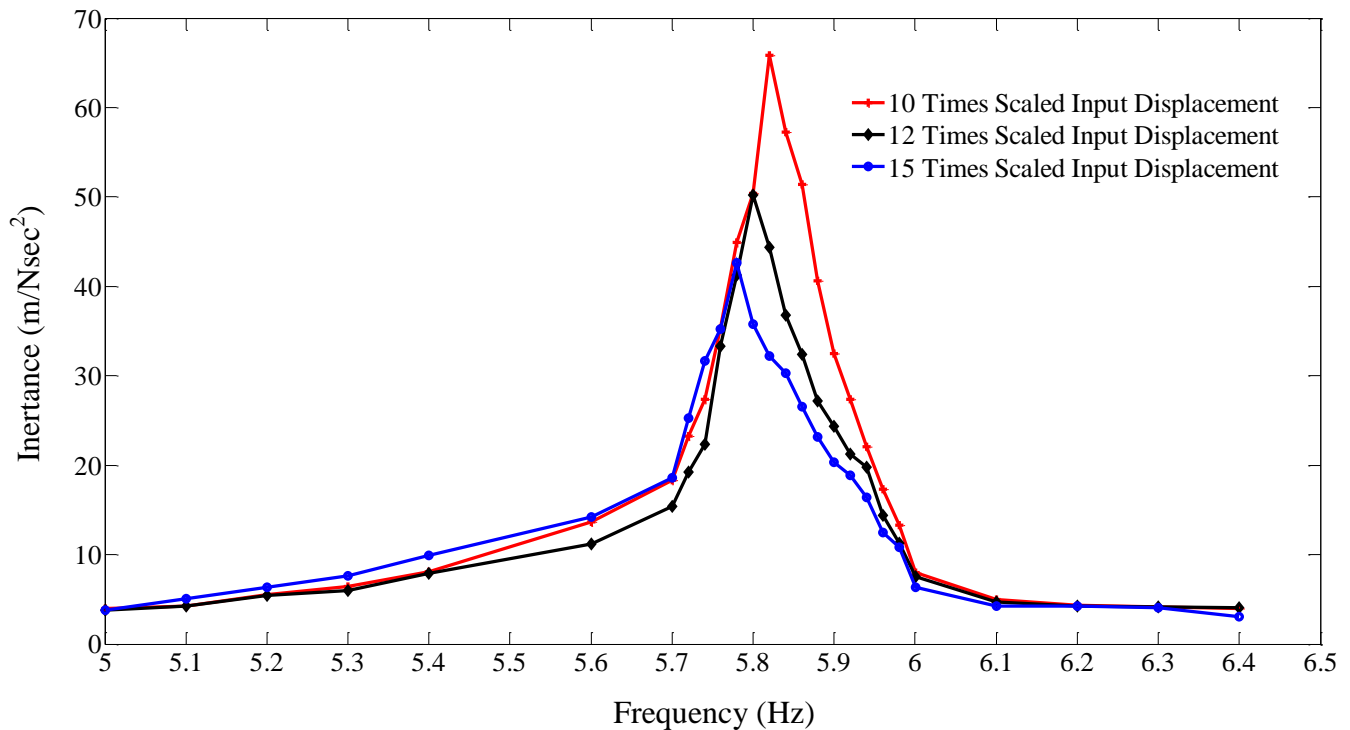
Figure 6.12: Nonlinear FRF Generated from a Step sine Test (Tightening Torque 13.55Nm)
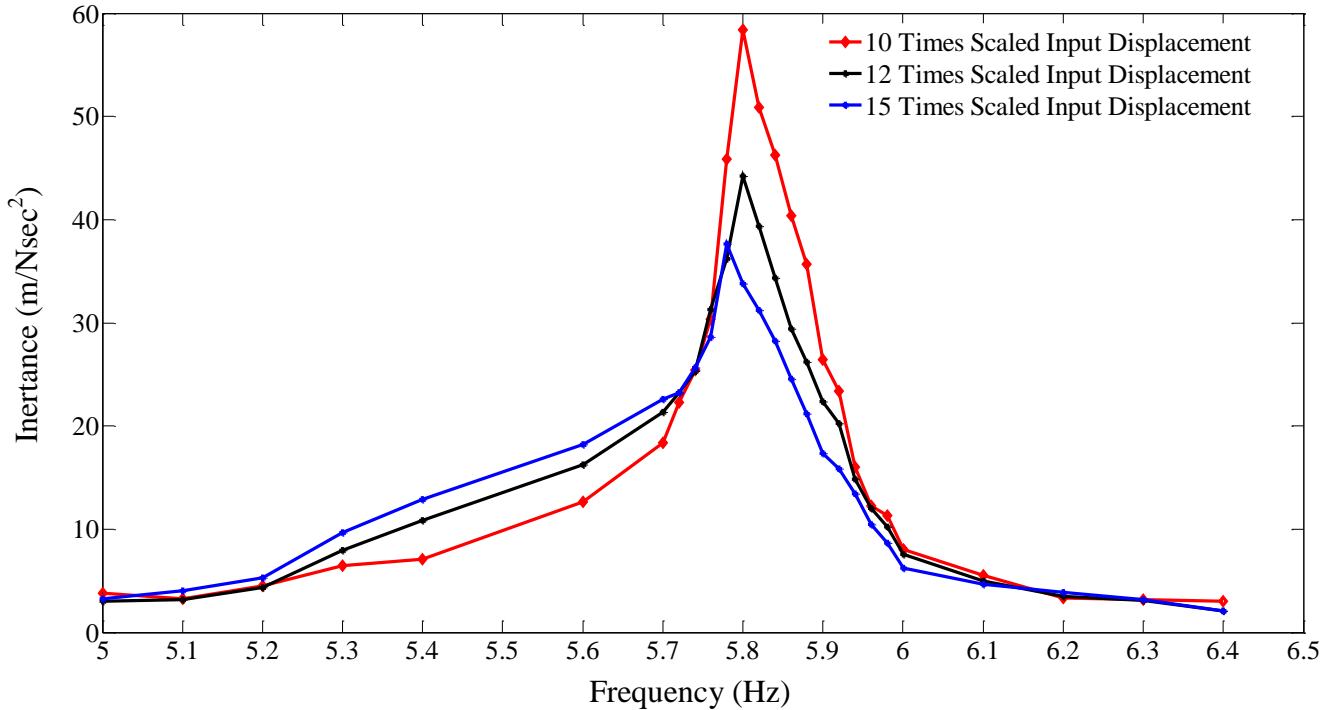
Figure 6.13: Nonlinear FRF Generated from a Step sine Test (Tightening Torque 9.03Nm)

6.2.4 Nonlinear Parameter Identification

Section 6.2.3 shows the nonlinear detection and characterization methodology in a base excited structure with joint connection. In this section, the nonlinear system identification methodology presented in Chapter 4 is applied to obtain the nonlinear parameters for each excitation frequency and for each preloading condition. The nonlinear parameter identification methodology consists: (i) reconstruction of force vector using the base excitation as an input, (ii) extraction of nonlinear restoring force at the measured DOFs and (iii) identification of parameters using the multilinear least square regression in a modal space. Since the identification of the nonlinear parameters involved integration of the measured acceleration signal to the displacement and velocity, the analytical integration algorithms is applied by using the measured steady state acceleration response data. Figure 6.14 shows the steady state acceleration response data, for an excitation frequency of 5.7 Hz measured at a distance of 0.65 m from the fixed end. This steady state

acceleration data is approximated by the analytical function by multilinear least square regression in each time step. Equation (3.33) is used to approximate the analytical function. The analytical approximated function and the measured relative acceleration are shown in Figure 6.15. The Goodness-of-Fit measured in terms of mean square error change is over 99%. The analytical function thus obtained is analytically integrated to obtain the velocity and displacement. The analytically integrated velocity and displacement signal are shown in Figure 6.16 and 6.17. The same procedure is repeated for each excitation frequency, each tightening torque, and each base displacement shown in Table 6.2. Having known the displacement, velocity and acceleration signal at each measured DOF and the mode shape matrix, it is possible to extract the nonlinear modal restoring force using Equation (4.17). The obtained nonlinear restoring force is then fitted with the first mode modal parameters using Equations (4.24-4.27). The procedure is repeated for each excitation frequency, each tightening torque and each scaled base displacement.
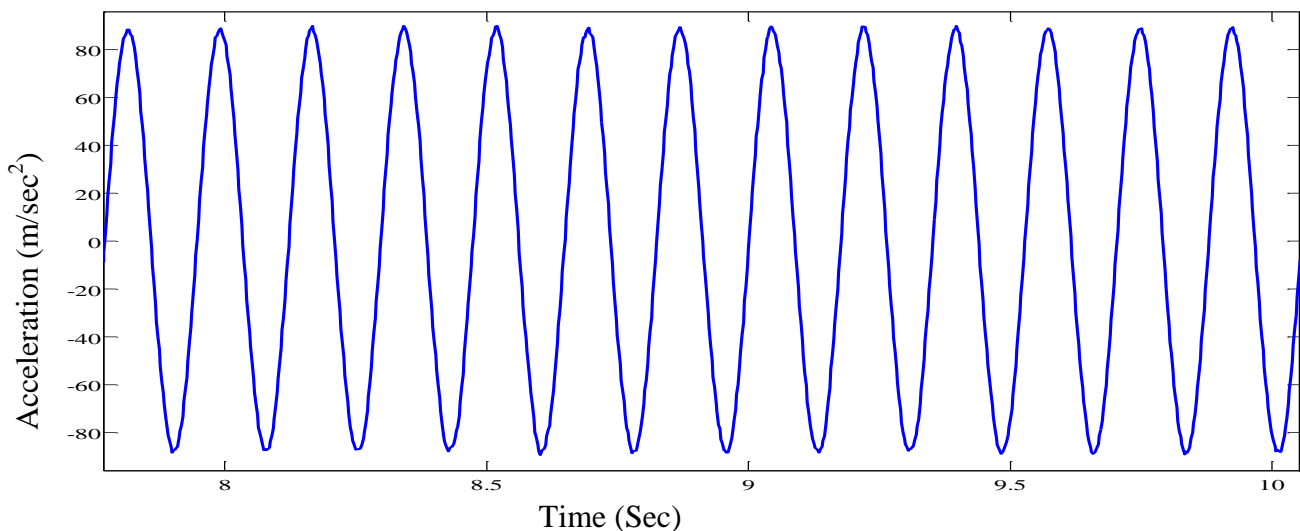
Figure 6.14: Steady state Acceleration Response of the Beam at a Distance of 0.65m from the

Fixed End (@ Tightening Torque 13.55Nm, Excitation Frequency5.7Hz)

128
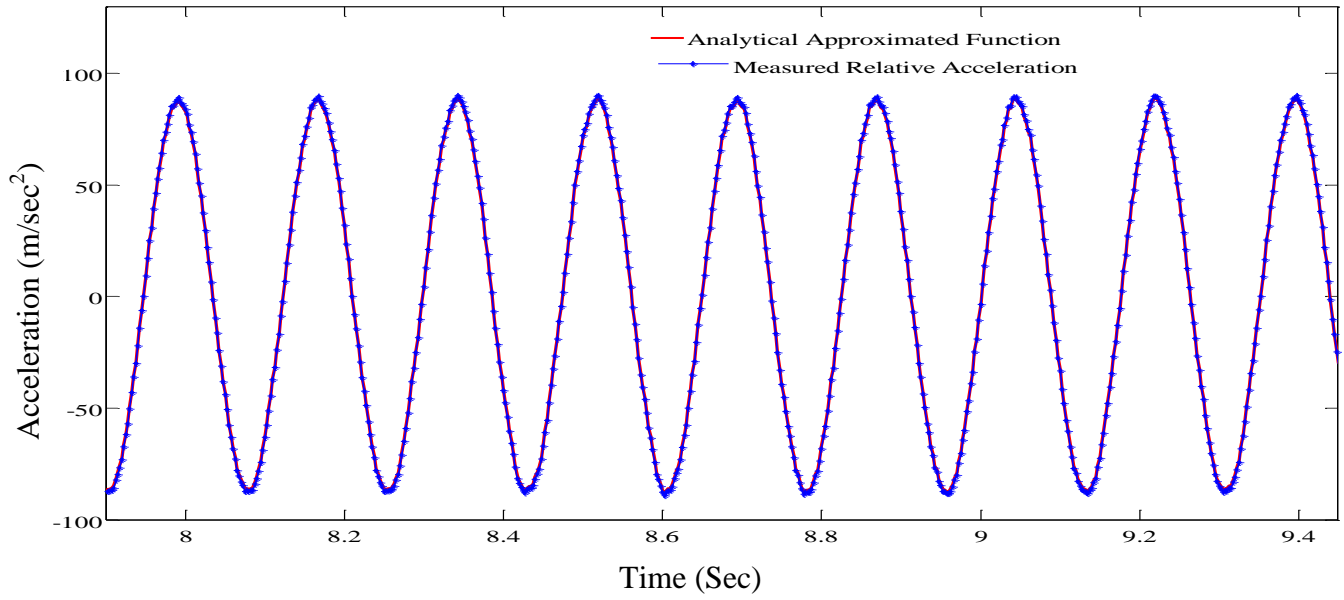
Figure 6.15: Measured and Fitted Acceleration Response of the Beam at a Distance of 0.65m

from the Fixed End (@ Tightening Torque 13.55Nm, Excitation Frequency5.7Hz)
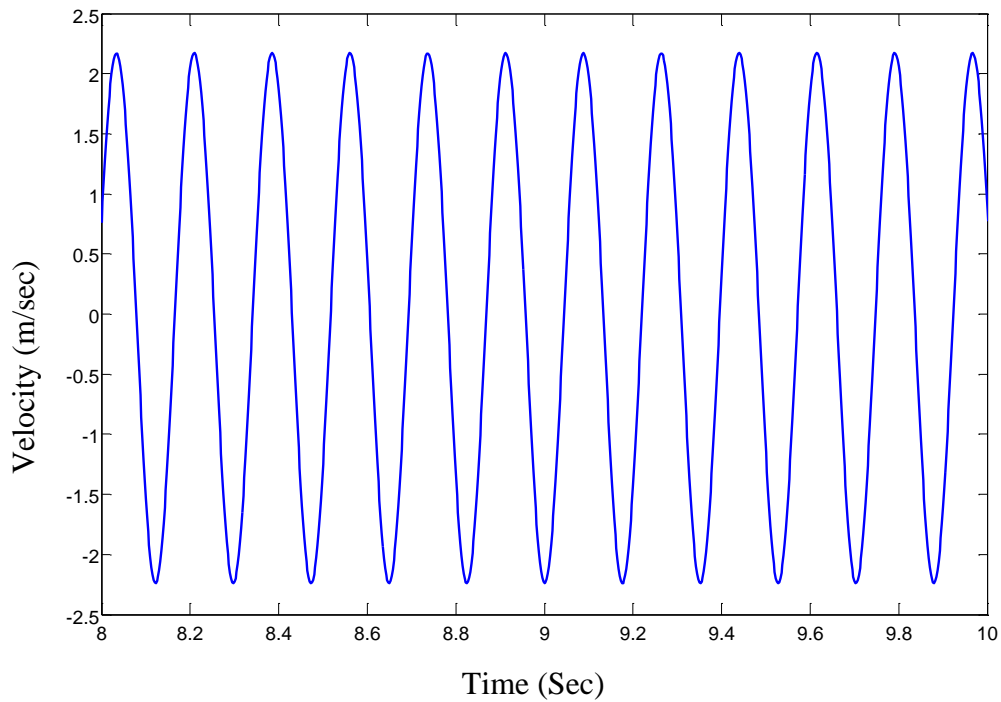
Figure 6.16: Analytically Integrated Velocity Response of the Beam at a Distance of 0.65m from
the Fixed End (@ Tightening torque 13.55Nm, Excitation Frequency5.7Hz)
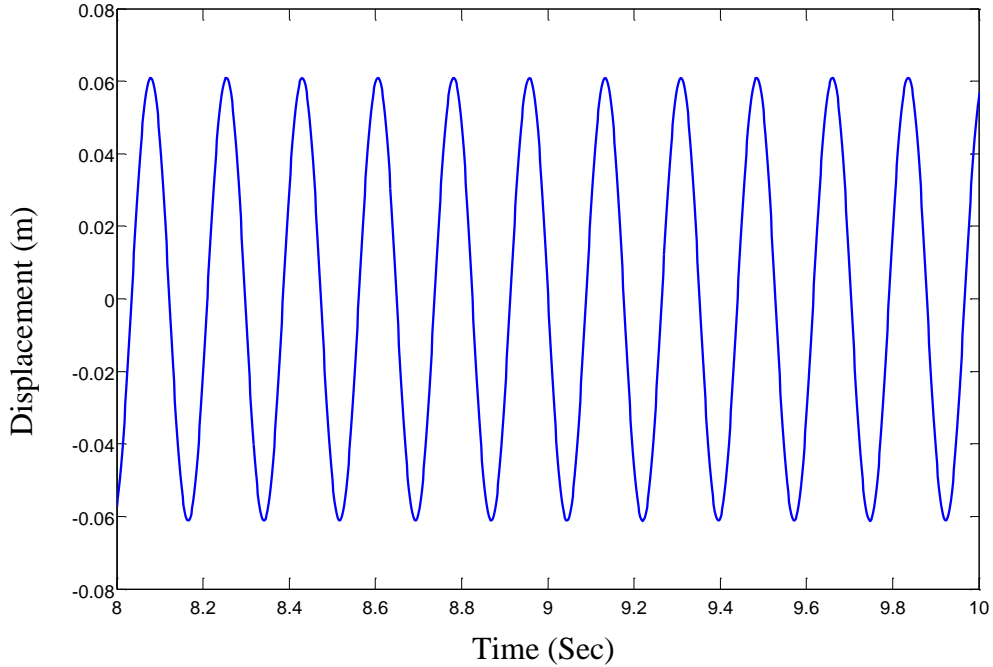
Figure 6.17: Analytically Integrated Displacement Response of the Beam at a Distance of 0.65m

from the Fixed End (@ Tightening Torque 13.55Nm, Excitation Frequency 5.7Hz)

Figures (6.18-6.20) represent the restoring force surface (A) and the hysteresis loop (B) generated for different excitation frequencies with the tightening torque of 13.55Nm. The base displacements at each excitation frequency are scaled to 12 times higher than that shown in Table 6.2. The obtained restoring force shown in each figure exhibits the significant softening effect and the energy dissipation due to slipping at the joint. The identified restoring force surface and the hysteresis loops are over plotted in the same figure in blue color. At the nonlinear natural frequency of 5.82Hz (Figure 6.20), the identified restoring force surface and the hysteresis loop shows the significant deviations. It is due to the fact that only two DOFs below and above the joint are taken to capture the entire dynamics. However, none of these figures show the coupling between the modes. The identified nonlinear parameters for each excitation frequency with 12 times scaled base displacement is tabulated in Table 6.4. Theoretically, the identified stiffness should be constant for each excitation frequency for a constant scaled base

130

displacement and a constant tightening torque. However, the results show the deviation of around 10%, the more being in resonance. Experiments are always susceptible to noise and uncertainty which may results in such a deviation. The maximum amplitude of displacement along with the identified equivalent damping coefficient for each excitation frequency is tabulated in Table 6.4. Having these two parameters it is possible to reconstruct the function to show the variations of damping as a function of maximum amplitude of displacement. Figure 6.21 shows such a plot where the experimentally observed data are shown in the blue dot and the identified function is shown in red. The identified function is obtained by estimating the coefficients in a least square sense using norm 2 error vectors. It should be noted that, to identify the coefficients, one can use the standard multilinear least square regression or norm 2 error vector. Both of the algorithms work in the least square sense and yield the same results.
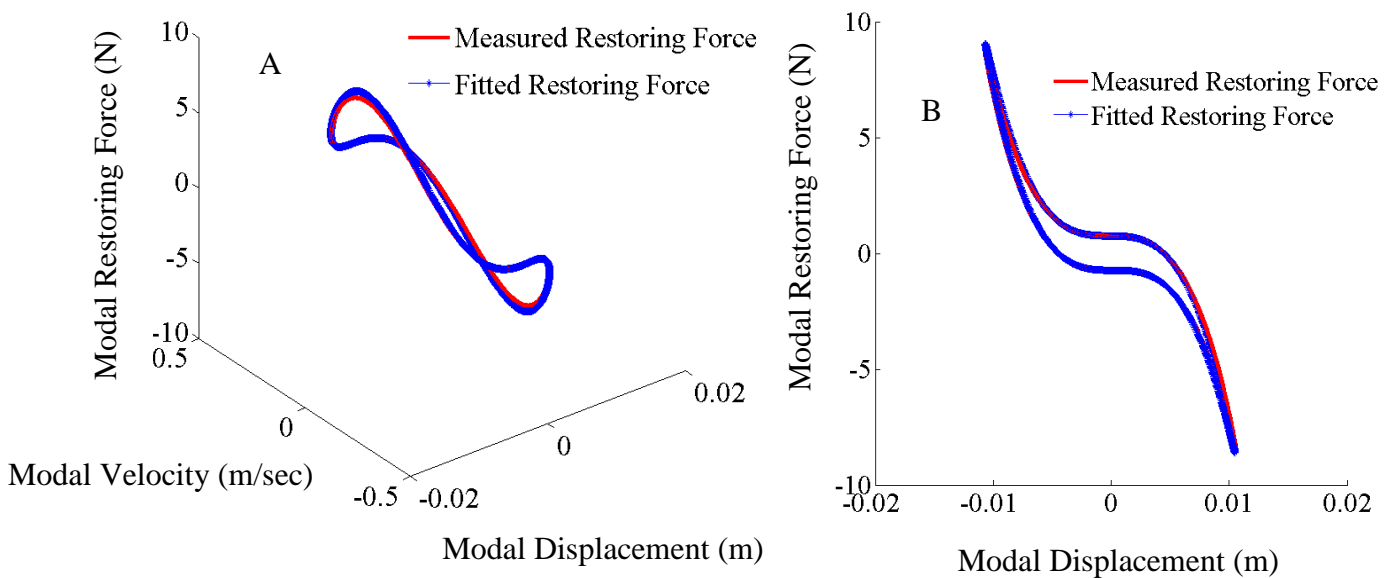
Figure 6.18: Restoring Force Surface (A:3D Surface,B: Slice View (X-Z) Projection, Excitation Frequency : 5.7 Hz, Tightening Torque : 13.55Nm)
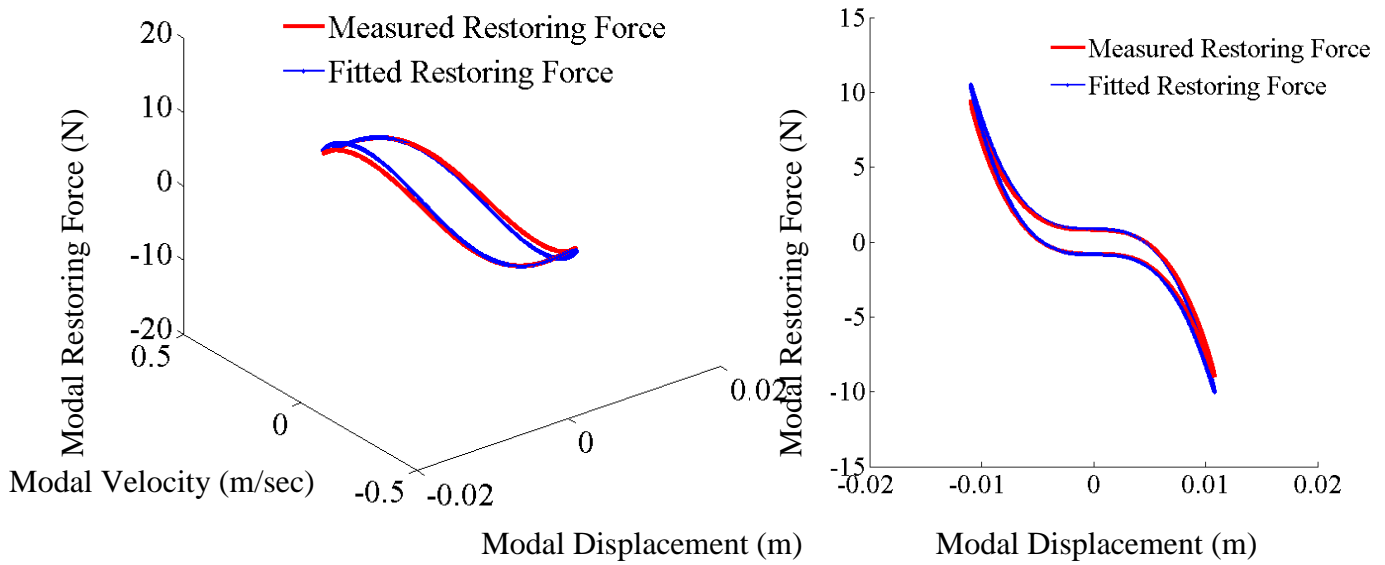
Figure 6.19: Restoring Force Surface (A:3D Surface,B: Slice View (X-Z) Projection, Excitation Frequency : 5.72 Hz, Tightening Torque : 13.55Nm)
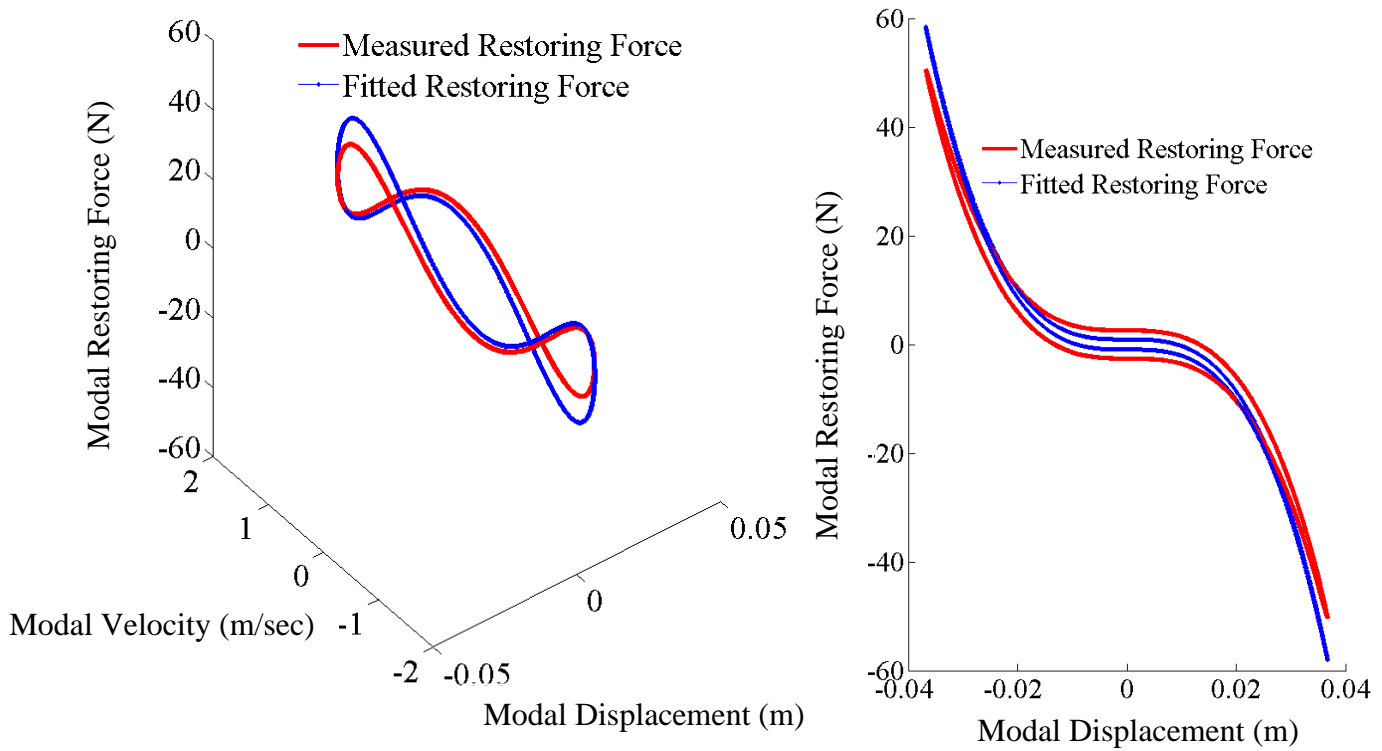
Figure 6.20: Restoring Force Surface (A: 3D Surface, B: Slice View (X-Z) Projection, Excitation Frequency: 5.80 Hz, Tightening Torque: 13.55Nm)

Table 6.3: Identified Nonlinear Parameters for Different Excitations (Tightening Torque (13.55Nm, Base Displacement 12 times Scaled)

Excitation Frequency (Hz)	Maximum Amplitude of Displacement $r_{max}(m)$	Equivalent Damping Coefficient c_{eq}(Nm\sec)	Nonlinear Stiffness $k_2(N/m^3)$
5.0	0.0037561	0.3719	6.45×10^6
5.1	0.004032564	0.3977	6.48×10^6
5.2	0.004119441	0.3859	7.23×10^6
5.3	0.005152218	0.4844	6.89×10^6
5.4	0.00582531	0.5501	7.45×10^6
5.5	0.007027474	0.6901	5.37×10^6
5.6	0.011041567	1.0964	5.49×10^6
5.7	0.01430621	1.5725	6.43×10^6
5.72	0.018007602	1.9305	5.41×10^6
5.74	0.021065172	2.3343	5.32×10^6
5.76	0.02696584	3.1785	6.56×10^6
5.78	0.034020338	4.3003	5.79×10^6
5.80	0.041965147	5.7102	6.94×10^6
5.82	0.034250879	4.3390	9.89×10^6
5.84	0.0331549196	4.3561	6.45×10^6
5.86	0.032892439	4.1127	6.63×10^6
5.88	0.029781333	3.6116	5.92×10^6
5.9	0.023627431	2.6904	6.32×10^6
5.92	0.019767518	2.3601	6.23×10^6
5.94	0.015829746	1.6569	6.05×10^6
5.96	0.012329365	1.2416	6.23×10^6

5.98	0.009449127	0.9225	6.48×10^6
6.0	0.005643001	0.5322	5.49×10^6
6.1	0.003403679	0.3192	6.49×10^6
6.2	0.002833501	0.3669	5.89×10^6
6.3	0.002680442	0.3530	5.29×10^6
6.4	0.002479834	0.3349	5.45×10^6
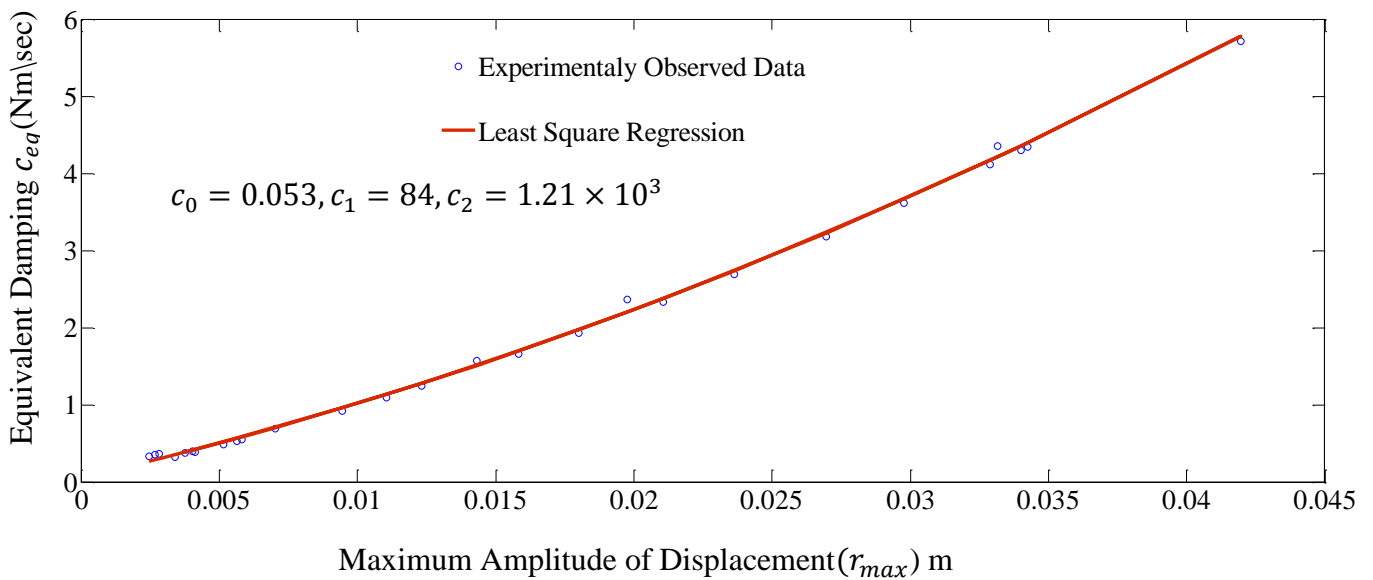
Figure 6.21: Viscous Damping Coefficient as a Function of Maximum Amplitude of Displacement

6.3   Summary

This chapter presents the identification algorithm for nonlinear bolt lap joint parameters using the base excitation as an input. The identification algorithm consists of: nonlinearity detection and characterization and the nonlinear parameter identification. The nonlinearity detection and characterization is carried out by exciting the system in a frequency band around the first natural frequency of the system and maintaining the constant equivalent excitation force in the excitation frequency range. The nonlinear parameter identification is carried out by using the theory

described in Chapter 4 of this thesis. A nonlinear single DOF model in the modal coordinate is chosen to demonstrate the approach numerically. The forward approach is carried out by assuming the nonlinear parameters to demonstrate the effects of the nonlinearity on the amplitude of vibration and the natural frequency of the system. The reverse approach is carried out to obtain the assumed nonlinear parameters. Following the numerical simulations, an experimental study is carried out on structure with two beams connected with a bolted joint. The nonlinearity detection, characterization and identification are carried out following the same procedure that is applied in the numerical model. The most significant result obtained from the experiment is that the presence of viscous damping as a quadratic function of the amplitude of displacement. The restoring force surface and the hysteresis plots provided the considerable validation of the identified stiffness and the viscous damping terms dependent upon the displacement amplitude.

Chapter 7

Conclusion and Future Work

This chapter presents a summary of the research findings, contribution to knowledge and recommendation for further research in this area.

7.1 Conclusion of the Research Work

Ground vehicle component durability testing is an important research topic, relevant to automotive industries. It encompasses multiple steps, like measuring the field test data, generating the accelerated loading profile, and implementing the loading profile in the laboratory. The engineering problem in the implementation of the loading profile is the unknown dynamics of the test components, such as stiffness and damping of the structures. These dynamics have adverse effects on the durability testing, for example, changing the failure mechanism of the test components.

Research in the structural dynamics includes various sub-areas, such as nonlinear system identification, stability studies of nonlinear systems, and the prediction of dynamic response for a nonlinear system. Although the research in the field of nonlinear system identification progressed for the last four decades, most developments have been restricted to the force excited structure, rather than the base excited structure. As durability tests are conducted through base excitation, to address the problems associated with the durability tests, the methodologies proposed in this thesis are specific to the parametric identification of nonlinear systems with base excitation. A test setup was developed such that the proposed methodologies can be demonstrated. The focus of this research is always kept on the practical implementation of the

proposed methodologies which can be integrated with the established tools like finite element analysis and modal analysis. The detailed conclusions on different topics are presented below.

7.1.1 Nonlinear System Identification Method for Base Excited Structures

For the base excited structure, the excitation force is distributed over the entire structure depending upon the mass distribution of the structure and is usually not feasible for measurements. Therefore, the conventional nonlinear system identification method cannot be applied in such cases. Two different strategies for nonlinear system identification of a base excited structure are proposed. The first methodology extracts the nonlinear parameters in the physical coordinates system, while the second methodology extracts the nonlinear parameters in the modal space. During demonstration, the second methodology is presented as it can extract maximum number of nonlinear terms. The crucial step in the nonlinear system identification of base excited structure is the extraction of the input in the form of force. A concise methodology based on the hybrid model technique is presented to reconstruct the force from the measured data where a closed-form solution is presented. The theory presented is validated with the numerical examples through simulations. This methodology can be used for both acceleration and displacement controlled tests.

7.1.2 Development of Experimental Setup for Nonlinear System Identification

An experimental setup specific to the proposed methodologies was designed, fabricated and installed. The system composes of a shaker table driven by the hydraulic system. The shaker table was constructed with the in-house knowledge and fabrication capability. The shaker table has the first natural frequency above 300Hz, which makes it significantly rigid. A procedure for the construction and the assembly of the small scale shaker table has been presented. The input to the system is displacements making it as a base excited system. The tests using harmonic

137

signals show that the displacements, as well as the acceleration time histories for the command and the response match well. However, some errors are noticed at low frequencies in the test signal which are due to the type of support bearings.

7.1.3 Demonstration of Force Reconstruction Technique in Base Excited Structure

Currently, in an automotive industry, prediction of the input force acting on a structure is a big challenge. Prediction of the input force is not only necessary for the vibration analysis of the structure but also for the stress-strain analysis of the structure. In this research study, the prediction of the input force acting on a structure is analyzed as an inverse but a well posed problem. A closed form solution is derived and is validated using the lumped parameter model. The theory is demonstrated by using a cantilever beam. A step sine input loading with constant base displacement is used to demonstrate the force reconstruction technique. Several results are shown to demonstrate the force reconstruction technique. The particular result from the experimentation is that the reconstructed input force vector is not equal to the equivalent excitation force vector. This is due to the fact that the unmeasured DOFs and unidentified modes project the force to the measured DOFs.

7.1.4 Experimental Demonstration of Nonlinear System Identification

Automotive engineers usually face difficulties when dealing with experimentally measured vibration data on a real life engineering structure. To overcome this difficulty, two methodologies specific to nonlinear system identification in a base excited structure are proposed in this thesis. Within the methodologies, two different integration algorithms are used to extract the nonlinear parameters: a single harmonic integration in frequency domain and an analytical integration of the measured steady state response data. The results are compared for both techniques using a cantilever beam as an example. The nonlinearities associated with the beam

are extracted by exciting the beam under high base motion. The natural frequencies found from the experiment are equivalent to the theoretical derived one, indicating that the beam is lightly damped. The modal damping ratios measured from the experiments are 0.028, 0.008 and 0.0065 for first, second and third mode, respectively. Several experimental results are presented to demonstrate the proposed methodology. At the first mode nonlinear identification test, there are no significant nonlinear damping terms. The cubic stiffness nonlinearity for first mode using two different integration algorithms at different excitations is compared. Results shows that the analytical integration technique is the best one as it can caters for multi-harmonic signal.

7.1.5   Nonlinear System Identification of Structures with Bolted Joint

Most of the body structures of ground vehicles are joined by means of bolting. It is known that the added flexibility introduced by the joint to the structure greatly affects its behavior and much of the energy is lost at the joint due to microslip. The energy losses at the joint introduce significant damping and stiffness nonlinearities. It is thus essential to develop the algorithm for the detection and characterization of nonlinearities (damping and stiffness) due to the bolted connection.

The nonlinearity detection and characterization methodology for the bolted lap joint structure using the base excitation as an input is developed. The methodology consists of exciting the system in a frequency band around each natural frequency of the system, while maintaining the constant equivalent excitation force. The proposed methodology is validated by taking a numerical example in the modal space using the simulation data. An experimental study is carried out using two beams connected with a bolted joint in the fixed free boundary condition. The nonlinearity detection and characterization for a bolted joint beam is carried out at several excitations frequencies, different base displacements and different pre-loadings (Tightening

Torque). Experimental results show that, when the bolt is sufficiently loosen, slipping behavior exist at the joints which results in the softening nonlinearity and the amplitude depending damping.

From the methodology and results obtained from the experiment conducted in this research study, it is concluded that the nonlinearity detection and characterization method presented thesis can be used for the initial stages of the analysis to get an idea about the nonlinear behavior of the structure. Based on the operating conditions, excitation ranges and relevant frequency, the nonlinearity can be further characterized. Once the nonlinearity is further characterized, the nonlinear parameter identification algorithm presented in this thesis can be used for any structure to identify the nonlinear parameters.

7.2   Limitations of the Current Work:

The limitations of the current research work are listed below.

- The nonlinear system identification methods proposed in this research work are based on the reverse explicit formulation. While formulating the theory, uncertainties in the dynamic systems are not considered. It is important to realize the source and type of uncertainties that exist in a dynamical system and a tool to cope with them.

- Several types of nonlinearities may exist in the real practical structure. Example include: discontinuous nonlinearities, non-smooth nonlinearities. It is important to realize such type of nonlinearities and test the proposed methodologies for such type of nonlinearities.

- Nonlinear system identification is an intermediate task. The bigger aim is the prediction of the system response. In order to predict the system response, it is important to understand the dynamics of the system in terms of stability.

7.3   Recommendation for Future Work

The research presented in this thesis started with the aim of developing the solution for the engineering problem, which is seen in the implementation phase of ground vehicle durability testing. The problem associated with the implementation phase is the generated loading profile in the MAST, using the controller iterative software does not match with the actual loading profile. The engineering problem associated with the loading profile replication is due to the nonlinear dynamics of the structure. There are two possible research areas that can address this. The first is to change the controller design software or iteration algorithm. The second is to identify the dynamics of the structure. Research presented in this thesis progressed in the second area which is the nonlinear system identification of the structures. Still at the end, certain questions remain unanswered. The research in the area of nonlinear system identification for a base excited structure can be taken further in the direction of topics presented below.

- The methods presented in this thesis are based on the normal modes concept. It would be an interesting research to extend the methods presented in this thesis, for a structure where complex modes exist.

- The identification methodologies presented in this thesis are demonstrated by using a single axis simulation table (SAST) as a base excitation. As demonstrated in Chapter 4, the modes cannot be isolated in a SAST. It would be better, if these methodologies are applied to the MAST, such that the modes can be isolated. There are several challenges while applying the proposed methodologies to the MAST. These includes, but not limited to; tuning the MAST (controlling the force at each DOF of the MAST); (ii) critical locations of the sensor; and, adaptation of excitation frequency and optimization of the base axis combination.

141

- The footprint library (collection of different nonlinearities), that address different types of nonlinearities for the base excited structures has not been developed yet. Developing such a footprint library containing different contribution of nonlinearities, would be beneficial.

- The nonlinear parameters associated with the structure are input dependent. In this research study the step sine and the single harmonic sinusoidal loading are used to detect, characterize and identify the nonlinearity. The step sine test is an extremely time consuming test for nonlinearity detection and characterization. Thus, it is essential to design the optimum input that can accurately detect, characterize and locate the nonlinearity. A tool which integrates the above four tasks would be worth researching.

References

1. Londhe, Abhijit, Suhas Kangde, and Narayana Moorthy. *Evaluation of Vehicle Systems Structural Durability Using PSD Based Fatigue Life Approach*. No. 2012-01-0953. SAE Technical Paper, 2012.

2. Halfpenny, Andrew. "Methods for Accelerating Dynamic Durability Tests."*nCode International Ltd, Sheffield* (2006).

3. Halfpenny, Andrew. "Accelerated vibration testing based on fatigue damage spectra." *White paper, nCode International,www.ncode.com*.

4. Johansson, Anders T. *Dynamic response reconstruction using passive components*. Chalmers University of Technology, 2012.

5. Nordberg, Patrik. *Time domain methods for load identification of linear and nonlinear systems*. Chalmers University of Technology, 2004.

6. Ewins, David J. *Modal testing: theory and practice*. Vol. 2. Letchworth: Research studies press, 1986.

7. Hermans, Luc, and Herman van der Auweraer. "Modal testing and analysis of structures under operational conditions: industrial applications." *Mechanical Systems and Signal Processing* 13.2 (1999): 193-216.

8. Lalanne, C., 2002. *"Mechanical Vibration & Shock,"* Volume II. Hermes Penton Ltd. London.

9. Peeters, Bart, and Guido De Roeck. "Reference-based stochastic subspace identification for output-only modal analysis." *Mechanical systems and signal processing* 13.6 (1999): 855-878.

10. Kerschen, Gaetan, et al. "Past, present and future of nonlinear system identification in structural dynamics." *Mechanical Systems and Signal Processing* 20.3 (2006): 505-592.

11. Billings, Stephen A. *Nonlinear system identification: NARMAX methods in the time, frequency, and spatio-temporal domains*. John Wiley & Sons, 2013.

12. Guo, Yuzhu, et al. "Identification of Nonlinear Systems with Non-Persistent Excitation using an Iterative Forward Orthogonal Least Squares Regression Algorithm."

13. Nayfeh, Ali H., and Dean T. Mook. *Nonlinear oscillations*. John Wiley & Sons, 2008.

14. Worden, Keith, and Geoffrey R. Tomlinson. *Nonlinearity in structural dynamics: detection, identification and modelling*. CRC Press, 2010.

15. Peeters, Bart, and Guido De Roeck. "Stochastic system identification for operational modal analysis: a review." *Journal of Dynamic Systems, Measurement, and Control* 123.4 (2001): 659-667.

16. Erlicher, Silvano, and Pierre Argoul. "Modal identification of linear non-proportionally damped systems by wavelet transform." *Mechanical Systems and signal processing* 21.3 (2007): 1386-1421.

17. Bashash, Saeid, A. Salehi-Khojinl, and Nader Jalili. "Forced vibration analysis of flexible Euler-Bernoulli beams with geometrical discontinuities." *American Control Conference, 2008*. IEEE, 2008.

18. Gondhalekar A., C., Petrov E. P., Imregun, M., 2009. "Parameters Identification for Nonlinear Dynamic Systems Via Genetic Algorithm Optimization", Journal of computational and nonlinear dynamics, 4(4), pp. 1-9.

19. Gondhalekar A., C., 2009. *"Strategies for Nonlinear System Identification."* Diss. University of London, 2009.

20. Marchesiello, Stefano, and Luigi Garibaldi. "A time domain approach for identifying nonlinear vibrating structures by subspace methods." *Mechanical Systems and Signal Processing* 22.1 (2008): 81-101.

21. Rosenberg, R. M. "0n Nonlinear Vibrations of Systems with Many Degrees of Freedom." *Advances in applied mechanics* 9 (1966): 155.

22. Shaw, S. W. "An invariant manifold approach to nonlinear normal modes of oscillation." *Journal of Nonlinear Science* 4.1 (1994): 419-448.

23. Pesheck, E., C. Pierre, and S. W. Shaw. "A new Galerkin-based approach for accurate non-linear normal modes through invariant manifolds." *Journal of sound and vibration* 249.5 (2002): 971-993.

24. Nayfeh, A. H., and S. A. Nayfeh. "On nonlinear modes of continuous systems."*Journal of Vibration and Acoustics* 116.1 (1994): 129-136.

25. Nayfeh, A. H., and S. A. Nayfeh. "Nonlinear normal modes of a continuous system with quadratic nonlinearities." *Journal of vibration and acoustics* 117.2 (1995): 199-205.

26. Nayfeh, Ali H., Char-Ming Chin, and Jon Pratt. "Perturbation methods in nonlinear dynamics—applications to machining dynamics." *Journal of Manufacturing Science and Engineering* 119.4A (1997): 485-493.

27. Mahmoodi, S. N., S. E. Khadem, and M. Rezaee. "Analysis of non-linear mode shapes and natural frequencies of continuous damped systems." *Journal of Sound and Vibration* 275.1 (2004): 283-298.

28. Masri, S. F., et al. "Identification of nonlinear vibrating structures: Part I-formulation." *Journal of Applied Mechanics* 54.4 (1987): 918-922.

29. Richards, C. M., and R. Singh. "Identification of multi-degree-of-freedom non-linear systems under random excitations by the "reverse path" spectral method." *Journal of Sound and Vibration* 213.4 (1998): 673-708.

30. Van Pelt, Tobin H., and Dennis S. Bernstein. "Non-linear system identification using Hammerstein and non-linear feedback models with piecewise linear static maps." *International Journal of Control* 74.18 (2001): 1807-1823.

31. He, J., and D. J. Ewins. "A simple method of interpretation for the modal analysis of nonlinear systems." *International Modal Analysis Conference, 5th, London, England*. 1987.

32. Feldman, Michael. "Hilbert transform in vibration analysis." *Mechanical Systems and Signal Processing* 25.3 (2011): 735-802.

33. Platten, Michael F., et al. "Identification of multi-degree of freedom non-linear systems using an extended modal space model." *Mechanical Systems and Signal Processing* 23.1 (2009): 8-29.

34. Platten, Michael F., et al. "Non-linear identification in modal space using a genetic algorithm approach for model selection." *International Journal of Applied Mathematics and Mechanics* 3.1 (2007): 72-89.

35. Siller, Hugo Ramon Elizalde. *Non-linear modal analysis methods for engineering structures*. Diss. University of London, 2004.

36. Jalali, Hassan, and Behzad T. Bonab. "Nonlinearity identification using sensitivity of frequency response functions." *Journal of Vibration and Control* (2012).

37. Jalali, H., B. T. Bonab, and H. Ahmadian. "Identification of weakly nonlinear systems using describing function inversion." *Experimental Mechanics* 51.5 (2011): 739-747.

38. Ku, Y. H., and C. F. Chen. "A new method for evaluating the describing function of hysteresis-type nonlinearities." *Journal of the Franklin Institute* 273.3 (1962): 226-241.

39. Watanabe K, Sato H (1988). "A modal analysis approach to nonlinear multidegrees-of-freedom systems." *ASME J Vibrations Stress Reliab* Des 189:110–410.

40. Kuran, B., and H. N. Özgüven. "A modal superposition method for non-linear structures." *Journal of Sound and vibration* 189.3 (1996): 315-339.

41. Besançon-Voda, Alina, and Petr Blaha. "Describing function approximation of a two-relay system configuration with application to Coulomb friction identification." *Control Engineering Practice* 10.6 (2002): 655-668.

42. Özer, Mehmet Bülent, H. Nevzat Özgüven, and Thomas J. Royston. "Identification of structural non-linearities using describing functions and the Sherman–Morrison method." *Mechanical Systems and Signal Processing* 23.1 (2009): 30-44.

43. Williams, Roger, John Crowley, and Havard Vold. "The multivariate mode indicator function in modal analysis." *International Modal Analysis Conference*. 1985.

44. Wright, J. R., J. E. Cooper, and M. J. Desforges. "Normal-mode force appropriation-theory and application." *Mechanical Systems and Signal Processing* 13.2 (1999): 217-240.

45. Sinapius, J. M. "Tuning of normal modes by multi-axial base excitation." *Mechanical systems and signal processing* 13.6 (1999): 911-924.

46. Füllekrug, U., and M. Sinapius. "Structural dynamics identification by means of multi-axial base excitation- Theory and application." *European Conference on Spacecraft Structures, Materials and Mechanical Testing, Braunschweig, Germany, Proceedings*. Vol. 4. No. 6. 1998.

47. Blondet, Marcial, and Carlos Esparza. "Analysis of shaking table-structure interaction effects during seismic simulation tests." *Earthquake engineering & structural dynamics* 16.4 (1988): 473-490.

48. Sjöberg, Jonas, et al. "Nonlinear black-box modeling in system identification: a unified overview." *Automatica* 31.12 (1995): 1691-1724.

49. Allison, Timothy Charles. *System Identification via the Proper Orthogonal Decomposition*. Diss. Virginia Polytechnic Institute and State University, 2007.

50. Saadat, Soheil, et al. "An intelligent parameter varying (IPV) approach for non-linear system identification of base excited structures." *International Journal of Non-Linear Mechanics* 39.6 (2004): 993-1004.

51. Halfpenny, A., 1999. "A Frequency Domain Approach for Fatigue Life Estimation from Finite Element Analysis," In: Proceedings of DAMAS 99 conference Dublin.

52. Marchesiello, Stefano, and Luigi Garibaldi. "A time domain approach for identifying nonlinear vibrating structures by subspace methods." *Mechanical Systems and Signal Processing* 22.1 (2008): 81-101.

53. Juditsky, Anatoli, et al. "Nonlinear black-box models in system identification: Mathematical foundations." *Automatica* 31.12 (1995): 1725-1750.

54. Schoukens, Johan, et al. "Frequency response function measurements in the presence of nonlinear distortions." *Automatica* 37.6 (2001): 939-946.

55. Magnevall, Martin. *Methods for Simulation and characterization of nonlinear mechanical structures*. Blekinge Institute of Technology, 2008.

56. Naylor, Steven, et al. "Identification of multi-degree of freedom systems with nonproportional damping using the resonant decay method." *Journal of vibration and acoustics* 126.2 (2004): 298-306.

57. Doranga, Sushil, and Christine Q. Wu. "Parameter Identification for Nonlinear Dynamic Systems via Multilinear Least Square Estimation." *Special Topics in Structural Dynamics, Volume 6*. Springer International Publishing, 2014. 169-182.

58. Chopra, Anil K., and Chatpan Chintanapakdee. "Drift spectrum vs. modal analysis of structural response to near-fault ground motions." *Earthquake Spectra* 17.2 (2001): 221-234.

59. Shih, C. Y., et al. "Complex mode indication function and its applications to spatial domain parameter estimation." *Mechanical Systems and Signal Processing* 2.4 (1988): 367-377.

60. Balmes, E. "Integration of existing methods and user knowledge in a mimo identification algorithm for structures with high modal densities." *International Modal Analysis Conference*. 1993.

61. Van der Auweraer, Herman, et al. "Optimum force vector conditioning in incremental sine testing." *International Modal Analysis Conference*. 1992.

62. Balmes, E., et al. "An evaluation of modal testing results based on the force appropriation method." *Proc. IMAC 13 International Modal Analysis Conference*. 1995.

63. Peeters, Bart, et al. "Modern solutions for ground vibration testing of large aircraft." *Sound and Vibration* 43.1 (2009): 8.

64. Salehi, M. A. H. D. I., and S. Ziaei-Rad. "Ground vibration test (GVT) and correlation analysis of an aircraft structure model." *IRANIAN JOURNAL OF SCIENCE AND TECHNOLOGY* 31.B (2007): 65.

65. Rodriguez-Vazquez, K., and Peter J. Fleming. "Multi-objective genetic programming for nonlinear system identification." *Electronics Letters* 34.9 (1998): 930-931.

66. Kyprianou, A., K. Worden, and M. Panet. "Identification of hysteretic systems using the differential evolution algorithm." *Journal of Sound and Vibration* 248.2 (2001): 289-314.

67. Charalampakis, A. E., and V. K. Koumousis. "Identification of Bouc–Wen hysteretic systems by a hybrid evolutionary algorithm." *Journal of Sound and Vibration* 314.3 (2008): 571-585.

68. Haupt, Randy L., and Sue Ellen Haupt. *Practical genetic algorithms*. John Wiley & Sons, 2004.

69. Jalali, Hassan, Hamid Ahmadian, and John E. Mottershead. "Identification of nonlinear bolted lap-joint parameters by force-state mapping." *International Journal of Solids and Structures* 44.25 (2007): 8087-8105.

70. Goege, Dennis, et al. "Advanced test strategy for identification and characterization of nonlinearities of aerospace structures." *AIAA journal* 43.5 (2005): 974-986.

71. Ma, X., L. Bergman, and A. Vakakis. "Identification of bolted joints through laser vibrometry." *Journal of Sound and Vibration* 246.3 (2001): 441-460.

72. Hartwigsen, Christian J., et al. "Experimental study of non-linear effects in a typical shear lap joint configuration." *Journal of Sound and Vibration* 277.1 (2004): 327-351.

73. Ahmadian, Hamid, and Hassan Jalali. "Identification of bolted lap joints parameters in assembled structures." *Mechanical Systems and Signal Processing* 21.2 (2007): 1041-1050.

74. Van Den Einde, Lelli, et al. "Development of the George E. Brown Jr. network for earthquake engineering simulation (NEES) large high performance outdoor shake table at the University of California, San Diego." *Proceedings of the 13th World Conference on Earthquake Engineering*. 2004.

75. Ozcelik, O., et al. "Experimental characterization, modeling and identification of the NEES-UCSD shake table mechanical system." *Earthquake Engineering & Structural Dynamics* 37.2 (2008): 243-264.

76. Luco, J. E., et al. "Experimental study of the dynamic interaction between the foundation of the NEES/UCSD Shake Table and the surrounding soil: Reaction block response." *Soil Dynamics and Earthquake Engineering* 31.7 (2011): 954-973.

77. Sinha, Piyush, and Durgesh C. Rai. "Development and performance of single-axis shake table for earthquake simulation." *Current science* 96.12 (2009): 1611-1620.

78. Doranga, S., and C. Q. Wu. "Development and Performance Analysis of Single Axis Simulation Table for Durability Testing." *Dynamics of Civil Structures, Volume 4*. Springer International Publishing, 2014. 227-234.

Appendix A

Nonlinear Parameter Extraction through Conventional Technique

This section presents how the nonlinear system identification in a base excited structure can be connected to the conventional nonlinear system identification strategy with multiple input force excited system. The algorithm follows the Figure 4.1, Stage III. If the reconstructed force vector, (Figure 4.1, Stage I) and the nonlinear restoring force (Figure 4.1, Stage II) are obtained, the conventional method can be used to estimate the nonlinear parameters. The nonzero elements of G in Equation (4.17) indicate nonlinearity at the corresponding degree of freedom. In [12] the nonlinear force extracted from the experimental data is formulated as a combined effect of three nonlinearities. The three nonlinearities are cubic stiffness, clearance and friction. Thus at the ith degree of freedom, the extracted nonlinear force can be written as,

$$G_i = g^{cubic} + g^{clearance} + g^{friction} \tag{A.1}$$

Where g^{cubic}, $g^{clearance}$ and $g^{friction}$ are the nonlinear force for cubic stiffness, clearance, and friction nonlinearities obtained from a first order harmonic balance method. The expressions for these forces are given in Table 2. The identification problem can be posed as an optimization problem by formulating the residual at the ith degree of freedom as

$$R_i = g^{cubic} + g^{clearance} + g^{friction} - G_i \tag{A.2}$$

Where G_i is the nonlinear force at the ith degree of freedom obtained from Equation (4.17), and the nonlinear forces are the same as those given in Table A.1. The total residual to be minimized for n_s selected points can be written as,

$$R = \frac{\sum_{j=1}^{n_s} (R_i)^2{}_j}{n_s} \tag{A.3}$$

The residual given in Equation (A.3) can be minimized to find the optimized values for n_p nonlinear parameters.

The nonlinear parameters now can be searched by using a genetic algorithm approach. There are a lot of literatures dealing with the genetic algorithm optimization. More detailed about optimization can be found in [18, 42, 52, 53 54].

Table A.1: Expression for Nonlinear Restoring Force [18]

Type of nonlinearity	Magnitude of non-linear force
Cubic stiffness	$$g^{cub} = \frac{3}{4}\beta(Y_i - Y_j)^2$$ Where β is the coefficient of cubic stiffness nonlinearity, Y_i and Y_j are the amplitudes of displacement at i^{th} and j^{th} degree of freedom respectively
Clearance	$$g^{cle} = \frac{K_z * (Y_i - Y_j)}{2\pi}[\pi - 2\theta_c + \sin(2\theta_c) - \frac{4y_c}{(Y_1 - Y_j)}cos\theta_c]$$ $$\theta_c = sin^{-1}\left(\frac{y_c}{(Y_1 - Y_j)}\right)$$ Where, K_z is the additional stiffness after the clearance gap is closed, y_c is the gap distance.
Friction	Stick region: $g^{fri} = \frac{K_d((Y_1 - Y_j))}{\pi}(\theta_l - sin_{\theta_l} cos_{\theta_l})$ Slip region: $g^{fri} = \frac{-4\mu N}{\pi}\left(1 - \frac{\mu N}{K_d(Y_1 - Y_j)}\right)$ $$\theta_l = cos^{-1}\left(1 - \frac{2\mu N}{K_d(Y_1 - Y_j)}\right)$$ Where, K_d is the tangential stiffness in stick region, N is the normal reaction, and μ is the coefficient of friction.

Technical Data for Bolt Clamping Loads (www.spaenaur.com/pdf/sectionD/D48.pdf)

Technical Data

Suggested Tightening Torque1 Values To Produce Corresponding Bolt Clamping Loads

Size	Bolt Dia. D (in.)	Tensile Stress Area A (sq. in.)	SAE Grade 2 Bolts Tensile Strength (min psi)	Proof Load (psi)	Clamp2 Load P (lb.)	Tightening Torque Dry K=0.20	Lub. K=0.15	SAE Grade 5 Bolts Tensile Strength (min psi)	Proof Load (psi)	Clamp2 Load P (lb.)	Tightening Torque Dry K=0.20	Lub. K=0.15	SAE Grade 73 Clamp2 Load P (lb.)	Tightening Torque Dry K=0.20	Lub. K=0.15	SAE Grade 84 Clamp2 Load P (lb.)	Tightening Torque Dry K=0.20	Lub. K=0.15
						lb. in.	lb. in.				lb. in.	lb. in.		lb. in.	lb. in.		lb. in.	lb. in.
4-40	0.1120	0.00604	74,000	55,000	240	5	4	120,000	85,000	380	8	6	480	11	8	540	12	9
4-48	0.1120	0.00661			280	6	5			420	9	7	520	12	9	600	13	10
6-32	0.1380	0.00909			380	10	8			580	16	12	720	20	15	820	23	17
6-40	0.1380	0.01015			420	12	9			640	18	13	800	22	17	920	25	19
8-32	0.1640	0.01400			580	19	14			900	30	22	1100	36	27	1260	41	31
8-36	0.1640	0.01474			600	20	15			940	31	23	1160	38	29	1320	43	32
10-24	0.1900	0.01750			720	27	21			1120	43	32	1380	52	39	1580	60	45
10-32	0.1900	0.02000			820	31	23			1285	49	36	1580	60	45	1800	68	51
1/4-20	0.2500	0.0318			1320	66	49			2020	96	75	2500	120	96	2860	144	108
1/4-28	0.2500	0.0364			1500	76	56			2320	120	86	2860	144	108	3280	168	120
						lb. ft.	lb. ft.				lb. ft.	lb. ft.		lb. ft.	lb. ft.		lb. ft.	lb. ft.
5/16-18	0.3125	0.0524			2160	11	8			3340	17	13	4120	21	16	4720	25	18
5/16-24	0.3125	0.0580			2400	12	9			3700	19	14	4560	24	18	5220	25	20
3/8-16	0.3750	0.0775			3200	20	15			4940	30	23	6100	40	30	7000	45	35
3/8-24	0.3750	0.0878			3620	23	17			5600	35	25	6900	45	45	7900	50	35
7/16-14	0.4375	0.1063			4380	30	24			6800	50	35	8400	60	45	9550	70	55
7/16-20	0.4375	0.1187			4900	35	25			7550	55	40	9350	70	50	10700	80	60
1/2-13	0.5000	0.1419			5840	50	35			9050	75	55	11200	95	70	12750	110	80
1/2-20	0.5000	0.1599			6600	55	40			10700	90	65	12600	100	80	14400	120	90
9/16-12	0.5625	0.1820			7500	70	55			11600	110	80	14350	135	100	16400	150	110
9/16-18	0.5625	0.2030			8400	80	60			12950	120	90	16000	150	110	18250	170	130
5/8-11	0.6250	0.2260			9300	100	75			14400	150	110	17800	190	140	20350	220	170
5/8-18	0.6250	0.2560			10600	110	85			16300	170	130	20150	210	160	23000	240	180
3/4-10	0.7500	0.3340			13800	175	130			21300	260	200	26300	320	240	30100	380	280
3/4-16	0.7500	0.3730			15400	195	145			23800	300	220	29400	360	280	33600	420	320
7/8-9	0.8750	0.4620	60,000	33,000	11400	165	125			29400	430	320	36400	520	400	41600	600	460
7/8-14	0.8750	0.5090			12600	185	140			32400	470	350	40100	580	440	45800	660	500
1-8	1.0000	0.6060			15000	250	190			38600	640	480	47700	800	600	54500	900	680
1-12	1.0000	0.6630			16400	270	200			42200	700	530	52200	860	660	59700	1000	740
1-1/8-7	1.1250	0.7630			18900	350	270	105,000	74,000	42300	800	600	60100	1120	840	68700	1280	960
1-1/8-12	1.1250	0.8560			21200	400	300			47500	880	660	67400	1260	940	77000	1440	1080
1-1/4-7	1.2500	0.9690			24000	500	380			53800	1120	840	76300	1580	1100	87200	1820	1360
1-1/4-12	1.2500	1.0730			26600	550	420			59600	1240	920	84500	1760	1320	96600	2000	1500
1-3/8-6	1.3750	1.1550			28600	660	490			64100	1460	1100	91000	2080	1560	104000	2380	1780
1-3/8-12	1.3750	1.3150			32500	740	560			73000	1680	1260	104000	2380	1780	118400	2720	2040
1-1/2-6	1.5000	1.4050			34800	870	650			78000	1940	1460	111000	2780	2080	126500	3160	2360
1-1/2-12	1.5000	1.5800			39100	980	730			87700	2200	1640	124005	3100	2320	142200	3560	2660

154